広島大学学位請求論文

Construction of a renormalization group improved effective potential in a two real scalar system

（二つの実スカラー系における繰り込み群で改善された有効ポテンシャルの構築）

２０１９年

広島大学大学院理学研究科

物理科学専攻

大兼　英朗

目次

１．主論文

Construction of a renormalization group improved effective potential in a two real scalar system

（二つの実スカラー系における繰り込み群で改善された有効ポテンシャルの構築）

PTEP 2019 (2019) no.4, 043B03

２．参考論文

(1) Precise Discussion of Time-Reversal Asymmetries in B-meson decays.

Takuya Morozumi, Hideaki Okane, Hiroyuki Umeeda

JHEP 1502 (2015) 174

(2) Phenomenological Aspects of Possible Vacua of a Neutrino Flavor Model.

Takuya Morozumi, Hideaki Okane, Hiroki Sakamoto

Yusuke Shimizu, Kenta Takagi, Hiroyuki Umeeda

Chin.Phys. C42 (2018) no.2, 023102

主論文

PTEP

Prog. Theor. Exp. Phys. **2019**, 043B03 (19 pages)
DOI: 10.1093/ptep/ptz022

Construction of a renormalization group improved effective potential in a two real scalar system

Hideaki Okane*

Graduate School of Science, Hiroshima University, Higashi-Hiroshima 739-8526, Japan
*E-mail: hideaki-ookane@hiroshima-u.ac.jp

Received January 20, 2019; Revised February 21, 2019; Accepted February 26, 2019; Published April 16, 2019

We study the improvement of an effective potential by a renormalization group (RG) equation in a two real scalar system. We clarify the logarithmic structure of the effective potential in this model. Based on the analysis of the logarithmic structure of it, we find that the RG improved effective potential up to Lth-to-leading log order can be calculated by the L-loop effective potential and $(L+1)$-loop β and γ functions. To obtain the RG improved effective potential, we choose the mass eigenvalue as a renormalization scale. If another logarithm at the renormalization scale is large, we decouple the heavy particle from the RG equation and we must modify the RG improved effective potential. In this paper we treat such a situation and evaluate the RG improved effective potential. Although this method was previously developed in a single scalar case, we implement the method in a two real scalar system. The feature of this method is that the choice of renormalization scale does not change even in a calculation of higher leading log order. Following our method one can derive the RG improved effective potential in a multiple scalar model.

Subject Index B32, B36

1. Introduction

Effective potentials improved by a renormalization group (RG) equation are widely applied in particle physics. In Refs. [1–6], the stability of an electroweak vacuum is studied through the evaluation of the RG improved effective potential on the high-energy scale. In addition, using the RG improved effective potential, the authors of Refs. [7–18] investigate the possibility that spontaneous symmetry breaking is realized by quantum correction to the effective potential. In this way, the RG improved effective potential is frequently utilized.

There has been a great deal of research into the RG improvement of the effective potential since a study by Coleman and Weinberg [7]. In Refs. [19–21], the RG improved effective potential in a single field is derived. If utilizing the RG invariance of the effective potential, the renormalization scale μ is set as a field-dependent mass $M(\phi,\mu)$; the logarithm $\log(M(\phi,\mu)^2/\mu^2)$ becomes zero. In that case, the logarithmic perturbative expansion of the effective potential including $(\log(M(\phi,\mu)^2/\mu^2))^L$ at the L-loop level is stable because of $\log(M(\phi,\mu)^2/\mu^2) = 0$. This is an essential point for the construction of the RG improved effective potential. If the theory includes multiple fields, the situation is not so simple. Taking $M(\phi,\mu)$ as a renormalization scale, one cannot guarantee that the logarithm $\log(M'(\phi,\mu)^2/\mu^2)$ coming from another field is always small. If the logarithm is large,

Funded by SCOAP[3]

it leads to the breakdown of the perturbative expansion for the effective potential. In Refs. [22–26], the methods of solving such a problem are studied. The methods are classified into two types. In Refs. [22–24], multiple renormalization scales are introduced and each logarithm is suppressed by the multiple renormalization scales. On the other hand, the decoupling theorem [27] is applied in Refs. [25,26]. If a large logarithm appears in the calculation of the effective potential, the heavy particle is decoupled. Since the remaining logarithm is only one of a light field, the calculation of the RG improved effective potential is the same as the method explained in the single field case. Note that these methods are applied to theory including only a single scalar field.

If multiple scalar fields are introduced, the analysis of the RG improved effective potential is complicated because the masses appearing in the logarithms depend on multiple classical background fields such as $M(\phi_1, \phi_2)$. The problem is addressed in Refs. [28–30]. In Ref. [28], the RG improved effective potential is calculated with the introduction of the multiple renormalization scale. In Ref. [29], which extends the method of Ref. [26], a step function for the automatic decoupling of a heavy particle is introduced in the effective potential. Moreover, effective action is analyzed to take wavefunction renormalization into account. In Ref. [30], a new method is suggested. The guiding principle for the method is to choose the renormalization scale so that the total loop correction vanishes. In Ref. [31] the RG improved effective potential in classical conformal theory is analyzed based on the method of Ref. [30]. In the present paper, we also approach the problem for the RG improvement of the effective potential.

In this paper, extending the method of Ref. [25], we construct the RG improved effective potential in a two real scalar theory. Since the method of Ref. [25] is based on the analysis of the logarithmic structure of the effective potential, we derive the expression of the effective potential expanded with respect to all the logarithms appearing in a two real scalar system. Based on the analysis of the logarithmic structure of the effective potential, we choose the field-dependent mass eigenvalue as a renormalization scale so that one of the logarithms vanishes. If another logarithm at the renormalization scale is small enough to be perturbative, the RG improved effective potential is calculated with the choice of the renormalization scale. If the logarithm is large, we absorb the logarithm into the new parameters defined in the low-energy scale and decouple the heavy particle from the theory. Since the logarithm to be considered is only one of a light particle, we can easily evaluate the RG improved effective potential. The advantages of this method are as follows. First, since this method is based on the logarithmic structure of the effective potential at any loop order, the choice of the renormalization scale does not need to be changed even at higher loop order. Second, we can derive the RG improved effective potential without introducing multiple renormalization scales or a step function for the decoupling. Finally, we can easily implement the decoupling theorem by expanding the effective potential coming from quantum correction with respect to ϕ^2/m^2 ($\phi^2 = \phi_1^2 + \phi_2^2$, m: decoupling scale).

This paper is organized as follows: In Sect. 2, we clarify the logarithmic structure of the effective potential and investigate the choice of the renormalization scale. In Sect. 3, the massless theory is treated and the RG improved effective potential is calculated based on the analysis of Sect. 2. In Sect. 4, we consider the massive model. In this section, we face a situation in which a large logarithm occurs. We decouple the heavy particle and construct the RG improved effective potential on the low-energy scale. In Sect. 5, we summarize the procedure of RG improvement in a multiple scalar model and discuss applications to other models. In Appendix A, the β and γ functions at the 1-loop level are given.

2. Logarithmic structure of effective potential and RG improvement

In this section, we clarify the logarithmic structure of the effective potential based on Ref. [25]. We then consider the choice of renormalization scale for the RG improvement of the effective potential. For a more specific explanation, we consider a two real scalar system as an example. The Lagrangian is given as follows:

$$\mathcal{L} = \frac{1}{2}(\partial\sigma)^2 + \frac{1}{2}(\partial\chi)^2 - \frac{m_1^2}{2}\sigma^2 - \frac{m_2^2}{2}\chi^2 - \frac{\lambda_1}{4!}\sigma^4 - \frac{\lambda_2}{4!}\chi^4 - \frac{\lambda_3}{4}\sigma^2\chi^2 - \Lambda. \tag{1}$$

We suppose that this model has $Z_2 \times Z_2$ symmetry: $\sigma \to -\sigma$ and $\chi \to -\chi$. Following Ref. [25], we factor out a coupling constant $1/\lambda_1$ from the Lagrangian[1]

$$\begin{aligned}\mathcal{L} = \frac{1}{\lambda_1}\Bigg(&\frac{1}{2}\left\{\partial(\sqrt{\lambda_1}\sigma)\right\}^2 + \frac{1}{2}\left\{\partial(\sqrt{\lambda_1}\chi)\right\}^2 - \frac{m_1^2}{2}(\sqrt{\lambda_1}\sigma)^2 - \frac{m_2^2}{2}(\sqrt{\lambda_1}\chi)^2 \\ &- \frac{1}{4!}(\sqrt{\lambda_1}\sigma)^4 - \frac{\lambda_2/\lambda_1}{4!}(\sqrt{\lambda_1}\chi)^4 - \frac{\lambda_3/\lambda_1}{4}(\sqrt{\lambda_1}\sigma)^2(\sqrt{\lambda_1}\chi)^2 - \lambda_1\Lambda\Bigg).\end{aligned} \tag{2}$$

Next, we shift the fields (σ, χ) by classical background fields (ϕ_1, ϕ_2), respectively:

$$\sigma \to \phi_1 + \sigma,$$
$$\chi \to \phi_2 + \chi,$$

and then redefine the quantum fields $\sqrt{\lambda_1}\sigma$ and $\sqrt{\lambda_1}\chi$ as σ and χ, respectively. After the shift and the redefinition, the Lagrangian becomes

$$\begin{aligned}\mathcal{L} = \frac{1}{\lambda_1}\Bigg(&\frac{1}{2}(\partial\sigma)^2 + \frac{1}{2}(\partial\chi)^2 - \frac{M_1^2}{2}\sigma^2 - \frac{M_2^2}{2}\chi^2 - M_3^2\sigma\chi \\ &- \frac{x_1}{3!}\sigma^3 - \frac{x_2 y_1}{3!}\chi^3 - \frac{y_2}{2}(x_2\sigma + x_1\chi)\sigma\chi \\ &- \frac{1}{4!}\sigma^4 - \frac{y_1}{4!}\chi^4 - \frac{y_2}{4}\sigma^2\chi^2 - \lambda_1 V^{(0)}\Bigg),\end{aligned} \tag{3}$$

where mass parameters (M_1^2, M_2^2, M_3^2), cubic coupling constants (x_1, x_2), and quartic coupling constants (y_1, y_2) are introduced as follows:

$$\begin{aligned} M_1^2 &= m_1^2 + \frac{\lambda_1}{2}\phi_1^2 + \frac{\lambda_3}{2}\phi_2^2, \\ M_2^2 &= m_2^2 + \frac{\lambda_3}{2}\phi_1^2 + \frac{\lambda_2}{2}\phi_2^2, \\ M_3^2 &= \lambda_3\phi_1\phi_2, \\ x_1 &= \sqrt{\lambda_1}\phi_1, \qquad x_2 = \sqrt{\lambda_1}\phi_2, \\ y_1 &= \frac{\lambda_2}{\lambda_1}, \qquad y_2 = \frac{\lambda_3}{\lambda_1}, \end{aligned}$$

[1] In this paper, we assume that all the quartic coupling constants are comparable to each other ($\mathcal{O}(\lambda_1) \sim \mathcal{O}(\lambda_2) \sim \mathcal{O}(\lambda_3)$) and perturbative. Under this assumption, the choice of λ_1 does not affect the final expression (28). That is to say, factoring out λ_2 (or λ_3) replaced by λ_1, one obtains the same result (28).

and $V^{(0)}$ is a tree-level effective potential:

$$V^{(0)} = \frac{m_1^2}{2}\phi_1^2 + \frac{m_2^2}{2}\phi_2^2 + \frac{\lambda_1}{4!}\phi_1^4 + \frac{\lambda_2}{4!}\phi_2^4 + \frac{\lambda_3}{4}\phi_1^2\phi_2^2 + \Lambda. \tag{4}$$

From the rewritten Lagrangian (3) and the tree potential (4), we can find that the theory is described by the following parameters:

$$\text{mass parameters :} \quad M_1^2,\ M_2^2,\ M_3^2, \tag{5}$$

$$\text{cubic coupling constants :} \quad x_1,\ x_2, \tag{6}$$

$$\text{quartic coupling constants :} \quad \lambda_1,\ y_1,\ y_2, \tag{7}$$

$$\text{constant term :} \quad \Lambda. \tag{8}$$

Moreover, since it is inconvenient for the mass matrix not to be diagonal, we rotate the mass matrix by introducing new states (σ_d and χ_d) and mixing angle (θ):

$$\begin{pmatrix}\sigma\\ \chi\end{pmatrix} = \begin{pmatrix}\cos\theta & -\sin\theta\\ \sin\theta & \cos\theta\end{pmatrix}\begin{pmatrix}\sigma_d\\ \chi_d\end{pmatrix}, \quad \tan(2\theta) = \frac{2M_3^2}{M_1^2 - M_2^2},$$

and then the mass matrix is diagonalized:

$$\begin{pmatrix}\sigma & \chi\end{pmatrix}\begin{pmatrix}M_1^2 & M_3^2\\ M_3^2 & M_2^2\end{pmatrix}\begin{pmatrix}\sigma\\ \chi\end{pmatrix} = \begin{pmatrix}\sigma_d & \chi_d\end{pmatrix}\begin{pmatrix}M_+^2 & 0\\ 0 & M_-^2\end{pmatrix}\begin{pmatrix}\sigma_d\\ \chi_d\end{pmatrix},$$

where the mass eigenvalues are

$$M_\pm^2 = \frac{1}{2}\left(M_1^2 + M_2^2 \pm \sqrt{(M_1^2 - M_2^2)^2 + 4M_3^4}\right).$$

For later discussion, the coordinate (ϕ_1, ϕ_2) is translated to the polar coordinate (ϕ, β):

$$\phi^2 = \phi_1^2 + \phi_2^2, \qquad \tan\beta = \frac{\phi_2}{\phi_1}. \tag{9}$$

From now on, the mass eigenvalues and the effective potential are written with the polar coordinate (ϕ, β).

At this stage, we can replace the three mass parameters (M_1^2, M_2^2, M_3^2) in Eq. (5) by mass eigenvalues $(M_\pm^2)$ and mixing angle (θ). Namely, the model is described in terms of the following parameters:

$$\text{mass eigenvalues :} \quad M_\pm^2, \tag{10}$$

$$\text{mixing angle :} \quad \theta, \tag{11}$$

$$\text{cubic coupling constants :} \quad x_1,\ x_2, \tag{12}$$

$$\text{quartic coupling constants :} \quad \lambda_1,\ y_1,\ y_2, \tag{13}$$

$$\text{constant term :} \quad \Lambda. \tag{14}$$

This information is so important that using these parameters we can write down the effective potential at the L-loop level as

$$V^{(L)} = \lambda_1^{L-1} M_-^4 \left[\text{function of } \log\left(\frac{M_-^2}{\mu^2}\right), \log\left(\frac{M_+^2}{\mu^2}\right), P\right], \tag{15}$$

where P is the generic term of $(p_1, \ldots, p_7)$:

$$p_1 = \frac{M_+^2}{M_-^2},\ p_2 = \theta,\ p_3 = \frac{x_1^2}{M_-^2},\ p_4 = \frac{x_2^2}{M_-^2}, \tag{16}$$

$$p_5 = y_1,\ p_6 = y_2,\ p_7 = \lambda_1 \frac{\Lambda}{M_-^4}. \tag{17}$$

Let us explain why the L-loop effective potential can be written as Eq. (15). Since λ_1 can be treated like an $\hbar$ in front of the action, the L-loop effective potential is proportional to λ_1^{L-1}. The part in the square brackets $[\cdots]$ in Eq. (15) is dimensionless because M_-^4 is extracted as a dimensionful part of $V^{(L)}$. So since we introduce dimensionless parameters $(p_1, \ldots, p_7)$ based on Eqs. (10)–(14), the part in the square brackets $[\cdots]$ can be written in terms of two logarithms ($\log(M_-^2/\mu^2)$ and $\log(M_+^2/\mu^2)$) and dimensionless parameters $(p_1, \ldots, p_7)$.

As is well known, since the L-loop effective potential $V^{(L)}$ contains the Lth power of the logarithm at most, one can express $V^{(L)}$ with respect to $\log(M_-^2/\mu^2)$ and $\log(M_+^2/\mu^2)$:

$$V^{(L)} = \frac{M_-^4}{\lambda_1} \sum_{l=0}^{L} \sum_{k=0}^{L-l} \lambda_1^l v^{(L)}_{L-(k+l),k}(P) s_1^{L-(l+k)} s_2^k, \tag{18}$$

where, multiplying each logarithm by λ_1, we define s_1 and s_2:

$$s_1 = \lambda_1 \log\left(\frac{M_-^2}{\mu^2}\right), \qquad s_2 = \lambda_1 \log\left(\frac{M_+^2}{\mu^2}\right).$$

Finally, by summing up $V^{(L)}$ from $L = 0$ to $L = \infty$, we obtain the total effective potential expressed in terms of s_1 and s_2:

$$V = \sum_{L=0}^{\infty} V^{(L)} = \frac{M_-^4}{\lambda_1} \sum_{l=0}^{\infty} \lambda_1^l f_l(P, s_1, s_2), \tag{19}$$

$$f_l(P, s_1, s_2) = \sum_{L=l}^{\infty} \sum_{k=0}^{L-l} v^{(L)}_{L-(l+k),k}(P) s_1^{L-(l+k)} s_2^k. \tag{20}$$

In this expression the power of λ_1 gives the order of the leading log-series expansion. In this sense, f_l means the lth-to-leading log function of the effective potential.

Next, we consider the choice of renormalization scale. As is well known, the effective potential satisfies the RG equation

$$\mathcal{D}V = \mu \frac{d}{d\mu} V = 0, \tag{21}$$

where the RG differential operator is given as

$$\mathcal{D} = \mu \frac{d}{d\mu} = \mu \frac{\partial}{\partial \mu} - \sum_X \gamma_X X \frac{\partial}{\partial X} + \sum_Y \beta_Y \frac{\partial}{\partial Y}, \tag{22}$$

where

$$\gamma_X = -\frac{\mu}{X} \frac{dX}{d\mu}, \qquad \beta_Y = \mu \frac{dY}{d\mu},$$

$$X = m_1^2, m_2^2, \Lambda, \phi_1, \phi_2, \qquad Y = \lambda_1, \lambda_2, \lambda_3. \tag{23}$$

These specific β and γ functions are given in Appendix A. We can then obtain the solution of the RG equation as

$$V(\phi, \beta, Q; \mu_0^2) = V\left(\bar{G}(t, \beta)\phi, \beta, \bar{Q}(t); \mu_0^2 e^{2t}\right), \tag{24}$$

where we use a shorthand notation $Q(= m_1^2, m_2^2, \lambda_1, \lambda_2, \lambda_3, \Lambda)$ and introduce t to express the renormalization scale μ^2 as $\mu^2(t) = \mu_0^2 e^{2t}$. Also, $\bar{G}(\beta, t)$ is defined as

$$\begin{aligned}\bar{\phi}_1(t)^2 + \bar{\phi}_2(t)^2 &= \left(\exp\left[-2\int_0^t ds \bar{\gamma}_{\phi_1}(s)\right]\cos^2\beta + \exp\left[-2\int_0^t ds \bar{\gamma}_{\phi_2}(s)\right]\sin^2\beta\right)\phi^2 \\ &\equiv \bar{G}(\beta, t)^2\phi^2.\end{aligned} \tag{25}$$

However, because of $\gamma_{\phi_1} = \gamma_{\phi_2} = 0$, from now on, we set $\bar{G}(\beta, t) = 1$. $\bar{Q}(t)$ is the solution of β or γ function and satisfies an initial value Q at an initial renormalization scale μ_0^2 or $t = 0$. The RG solution of Eq. (24) for the effective potential means that it is independent of the renormalization scale t. Since we can freely choose the renormalization scale, we look for the best choice of it. Let us take the renormalization scale as follows:

$$\mu^2 = \bar{M}_-(t)^2. \tag{26}$$

Since this choice leads to $\bar{s}_1(t) = 0$, the RG improved effective potential expressed with Eq. (19) becomes

$$V = \bar{M}_-(t)^4 \sum_{l=0}^{\infty} \bar{\lambda}_1(t)^{l-1} f_l(\bar{P}, \bar{s}_1 = 0, \bar{s}_2),$$

where from Eq. (20)

$$f_l(\bar{P}, \bar{s}_1 = 0, \bar{s}_2) = \sum_{L=l}^{\infty} v_{0,L-l}^{(L)}(\bar{P})\bar{s}_2^{L-l}.$$

Here, if we assume $\bar{s}_2 \lesssim \mathcal{O}(\bar{\lambda}_1)$, one gets the lth-to-leading log function:

$$f_l(\bar{P}, \bar{s}_1 = 0, \bar{s}_2) = v_{0,0}^{(l)}(\bar{P}) + \mathcal{O}\left(\bar{\lambda}_1\right). \tag{27}$$

If $\bar{s}_2 \lesssim \mathcal{O}(\bar{\lambda}_1)$ and we would like to evaluate the effective potential up to Lth-to-leading log order, the expression is written as

$$\begin{aligned}V &= \bar{M}_-(t)^4 \sum_{l=0}^{L} \bar{\lambda}_1(t)^{l-1} f_l(\bar{P}, \bar{s}_1 = 0, \bar{s}_2)\Big|_{\bar{s}_2 \lesssim \mathcal{O}(\bar{\lambda}_1)} \\ &= \bar{M}_-(t)^4 \sum_{l=0}^{L} \bar{\lambda}_1(t)^{l-1} v_{0,0}^{(l)}(\bar{P})\Big|_{\mu^2 = \bar{M}_-^2} + \mathcal{O}\left(\bar{\lambda}_1^L\right) \\ &= \sum_{l=0}^{L} V^{(l)}(\phi, \beta, \bar{Q}(t); \mu_0^2 e^{2t})\Big|_{\mu^2 = \bar{M}_-^2} + \mathcal{O}\left(\bar{\lambda}_1^L\right).\end{aligned} \tag{28}$$

We notice that the term of $\mathcal{O}\left(\bar{\lambda}_1\right)$ in Eq. (27) contributes to the effective potential beyond the Lth-to-leading log order. Note that the RG improved effective potential is exactly correct up to Lth-to-leading log order only if the RG equations for the parameters are solved up to the $(L+1)$ loop level. In summary, if one prepares the L-loop effective potential and $(L+1)$-loop β and γ functions, one can construct the RG improved effective potential (28) up to Lth-to-leading log order for the case of $\bar{s}_2 \lesssim \mathcal{O}\left(\bar{\lambda}_1\right)$.

We comment on the variables of the effective potential. Originally, the effective potential has three variables (ϕ, β, t). However, now that $\mu(t)^2$ is taken to be equal to $\bar{M}_-(\phi,\beta,t)^2$, these variables are related. In our paper, we show that we can solve $\mu(t)^2 = \bar{M}_-(\phi,\beta,t)^2$ analytically with respect to ϕ and construct the RG improved effective potential by using the solution of ϕ.[2]

Since the above prescription is correct only in the case of $\bar{s}_2 \lesssim \mathcal{O}\left(\bar{\lambda}_1\right)$, we must consider the method of the RG improvement for the case of $\bar{s}_2 > \mathcal{O}\left(\bar{\lambda}_1\right)$. In that case, as seen from the logarithm $\log\left(\bar{M}_+(t)^2/\bar{M}_-(t)^2\right)$ of $\bar{s}_2$, the relative magnitude of the mass eigenvalues is large. In such a case, we make use of the decoupling theorem [25]. The decoupling of the heavy particle means that the logarithm of the particle is absorbed into the parameters defined in the effective theory. The remaining logarithm is only one of a light particle. If the theory includes only a single logarithm, by setting the renormalization scale as the light mass, the RG improved effective potential can be calculated. We discuss this situation more specifically in Sect. 4.

3. RG improved effective potential in a two real scalar system (massless case)

We specifically calculate the RG improved effective potential by the method constructed in Sect. 2. In this section we treat the two real scalar model without mass parameters. The procedure for the construction of the RG effective potential is as follows. Because of taking the renormalization scale as $\mu_0^2 e^{2t} = \bar{M}_-(t)^2$, we solve it with respect to ϕ. Substituting the ϕ into the mass eigenvalue M_+^2 and the effective potential, we can evaluate $\log(\bar{M}_+(t)^2/\bar{M}_-(t)^2)$ and the effective potential. If the logarithm is small enough for $\bar{s}_2$ to be of the order of $\bar{\lambda}_1$, we can use the expression of Eq. (28) as the effective potential up to Lth-to-leading log order.

In order to obtain ϕ with $\mu_0^2 e^{2t} = \bar{M}_-(t)^2$ satisfied, we solve it in terms of ϕ. In the present model, the mass eigenvalues $M_\pm^2$ are written as

$$\begin{aligned} M_\pm^2 &= \frac{\phi^2}{4}\Big((\lambda_1+\lambda_3)\cos^2\beta + (\lambda_3+\lambda_2)\sin^2\beta \\ &\qquad \pm \sqrt{\left((\lambda_1-\lambda_3)\cos^2\beta + (\lambda_3-\lambda_2)\sin^2\beta\right)^2 + 16\lambda_3^2\sin^2\beta\cos^2\beta}\Big) \\ &\equiv \lambda_\pm(\beta)\phi^2. \end{aligned}$$

So we can easily obtain ϕ from $\mu_0^2 e^{2t} = \bar{M}_-(t)^2$:

$$\phi^2 = \frac{\mu_0^2 e^{2t}}{\bar{\lambda}_-(\beta,t)}. \tag{29}$$

[2] Moreover, note that although the dimensionless parameters P are introduced for the derivation of the logarithmic structure of the effective potential, the final expression is written in terms of the parameters Q. Namely, we do not use the dimensionless parameters P but the parameters Q for the calculation of the RG improved effective potential (28) .

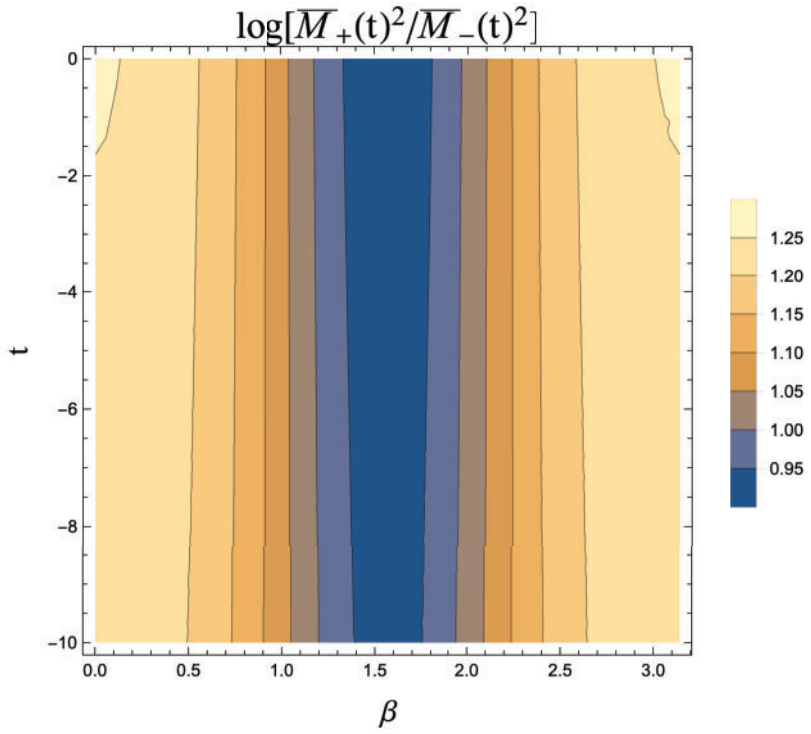

Fig. 1. A contour plot of $\log(\bar{M}_+^2/\bar{M}_-^2)$ in the regions of $\beta \in (0,\pi)$ and $t \in (-10,0)$. We take $\lambda_1 = 0.7$, $\lambda_2 = 0.5$, $\lambda_3 = 0.2$, and $\phi = 10$ at $\mu_0^2 = M_-^2$ as an initial condition.

As mentioned above, now ϕ is not the variable of the effective potential and is determined by β and t. The ϕ appearing in the mass eigenvalue $\bar{M}_+^2$ and the effective potential is calculated with Eq. (29).

The logarithm of $\bar{s}_2$ is written as

$$\log\left(\frac{\bar{M}_+(t)^2}{\mu(t)^2}\right)\Bigg|_{\mu(t)^2=\bar{M}_-(t)^2} = \log\left(\frac{\bar{\lambda}_+(\beta,t)}{\bar{\lambda}_-(\beta,t)}\right), \tag{30}$$

where ϕ is canceled out because of the massless model. At this stage we assign initial values of $(\lambda_1, \lambda_2, \lambda_3)$ for performing the numerical calculation. Taking $\lambda_1 = 0.7, \lambda_2 = 0.5, \lambda_3 = 0.2$, and $\phi = 10$ at $\mu_0^2 = M_-^2$, we calculate $\log(\bar{M}_+(t)^2/\bar{M}_-(t)^2)$ for the range of $\beta \in (0,\pi)$ and $t \in (-10,0)$ by 1-loop β functions in Fig. 1. In Fig. 1 we see that $\log(\bar{M}_+(t)^2/\bar{M}_-(t)^2) \approx 1$ in the regions of (β,t). Thus, since we can conclude that $\bar{s}_2 \approx \bar{\lambda}_1$, Eq. (28) can be used as the RG improved effective potential. Using the tree-level effective potential and the 1-loop β function, the RG improved effective potential at the leading log order is given as

$$V = \left(\frac{\bar{\lambda}_1(t)}{4!}\cos^4\beta + \frac{\bar{\lambda}_2(t)}{4!}\sin^4\beta + \frac{\bar{\lambda}_3(t)}{4}\sin^2\beta\cos^2\beta\right)\phi^4 \quad \text{with} \quad \phi^2 = \frac{\mu_0^2 e^{2t}}{\bar{\lambda}_-(\beta,t)}, \tag{31}$$

where the condition for ϕ^2 originates from the choice of the renormalization scale $\mu^2 = \bar{M}_-(t)^2$, as seen in Eq. (29). Clearly the RG improved effective potential is determined by β and t. In Fig. 2, the RG improved effective potential is plotted as axes of $(\phi_1/\mu_0, \phi_2/\mu_0)$ for the regions of $\beta \in (0,\pi)$ and $t \in (-10,0)$.

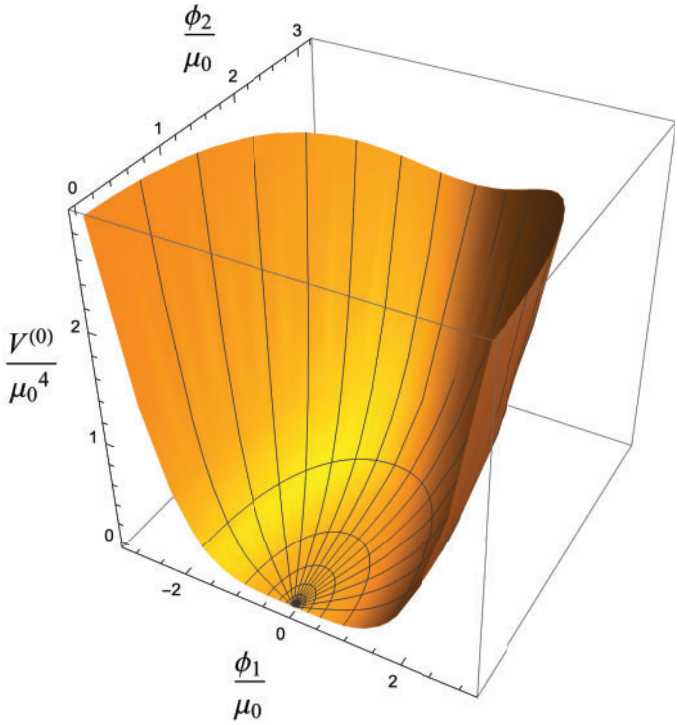

Fig. 2. A 3D plot of the RG improved effective potential at the leading log order divided by the initial renormalization scale μ_0^4 as axes of $(\phi_1/\mu_0, \phi_2/\mu_0)$. This is plotted in the regions of $\beta \in (0, \pi)$ and $t \in (-10, 0)$. The initial condition is the same as in Fig. 1.

4. RG improved effective potential in a two real scalar system (massive case)

In this section we consider the massive theory in a two real scalar model. In particular, we treat the effective potential causing spontaneous symmetry breaking. The procedure for the construction of the RG improved effective potential is the same as the previous method. We solve Eq. (26) for ϕ in the massive case. In this case, because of the mass parameters, the equation is a little complicated but it can be analytically solved. Equation (26) is written as follows:

$$A = \sqrt{B}, \tag{32}$$

where

$$A = m_1^2 + m_2^2 - 2\mu^2 + \frac{1}{2}\Big((\lambda_1 + \lambda_3)\cos^2\beta + (\lambda_2 + \lambda_3)\sin^2\beta\Big)\phi^2,$$

$$B = \left\{m_1^2 - m_2^2 + \frac{1}{2}\Big((\lambda_1 - \lambda_3)\cos^2\beta + (\lambda_3 - \lambda_2)\sin^2\beta\Big)\phi^2\right\}^2 + 4\lambda_3^2\sin^2\beta\cos^2\beta\phi^4.$$

Squaring both sides of $A = \sqrt{B}$, a quadratic equation for ϕ^2 is given as

$$a\phi^4 + 2b\phi^2 + c = 0, \tag{33}$$

where

$$a = \lambda_1\lambda_3\cos^4\beta + \lambda_2\lambda_3\sin^4\beta + (\lambda_1\lambda_2 - 3\lambda_3^2)\sin^2\beta\cos^2\beta,$$

$$b = (\lambda_3 \cos^2\beta + \lambda_2 \sin^2\beta)(m_1^2 - \mu^2) + (\lambda_1 \cos^2\beta + \lambda_3 \sin^2\beta)(m_2^2 - \mu^2),$$
$$c = 4(m_1^2 - \mu^2)(m_2^2 - \mu^2).$$

We can obtain the solution ϕ^2 as

$$\phi^2 = \frac{-b \pm \sqrt{b^2 - ac}}{a}. \tag{34}$$

Since we solve the quadratic equation, there are two solutions for ϕ^2. However, because the original equation is $A = \sqrt{B}$, the solution satisfies the following conditions:

$$A > 0 \quad \text{and} \quad B > 0. \tag{35}$$

Although it is difficult to analytically prove whether either solution satisfies the condition or not, by using the initial values as inputs in the following subsections we confirm numerically the following results:

$$\phi^2 = \frac{-b + \sqrt{b^2 - ac}}{a} \quad \rightarrow \quad A > 0 \quad \text{and} \quad B > 0,$$
$$\phi^2 = \frac{-b - \sqrt{b^2 - ac}}{a} \quad \rightarrow \quad A < 0 \quad \text{and} \quad B < 0.$$

Therefore we adopt the solution ϕ as

$$\phi^2 = \frac{-b + \sqrt{b^2 - ac}}{a}. \tag{36}$$

Since we get the solution ϕ for Eq. (26), we can construct the RG improved effective potential. The expression is provided at leading log order as

$$V = \frac{1}{2}(\bar{m}_1(t)^2 \cos^2\beta + \bar{m}_2(t)^2 \sin^2\beta)\phi^2 + \frac{1}{4!}(\bar{\lambda}_1(t)\cos^4\beta + \bar{\lambda}_2(t)\sin^4\beta + 6\bar{\lambda}_3(t)\sin^2\beta\cos^2\beta)\phi^4 + \bar{\Lambda}(t)$$
$$\text{with} \qquad \phi^2 = \frac{-\bar{b}(\beta,t) + \sqrt{\bar{b}(\beta,t)^2 - \bar{a}(\beta,t)\bar{c}(t)}}{\bar{a}(\beta,t)}. \tag{37}$$

In the following subsections, we consider two situations for inputting the initial value of the renormalization scale. First, taking $(m_1^2 < 0, m_2^2 < 0, -m_1^2 \sim -m_2^2)$ as the mass parameters, we set the initial renormalization scale on the vacuum, which is determined by the stationary condition of the effective potential. Increasing the renormalization scale from the low-energy scale at the vacuum, we analyze the behavior of the RG improved effective potential in the high-energy region. Second, we input the initial values of the parameters on the high-energy scale and decrease the renormalization scale to the low-energy scale. Assuming $(m_1^2 < 0, m_2^2 > 0, -m_1^2 \ll m_2^2)$ for the mass parameters, we investigate the RG improved effective potential in the low-energy region. As the renormalization scale decreases, the mass eigenvalue $\bar{M}_-^2$ also declines and reaches m_2^2 at a scale. Since $\bar{M}_-^2$ continues to decline below the scale, we find the logarithm of $\bar{s}_2$ large. In order to avoid the breakdown of the logarithmic perturbation, we utilize the decoupling theorem. Applying the decoupling theorem, we derive the RG improved effective potential in the low-energy scale and visualize the behavior including the minimum value of the RG improved effective potential.

4.1. $-m_2^2 \sim -m_1^2$

Since we set the initial condition on the vacuum in this subsection, we derive the stationary condition for the effective potential. Introducing a convenient notation for the mass parameter and quartic coupling constant:

$$m(\beta)^2 = m_1^2 \cos^2\beta + m_2^2 \sin^2\beta,$$
$$\lambda(\beta) = \lambda_1 \cos^4\beta + \lambda_2 \sin^4\beta + 6\lambda_3 \sin^2\beta \cos^2\beta,$$

we can write the effective potential at a tree level:

$$V^{(0)} = \frac{m(\beta)^2}{2}\phi^2 + \frac{\lambda(\beta)}{4!}\phi^4 + \Lambda.$$

We calculate the stationary conditions for the effective potential:

$$\frac{\partial V^{(0)}}{\partial \phi} = 0, \quad \frac{\partial V^{(0)}}{\partial \beta} = 0. \tag{38}$$

From $\frac{\partial V^{(0)}}{\partial \phi} = 0$, we derive the following condition:

$$\phi^2 = -6\frac{m(\beta)^2}{\lambda(\beta)}. \tag{39}$$

Combining this condition and $\frac{\partial V^{(0)}}{\partial \beta} = 0$, we get the stationary condition for β:

$$\beta = \arccos\left[\frac{\lambda_2 m_1^2 - 3\lambda_3 m_2^2}{(\lambda_2 - 3\lambda_3)m_1^2 + (\lambda_1 - 3\lambda_3)m_2^2}\right]. \tag{40}$$

Substituting this β for Eq. (39), we can obtain ϕ on the stationary point:

$$\phi^2 = -6\frac{(\lambda_2 - 3\lambda_3)m_1^2 + (\lambda_1 - 3\lambda_3)m_2^2}{\lambda_1\lambda_2 - 9\lambda_3^2}. \tag{41}$$

Using Eqs. (41)–(40), we can calculate the vacuum expectation value and also estimate the initial renormalization scale $\mu_0^2 = \bar{M}_-(t=0)^2 = M_-^2$. For simplicity, in this section we impose $\Lambda = 0$ at the initial point.

Taking [$\lambda_1 = 0.7$, $\lambda_2 = 0.5$, $\lambda_3 = 0.1$, $m_1^2 = -(160\ \text{GeV})^2$, and $m_2^2 = -(170\ \text{GeV})^2$] as an initial condition, we get the vacuum expectation value $(\phi, \beta) = (591\ \text{GeV}, 0.94)$, the initial renormalization scale $\mu_0 = M_- = 135$ GeV, and the mass eigenvalue $M_+ = 236$ GeV. We regard the vacuum expectation value and the initial renormalization scale as a starting point for the RG improved effective potential and the running parameters. Then, we run $\log(\bar{M}_+(t)^2/\bar{M}_-(t)^2)$ by the RG equations in the regions of $t \in (0, 5)$ and $\beta \in (0, \frac{\pi}{2})$. Figure 3 shows the result of the logarithm. On $\beta = 0$ and $\beta = \frac{\pi}{2}$ in Fig. 3, the logarithm takes 2–3 in the range of $t = (0, 2)$ and less than 2 for $t > 2$. In $\beta = \frac{\pi}{4}$, the logarithm is less than 1 for the whole scale of t. If the magnitude of the logarithm as $\log(\bar{M}_-^2/\bar{M}_+^2) \lesssim 3$ is accepted in the context of a logarithmic perturbative expansion, the RG improved effective potential is calculated with Eq. (37). The result is shown in Fig. 4. In the left panel of Fig. 4, the dot-dashed green, dotted orange, and solid blue lines correspond to the RG improved effective potential in $\beta = 0$, $\beta = \frac{\pi}{4}$, and $\beta = \frac{\pi}{2}$, respectively. In the right panel of Fig. 4, the dot-dashed green, dotted orange, and solid blue lines correspond to ϕ in $\beta = 0$, $\beta = \frac{\pi}{4}$, and

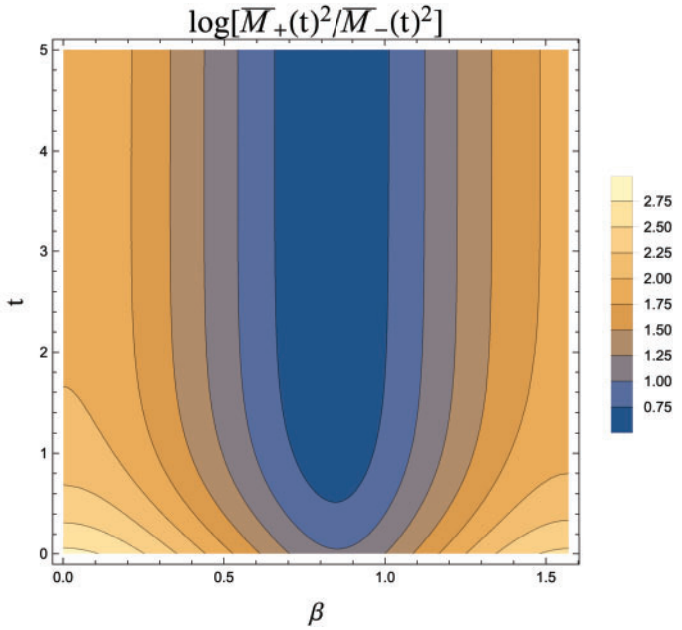

Fig. 3. The logarithm of the ratio of $\bar{M}_+(t)^2$ to $\bar{M}_-(t)^2$ is plotted in the ranges of $\beta \in (0, \frac{\pi}{2})$ and $t \in (0, 5)$. The result is produced by taking $\lambda_1 = 0.7$, $\lambda_2 = 0.5$, $\lambda_3 = 0.1$, $m_1^2 = -(160\ \text{GeV})^2$, and $m_2^2 = -(170\ \text{GeV})^2$ as an initial condition for the RG equation.

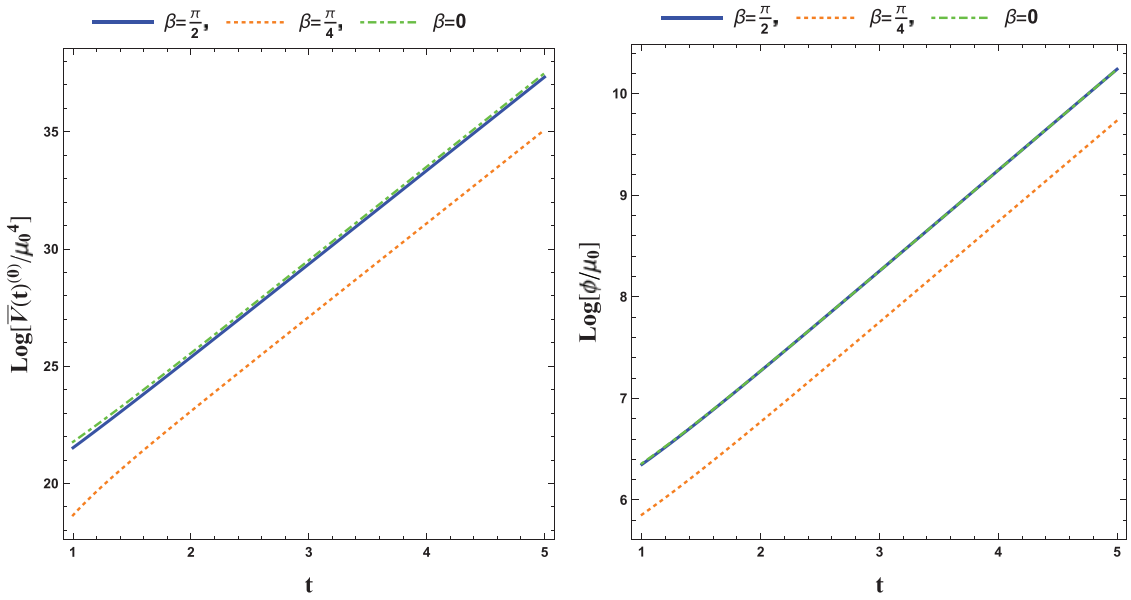

Fig. 4. Left: The dot-dashed green, dotted orange, and solid blue lines correspond to the RG improved effective potential in $\beta = 0$, $\beta = \frac{\pi}{4}$, and $\beta = \frac{\pi}{2}$, respectively. Right: The dot-dashed green, dotted orange, and solid blue lines correspond to ϕ in $\beta = 0$, $\beta = \frac{\pi}{4}$, and $\beta = \frac{\pi}{2}$, respectively. The initial condition for the RG equation is the same as in Fig. 3.

$\beta = \frac{\pi}{2}$, respectively (ϕ in $\beta = 0$ and $\frac{\pi}{2}$ are ϕ_1 and ϕ_2, respectively). In both panels of Fig. 4, the lines at $\beta = 0$ and $\frac{\pi}{2}$ overlap with each other.

We give a more complete discussion for the logarithmic perturbative expansion. As explained above, there are regions in which the logarithm is beyond 1. If the logarithm is considered to be large, the heavy field with mass $\bar{M}_+$ should be decoupled from the theory. Due to this decoupling,

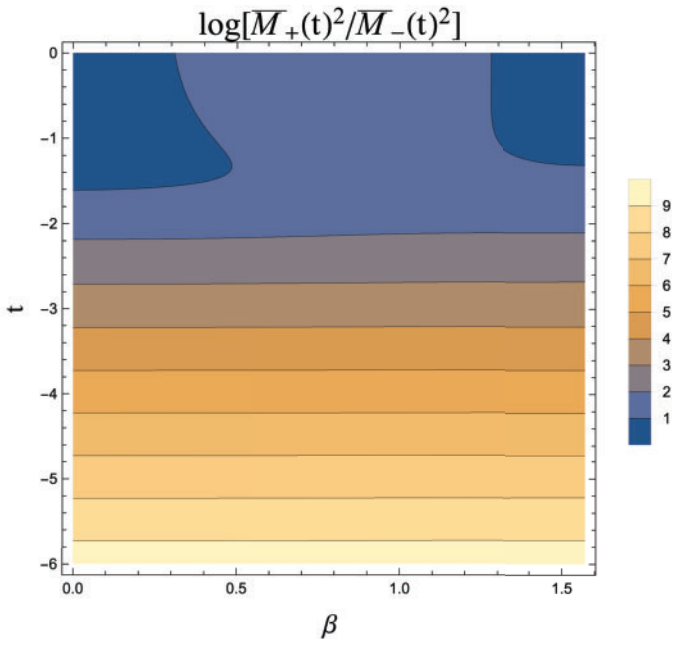

Fig. 5. The logarithm of the ratio of $\bar{M}_+(t)^2$ to $\bar{M}_-(t)^2$ is plotted in the regions of $\beta \in (0, \frac{\pi}{2})$ and $t \in (-6, 0)$. The initial condition is given as $\lambda_1 = 0.7, \lambda_2 = 0.6, \lambda_3 = 0.4, m_1^2 = -(200\ \text{GeV})^2, m_2^2 = (3000\ \text{GeV})^2, \Lambda = 0$ at $(\phi, \beta) = (40\,000\ \text{GeV}, \frac{\pi}{4})$.

the remaining logarithm is only $\log(\bar{M}_-^2/\mu^2)$. Since the single logarithm can be suppressed by using the degree of freedom of the renormalization scale μ, the logarithmic perturbation is stable. Such a procedure is explained in the next subsection.

4.2. $m_2^2 \gg -m_1^2$

In this subsection we impose the initial condition at a high-energy scale and gradually decrease the renormalization scale to a scale around $-m_1^2$. Also we suppose that $m_2^2 \gg -m_1^2 > 0$. Setting the following initial condition:

$$\lambda_1 = 0.7,\ \lambda_2 = 0.6,\ \lambda_3 = 0.4,$$
$$m_1^2 = -(200\ \text{GeV})^2,\ m_2^2 = (3000\ \text{GeV})^2,\ \Lambda = 0,$$

at $(\phi, \beta) = (40\,000\ \text{GeV}, \frac{\pi}{4})$, we evaluate the logarithm of the ratio of $\bar{M}_+(t)^2$ to $\bar{M}_-(t)^2$ in Fig. 5. Clearly, the logarithm becomes large as the renormalization scale decreases to the low-energy scale. This indicates the breakdown of the logarithmic perturbative expansion in the low-energy region. For more detail, we evaluate the ratio of $\bar{M}_-(t)^2$ to $\bar{m}_2(t)^2$ in the left panel of Fig. 6. As seen from the left panel in Fig. 6, $\bar{M}_-(t)$ steadily falls with decreasing renormalization scale t. The ratio of $\bar{M}_+(t)^2$ to m_2^2 is calculated in the right panel of Fig. 6. In contrast to the figure on the left, the figure shows that the value of $\bar{M}_+(t)$ is comparable to $\bar{m}_2(t)$ below $t = -1$. Therefore in Fig. 6 we find out that the ratio of $\bar{M}_+(t)^2$ to $\bar{M}_-(t)^2$ increases with lower renormalization scale because $\bar{M}_-(t)$ is smaller than $\bar{m}_2(t)$ while $\bar{M}_+(t)$ is comparable to $\bar{m}_2(t)$.

In order to avoid a large logarithm, we should modify the RG improved effective potential for the low-energy scale. The way to modify the RG improvement is to utilize the decoupling theorem. In the present case, since $\bar{M}_+(t)$ is heavier than $\bar{M}_-(t)$, the field with the mass $\bar{M}_+(t)$ should be decoupled. Moreover, as seen in the right panel of Fig. 6, since $\bar{M}_+(t)$ is comparable to $\bar{m}_2(t)$, we

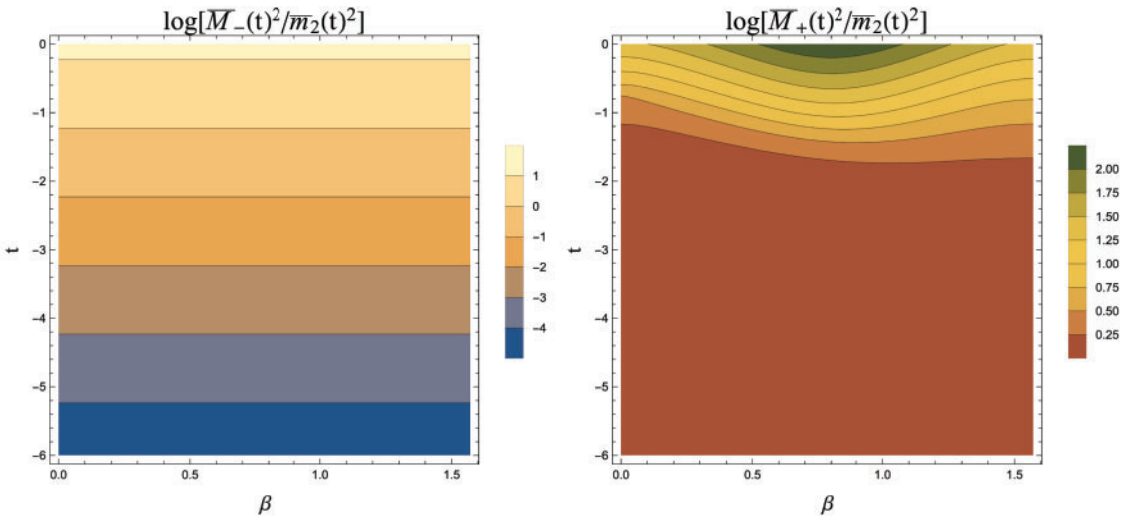

Fig. 6. Left: The logarithm of the ratio of $\bar{M}_-(t)^2$ to $\bar{m}_2(t)^2$ is evaluated in the regions of $\beta \in (0, \frac{\pi}{2})$ and $t \in (-6, 0)$. Right: The logarithm of the ratio of $\bar{M}_+(t)^2$ to $\bar{m}_2(t)^2$ is calculated in the regions of $\beta \in (0, \frac{\pi}{2})$ and $t \in (-6, 0)$.

factor out $\bar{m}_2(t)^2$ from the expression of $\bar{M}_+(t)^2$. Hereafter we omit the bar of the parameters to reduce the bother. To implement it, we expand M_+^2 with respect to $\frac{\phi^2}{m_2^2}$:

$$M_+^2 = m_2^2(1+\Delta),$$
$$\Delta = \left(\frac{\lambda_3}{2}\cos^2\beta + \frac{\lambda_2}{2}\sin^2\beta\right)\frac{\phi^2}{m_2^2} + \lambda_3^2\sin^2\beta\cos^2\beta\left(\frac{\phi^4}{m_2^4}\right).$$

Additionally, we expand the 1-loop effective potential with M_+^2 in terms of $\frac{\phi^2}{m_2^2}$:

$$\begin{aligned} V_+^{(1)} &= \frac{M_+^4}{64\pi^2}\left(\log\left(\frac{M_+^2}{\mu^2}\right) - \frac{3}{2}\right) \\ &= \frac{m_2^4}{64\pi^2}\left(\log\left(\frac{m_2^2}{\mu^2}\right) - \frac{3}{2}\right) + \frac{m_2^2}{64\pi^2}(\lambda_3\cos^2\beta + \lambda_2\sin^2\beta)\left(\log\left(\frac{m_2^2}{\mu^2}\right) - 1\right)\phi^2 \\ &\quad + \frac{1}{64\pi^2}\left\{2\lambda_3^2\sin^2\beta\cos^2\beta\left(\log\left(\frac{m_2^2}{\mu^2}\right) - 1\right) + \frac{1}{4}\left(\lambda_3\cos^2\beta + \lambda_2\sin^2\beta\right)^2\log\left(\frac{m_2^2}{\mu^2}\right)\right\}\phi^4 \\ &\quad + \mathcal{O}\left(\frac{\phi^6}{m_2^2}\right). \end{aligned} \tag{42}$$

In this expression we see that $\log(m_2^2/\mu^2)$ leads to a large logarithm, which is not suppressed with the choice of $\mu^2 = M_-^2$. The concept of the decoupling theorem is to absorb the large logarithm into new parameters by the redefinition of the parameters. Hence we combine the 1-loop effective potential with the tree effective potential and redefine the new parameters to renormalize the large logarithm:

$$V^{(0)} + V_+^{(1)} = \frac{\phi^2}{2}(\tilde{m}_1^2\cos^2\beta + \tilde{m}_2^2\sin^2\beta)$$

$$+\frac{\phi^4}{4!}(\tilde{\lambda}_1\cos^4\beta+\tilde{\lambda}_2\sin^4\beta+6\tilde{\lambda}_3\sin^2\beta\cos^2\beta)+\tilde{\Lambda}, \tag{43}$$

where

$$\tilde{m}_1^2=m_1^2+\frac{\lambda_3 m_2^2}{32\pi^2}\left(\log\left(\frac{m_2^2}{\mu^2}\right)-1\right), \tag{44}$$

$$\tilde{m}_2^2=m_2^2+\frac{\lambda_2 m_2^2}{32\pi^2}\left(\log\left(\frac{m_2^2}{\mu^2}\right)-1\right), \tag{45}$$

$$\tilde{\lambda}_1=\lambda_1+\frac{3\lambda_3^2}{32\pi^2}\log\left(\frac{m_2^2}{\mu^2}\right), \tag{46}$$

$$\tilde{\lambda}_2=\lambda_2+\frac{3\lambda_2^2}{32\pi^2}\log\left(\frac{m_2^2}{\mu^2}\right), \tag{47}$$

$$\tilde{\lambda}_3=\lambda_3+\frac{\lambda_3^2}{8\pi^2}\left(\log\left(\frac{m_2^2}{\mu^2}\right)-1\right)+\frac{\lambda_2\lambda_3}{32\pi^2}\log\left(\frac{m_2^2}{\mu^2}\right), \tag{48}$$

$$\tilde{\Lambda}=\Lambda+\frac{m_2^4}{64\pi^2}\left(\log\left(\frac{m_2^2}{\mu^2}\right)-\frac{3}{2}\right). \tag{49}$$

Note that because there is no contribution to the wavefunction renormalization in this model, the classical background fields do not change:

$$\tilde{\phi}_1=\phi_1, \qquad \tilde{\phi}_2=\phi_2. \tag{50}$$

Since we use the parameters in the low-energy effective theory below $\mu^2=m_2^2$, we derive the β and γ functions for the redefined parameters. To derive them, the RG differential operator in Eq. (22) is rewritten in terms of the new parameters:

$$\begin{aligned}\mathcal{D}=\mu\frac{d}{d\mu}&=(\mathcal{D}\mu)\frac{\partial}{\partial\mu}+\sum_{\tilde{X}}(\mathcal{D}\tilde{X})\frac{\partial}{\partial\tilde{X}}+\sum_{\tilde{Y}}(\mathcal{D}\tilde{Y})\frac{\partial}{\partial\tilde{Y}},\\&=\mu\frac{\partial}{\partial\mu}-\sum_{\tilde{X}}\gamma_{\tilde{X}}\tilde{X}\frac{\partial}{\partial\tilde{X}}+\sum_{\tilde{Y}}\beta_{\tilde{Y}}\frac{\partial}{\partial\tilde{Y}},\end{aligned} \tag{51}$$

where

$$\tilde{X}=\tilde{m}_1^2,\tilde{m}_2^2,\tilde{\Lambda},\tilde{\phi}_1,\tilde{\phi}_2, \qquad \tilde{Y}=\tilde{\lambda}_1,\tilde{\lambda}_2,\tilde{\lambda}_3. \tag{52}$$

Hence we can get the β and γ functions defined by the tilde parameters:

$$\beta_{\tilde{\lambda}_1}=\frac{3\tilde{\lambda}_1^2}{16\pi^2}, \qquad \beta_{\tilde{\lambda}_2}=\frac{3\tilde{\lambda}_3^2}{16\pi^2}, \qquad \beta_{\tilde{\lambda}_3}=\frac{\tilde{\lambda}_1\tilde{\lambda}_3}{16\pi^2}, \tag{53}$$

$$\gamma_{\tilde{m}_1^2}=-\frac{\tilde{\lambda}_1}{16\pi^2}, \qquad \gamma_{\tilde{m}_2^2}=-\frac{\tilde{\lambda}_3\tilde{m}_1^2}{16\pi^2\tilde{m}_2^2}, \qquad \gamma_{\tilde{\Lambda}}=-\frac{\tilde{m}_1^4}{32\pi^2\tilde{\Lambda}} \tag{54}$$

$$\gamma_{\tilde{\phi}_1}=0, \qquad \gamma_{\tilde{\phi}_2}=0. \tag{55}$$

We notice that the effect of the heavy field disappears from the RG equation in Eqs. (53)–(55). In this sense the heavy field is decoupled from theory in the low-energy scale. We can construct the RG

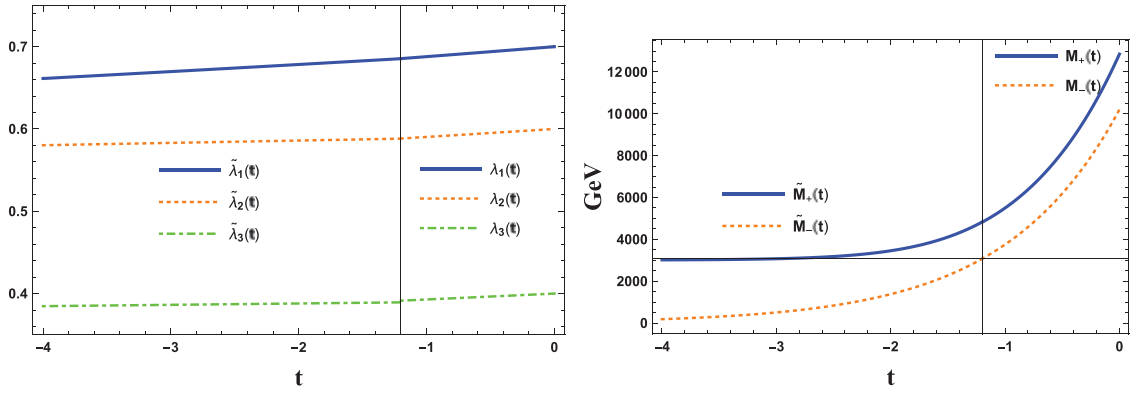

Fig. 7. Left: The running of the quartic coupling constants is solved. The solid blue, dotted orange, and dot-dashed green lines denote the running of λ_1, λ_2, and λ_3, respectively. The vertical line is the decoupling scale with $t = -1.2$. Right: The dependence of the mass eigenvalues (M_-^2, M_+^2) on the renormalization scale t is plotted.

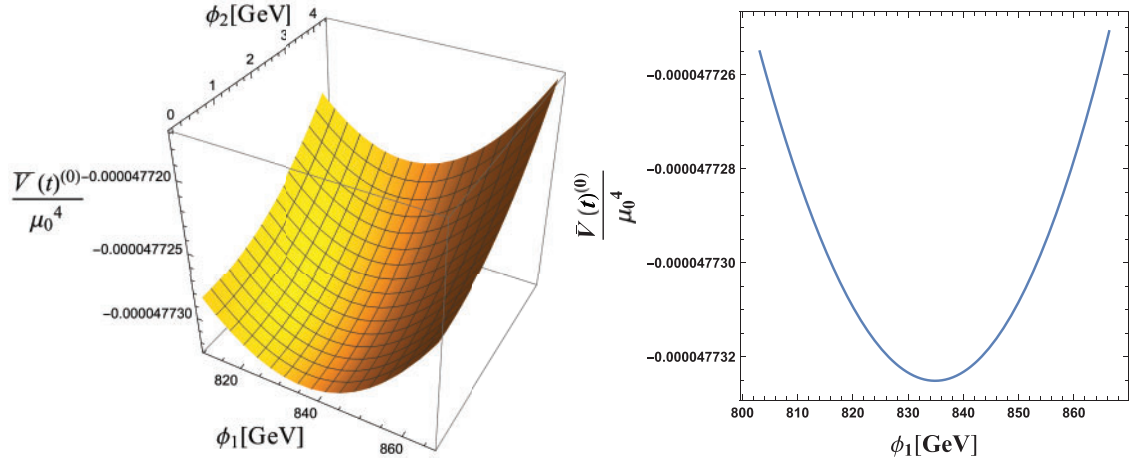

Fig. 8. Left: The 3D plot of the RG improved effective potential is evaluated as a function of (ϕ_1, ϕ_2). Right: The RG improved effective potential is plotted as a function of ϕ_1 with ϕ_2 equal to zero ($\phi_2 = 0$). From the minimum point of the RG improved effective potential, the vacuum expectation value is estimated as $(\beta = 0, t = -3.25)$.

improved effective potential by replacing the parameters with the tilde parameters for the effective potential in Eq. (37).

Let us consider a decoupling point at which the theory is separated into the full theory and the low-energy effective theory. From the left panel of Fig. 6, we see that $\bar{M}_-(t)$ coincides with $\bar{m}_2(t)$ around $t = -1$. Actually, as we can identify the scale as $t = -1.2$ and $\bar{M}_-(t)$ do not vary in the range of $\beta \in (0, \frac{\pi}{2})$, we use $(\beta, t) = (\frac{\pi}{2}, -1.2)$ as a decoupling point. The choice of the decoupling point is valid because the logarithm in Eqs. (44)–(50) is suppressed at the scale when $\bar{M}_-(t)$ becomes equal to $\bar{m}_2(t)$. Now we can solve the RG equations for all the parameters from the initial scale to the low-energy scale. In the left panel of Fig. 7, the quartic coupling constants are solved from $t = 0$ to $t = -4$. We can confirm the slight threshold correction for $\bar{\lambda}_3$. The difference between $\bar{\lambda}_3(t = -1.2)$ and $\bar{\tilde{\lambda}}_3(t = -1.2)$ normalized by $\bar{\lambda}_3(t = -1.2)$ is 0.02. In the right panel of Fig. 7, we run the mass eigenvalues in the same range. The $\bar{\tilde{M}}_-^2$ continues to decrease as the renormalization scale is lowered, while the $\bar{\tilde{M}}_+^2$ converges to about 3000 GeV. In the left panel of Fig. 8, the RG improved

effective potential is plotted as a function of (ϕ_1, ϕ_2). We can find the minimum value of the RG improved effective potential. This point corresponds to the vacuum in the present model. The right panel of Fig. 8 shows the behavior of the RG improved effective potential as a function of ϕ_1 with ϕ_2 equal to zero ($\phi_2 = 0$). From the evaluation of the RG improved effective potential, the vacuum expectation value corresponds to $(\beta, t) = (0, -3.25)$. Substituting them into the mass eigenvalues, we obtain the values of the masses:

$$\bar{\tilde{M}}_-\Big|_{\substack{\beta=0\\ t=-3.25}} = 396 \text{ GeV}, \qquad \bar{\tilde{M}}_+\Big|_{\substack{\beta=0\\ t=-3.25}} = 3007 \text{ GeV}. \tag{56}$$

5. Summary and discussion

In this paper we have studied the RG improvement of the effective potential in a two real scalar system. In Sect. 2 we clarify the logarithmic structure of the effective potential. If we choose $\mu_0^2 e^{2t} = \bar{M}_-^2(t)$ as a renormalization scale and the logarithm of $\bar{s}_2$ is less than $\mathcal{O}(1)$, we find that the RG improved effective potential up to Lth-to-leading log order can be calculated by an L-loop effective potential and $(L+1)$-loop β and γ functions. In Sects. 3 and 4, we solve $\mu_0^2 e^{2t} = \bar{M}_-^2(t)$ with respect to ϕ. This means that ϕ is not a variable of the effective potential but becomes a function of β and t. By using ϕ we can evaluate the mass eigenvalue $\bar{M}_+^2$ and the RG improved effective potential. Then, we examine if the logarithm of the ratio of $\bar{M}_+(t)^2$ to $\bar{M}_-(t)^2$ satisfies $\bar{s}_2 \lesssim \mathcal{O}(\bar{\lambda}_1)$. If it is satisfied, the RG improved effective potential can be obtained as mentioned above. On the other hand, if $\bar{s}_2 > \mathcal{O}(\bar{\lambda}_1)$, the heavy particle should be decoupled. In Sect. 4, we study such a situation. We absorb the large logarithm into the new parameters defined in the low-energy scale and derive the RG equations described in terms of the redefined parameters. The RG improved effective potential can then be constructed in the low-energy region.

There are three features in this method. First, we do not need to change the choice of the renormalization scale beyond the leading log order. This is because, since we analyze the logarithmic structure of the effective potential at any loop order, the choice $\mu_0^2 e^{2t} = \bar{M}_-(t)^2$ is valid for the RG improvement up to arbitrary lth-to-leading log order. Due to this, the ϕ that satisfies $\mu_0^2 e^{2t} = \bar{M}_-^2(t)$ is the same as the one in the leading log order. So we do not need to resolve $\mu_0^2 e^{2t} = \bar{M}_-(t)^2$ with respect to ϕ. Note that the RG equations must be solved in a loop level corresponding to the desired leading log order. Second, we can derive the RG improved effective potential without introducing multiple renormalization scales or a step function by which the heavy particle is automatically decoupled. Third, we can decouple the heavy particle from the theory by expanding the quantum correction to the effective potential with respect to ϕ^2/m^2. If the logarithm $\log\left(\phi^2/m^2\right)$ is absorbed into the parameters in the low-energy scale, we can derive the RG improved effective potential.

Our method can be applied to other multiple scalar models. If multiple scalar fields are introduced in a model, one represents the classical background fields in terms of polar coordinates such as $(\phi_1, \phi_2) = (\phi\cos\beta, \phi\sin\beta)$. With $\mu_0^2 e^{2t} = \bar{M}_{\text{lightest}}(t)^2$ chosen as a renormalization scale, the ϕ corresponding to a radius of the polar coordinate becomes a function of the renormalization scale t and angles in the polar coordinate apart from whether it can be solved analytically. If one reaches this stage, one can implement the calculation of the RG improved effective potential in the same way as in this paper. Finally, since the stability issue and the origin of spontaneous symmetry breaking are investigated through the RG improved effective potential, our work contributes to such studies in a multiple scalar theory.

Acknowledgements

We thank T. Morozumi and Y. Shimizu for reading our manuscript and giving useful comments.

Funding

Open Access funding: SCOAP[3].

Appendix A. β and γ functions in a two real scalar model

In this appendix, we provide the β and γ functions in a two real single scalar model:

$$\begin{aligned}
\beta_{\lambda_1} &= \frac{3}{16\pi^2}(\lambda_1^2 + \lambda_3^2),\\
\beta_{\lambda_2} &= \frac{3}{16\pi^2}(\lambda_2^2 + \lambda_3^2),\\
\beta_{\lambda_3} &= \frac{\lambda_3}{16\pi^2}(\lambda_1 + \lambda_2 + 4\lambda_3),\\
\gamma_{m_1^2} &= -\frac{1}{16\pi^2 m_1^2}(\lambda_1 m_1^2 + \lambda_3 m_2^2),\\
\gamma_{m_2^2} &= -\frac{1}{16\pi^2 m_2^2}(\lambda_2 m_2^2 + \lambda_3 m_1^2),\\
\gamma_{\Lambda} &= -\frac{1}{32\pi^2\Lambda}(m_1^4 + m_2^4)\\
\gamma_{\phi_1} &= 0,\\
\gamma_{\phi_2} &= 0.
\end{aligned}$$

References

[1] J. Elias-Miro, J. R. Espinosa, G. F. Giudice, G. Isidori, A. Riotto, and A. Strumia, Phys. Lett. B **709**, 222 (2012) [arXiv:1112.3022 [hep-ph]] [Search INSPIRE].
[2] G. Degrassi, S. Di Vita, J. Elias-Miró, J. R. Espinosa, G. F. Giudice, G. Isidori, and A. Strumia, J. High Energy Phys. **1208**, 098 (2012) [arXiv:1205.6497 [hep-ph]] [Search INSPIRE].
[3] F. Bezrukov, M. Y. Kalmykov, B. A. Kniehl, and M. Shaposhnikov, J. High Energy Phys. **1210**, 140 (2012) [arXiv:1205.2893 [hep-ph]] [Search INSPIRE].
[4] S. Alekhin, A. Djouadi, and S. Moch, Phys. Lett. B **716**, 214 (2012) [arXiv:1207.0980 [hep-ph]] [Search INSPIRE].
[5] I. Masina, Phys. Rev. D **87**, 053001 (2013) [arXiv:1209.0393 [hep-ph]] [Search INSPIRE].
[6] D. Buttazzo, G. Degrassi, P. P. Giardino, G. F. Giudice, F. Sala, A. Salvio, and A. Strumia, J. High Energy Phys. **1312**, 089 (2013) [arXiv:1307.3536 [hep-ph]] [Search INSPIRE].
[7] S. Coleman and E. Weinberg, Phys. Rev. D **7**, 1888 (1973).
[8] R. Hempfling, Phys. Lett. B **379**, 153 (1996) [arXiv:hep-ph/9604278] [Search INSPIRE].
[9] K. A. Meissner and H. Nicolai, Phys. Lett. B **648**, 312 (2007) [arXiv:hep-th/0612165] [Search INSPIRE].
[10] W.-F. Chang, J. N. Ng, and J. M. S. Wu, Phys. Rev. D **75**, 115016 (2007) [arXiv:hep-ph/0701254] [Search INSPIRE].
[11] R. Foot, A. Kobakhidze, K. L. McDonald, and R. R. Volkas, Phys. Rev. D **77**, 035006 (2008) [arXiv:0709.2750 [hep-ph]] [Search INSPIRE].
[12] S. Iso, N. Okada, and Y. Orikasa, Phys. Lett. B **676**, 81 (2009) [arXiv:0902.4050 [hep-ph]] [Search INSPIRE].
[13] M. Holthausen, M. Lindner, and M. A. Schmidt, Phys. Rev. D **82**, 055002 (2010) [arXiv:0911.0710 [hep-ph]] [Search INSPIRE].

[14] L. Alexander-Nunneley and A. Pilaftsis, J. High Energy Phys. **1009**, 021 (2010) [arXiv:1006.5916 [hep-ph]] [Search INSPIRE].
[15] K. Ishiwata, Phys. Lett. B **710**, 134 (2012) [arXiv:1112.2696 [hep-ph]] [Search INSPIRE].
[16] M. Holthausen, J. Kubo, K. S. Lim, and M. Lindner, J. High Energy Phys. **1312**, 076 (2013) [arXiv:1310.4423 [hep-ph]] [Search INSPIRE].
[17] N. Haba, H. Ishida, N. Kitazawa, and Y. Yamaguchi, Phys. Lett. B **755**, 439 (2016) [arXiv:1512.05061 [hep-ph]] [Search INSPIRE].
[18] K. Endo and Y. Sumino, J. High Energy Phys. **1505**, 030 (2015) [arXiv:1503.02819 [hep-ph]] [Search INSPIRE].
[19] B. Kastening, Phys. Lett. B **283**, 287 (1992).
[20] M. Bando, T. Kugo, N. Maekawa, and H. Nakano, Phys. Lett. B **301**, 83 (1993) [arXiv:hep-ph/9210228] [Search INSPIRE].
[21] C. Ford, D. R. T. Jones, P. W. Stephenson, and M. B. Einhorn, Nucl. Phys. B **395**, 17 (1993) [arXiv:hep-lat/9210033] [Search INSPIRE].
[22] M. B. Einhorn and D. R. Timothy Jones, Nucl. Phys. B **230**, 261 (1984).
[23] C. Ford and C. Wiesendanger, Phys. Rev. D **55**, 2202 (1997) [arXiv:hep-ph/9604392] [Search INSPIRE].
[24] C. Ford and C. Wiesendanger, Phys. Lett. B **398**, 342 (1997) [arXiv:hep-th/9612193] [Search INSPIRE].
[25] M. Bando, T. Kugo, N. Maekawa, and H. Nakano, Prog. Theor. Phys. **90**, 405 (1993) [arXiv:hep-ph/9210229] [Search INSPIRE].
[26] J. A. Casas, V. Di Clemente, and M. Quirós, Nucl. Phys. B **553**, 511 (1999) [arXiv:hep-ph/9809275] [Search INSPIRE].
[27] T. Appelquist and J. Carazzone, Phys. Rev. D **11**, 2856 (1975).
[28] T. G. Steele, Z.-W. Wang, and D. G. C. McKeon, Phys. Rev. D **90**, 105012 (2014) [arXiv:1409.3489 [hep-ph]] [Search INSPIRE].
[29] S. Iso and K. Kawana, J. High Energy Phys. **1803**, 165 (2018) [arXiv:1801.01731 [hep-ph]] [Search INSPIRE].
[30] L. Chataignier, T. Prokopec, M. G. Schmidt, and B. Świeżewska, J. High Energy Phys. **1803**, 014 (2018) [arXiv:1801.05258 [hep-ph]] [Search INSPIRE].
[31] L. Chataignier, T. Prokopec, M. G. Schmidt, and B. Świeżewska, J. High Energy Phys. **1808**, 083 (2018) [arXiv:1805.09292 [hep-ph]] [Search INSPIRE].

参考論文

(1) Precise Discussion of Time-Reversal Asymmetries in B-meson decays.

Takuya Morozumi, Hideaki Okane, Hiroyuki Umeeda

JHEP 1502 (2015) 174

(2) Phenomenological Aspects of Possible Vacua of a Neutrino Flavor Model.

Takuya Morozumi, Hideaki Okane, Hiroki Sakamoto

Yusuke Shimizu, Kenta Takagi, Hiroyuki Umeeda

Chin.Phys. C42 (2018) no.2, 023102

Published for SISSA by Springer

Received: November 11, 2014
Revised: January 13, 2015
Accepted: January 23, 2015
Published: February 26, 2015

Precise discussion of time-reversal asymmetries in B-meson decays

Takuya Morozumi, Hideaki Okane and Hiroyuki Umeeda

Graduate School of Science, Hiroshima University,
Higashi-Hiroshima, Hiroshima 739-8526, Japan
Core of Research for the Energetic Universe, Hiroshima University,
Higashi-Hiroshima, Hiroshima 739-8526, Japan

E-mail: morozumi@hiroshima-u.ac.jp, hideaki-ookane@hiroshima-u.ac.jp, umeeda@theo.phys.sci.hiroshima-u.ac.jp

Abstract: BaBar collaboration announced that they observed time reversal (T) asymmetry through B meson system. In the experiment, time dependencies of two distinctive processes, $B_- \to \bar{B}^0$ and $\bar{B}^0 \to B_-$ ($-$ expresses CP value) are compared with each other. In our study, we examine event number difference of these two processes. In contrast to the BaBar asymmetry, the asymmetry of events number includes the overall normalization difference for rates. Time dependence of the asymmetry is more general and it includes terms absent in one used by BaBar collaboration. Both of the BaBar asymmetry and ours are naively thought to be T-odd since two processes compared are related with flipping time direction. We investigate the time reversal transformation property of our asymmetry. Using our notation, one can see that the asymmetry is not precisely a T-odd quantity, taking into account indirect CP and CPT violation of K meson systems. The effect of ϵ_K is extracted and gives rise to $\mathcal{O}(10^{-3})$ contribution. The introduced parameters are invariant under rephasing of quarks so that the coefficients of our asymmetry are expressed as phase convention independent quantities. Some combinations of the asymmetry enable us to extract parameters for wrong sign decays of B_d meson, CPT violation, etc. We also study the reason why the T-even terms are allowed to contribute to the asymmetry, and find that several conditions are needed for the asymmetry to be a T-odd quantity.

Keywords: B-Physics, CP violation, Kaon Physics

ArXiv ePrint: 1411.2104

doi:10.1007/JHEP02(2015)174

Contents

JHEP02(2015)174

1 Introduction

T-symmetry is fundamental symmetry in particle physics. T-transformation exchanges an initial state and final state, flipping the momentum and spin of particles. If some rate of a process deviates from the rate of time reversed one, it implies T-violation. T-violation is worth pursuit since it reflects the characterized feature of theory.

In EPR correlating B meson system, if one of a pair of B meson is tagged, another side of B meson is determined as orthogonal state with tagged side B meson. In refs. [1]–[3], a method to observe T-violation using B meson system is suggested. Their idea is based on the difference of the time dependencies for two distinctive processes, $B_- \to \bar{B}^0$ and $\bar{B}^0 \to B_-$. In refs. [1]–[3], it is considered to be T-asymmetry since two distinctive processes are related with flipping time direction. Then, BaBar collaboration announced [4]

that they measured non-zero asymmetry and this observation is direct demonstration of T-violation. A review for the BaBar asymmetry and the other T and CPT asymmetries is given in ref. [5].

However, their statement includes ambiguity since we cannot exactly identify B meson such as $\bar{B}^0$ or B_-. In the BaBar experiment, two methods to identify $\bar{B}^0$ and B_- are implemented. The first one is referred as flavor tagging which enables one to identify $\bar{B}^0$, using the semi-leptonic decay mode of B meson. Another one is referred as CP tagging which allows us to identify B_- with final state ψK_S.

In ref. [6], it is pointed out that there exist subtleties in BaBar measurement. The main point in ref. [6] is that they consider a process and its authentically time reversed process. Note that the authentic time reversed process includes inverse decay such like $l^- X \to \bar{B}^0$ and $\psi K_L \to B^0$. Since an authentic time reversed process is experimentally hard to observe, they substitute another process which does not include inverse decays. Therefore, they derive the conditions that BaBar asymmetry is identical with a T-odd quantity, taking into account inverse decays. The derived conditions are (1) the absence of the wrong sign semi-leptonic B meson decays, (2) the absence of the wrong strangeness decays, (3) the absence of CPT violation of the strangeness changing decays. All the conditions are derived by assuming that ψK_S and ψK_L are exact CP eigenstates.

In this paper, we conduct model-independent analysis of an event number asymmetry. Our analysis is extension of the work [6], incorporating the difference of overall constants for the rates that form the asymmetry into calculation. We also include the effect of indirect CP and CPT violation of K meson system. Furthermore, the asymmetry is written in terms of the phase convention independent parameters and one can find contribution of ϵ_K explicitly. Some combinations of the coefficients enable one to constrain model-independent parameters. We also discuss the T-even parts of the asymmetry. One can find that the asymmetry is a T-odd quantity when several conditions are satisfied.

In section 2, we introduce the asymmetry of entangled B meson system. In section 3, we define parameters which are definitively T-odd or T-even and describe the relation between notation in [6] and ours. It is also shown that the parameters are phase convention independent quantities. The method to extract the effect of indirect CP violation in Kaon system is also considered in section 3. In section 4, we write the event number asymmetry in terms of the parameters defined in section 3 and show that the asymmetry consists of not only the T-odd part but also T-even part, using our notation. In sections 4.1–4.3, rather than discussing T-transformation property of the asymmetry, some methods to extract the parameters from the asymmetry are investigated. In section 5, we derive the conditions that T-even parts of the asymmetry vanish and examine the intuitive reason why these conditions are required. The conditions are categorized as two types. The first condition is in regards to B meson states that appear in the processes. Including the effect of indirect CP violation, we evaluate how the first condition is violated, in comparison with the result in [6]. The second condition is in regards to overall constant which forms the asymmetry. We find that the second condition is needed when one takes account of the difference of overall constant of the two rates. Section 6 is devoted to summary of our study.

JHEP02(2015)174

2 Formula for asymmetry of entangled systems

In ref. [6], a formula for the time-dependent decay rate of the entangled $B\bar{B}$ system is derived. When f_1 and f_2 denote the final states of a tagging side and a signal side, respectively, it is written as,

$$\begin{aligned}\Gamma_{(f_1)\perp,f_2} &= e^{-\Gamma(t_1+t_2)}N_{(1)\perp,2}\big[\kappa_{(1)\perp,2}\cosh(y\Gamma t)+\sigma_{(1)\perp,2}\sinh(y\Gamma t)\\ &\quad +\mathcal{C}_{(1)\perp,2}\cos(x\Gamma t)+\mathcal{S}_{(1)\perp,2}\sin(x\Gamma t)\big]\\ &= e^{-\Gamma(t_1+t_2)}N_{(1)\perp,2}\kappa_{(1)\perp,2}\bigg[\cosh(y\Gamma t)+\frac{\sigma_{(1)\perp,2}}{\kappa_{(1)\perp,2}}\sinh(y\Gamma t)\\ &\quad +\frac{\mathcal{C}_{(1)\perp,2}}{\kappa_{(1)\perp,2}}\cos(x\Gamma t)+\frac{\mathcal{S}_{(1)\perp,2}}{\kappa_{(1)\perp,2}}\sin(x\Gamma t)\bigg],\end{aligned} \tag{2.1}$$

where

$$\Gamma=\frac{\Gamma_H+\Gamma_L}{2},\quad x=\frac{m_H-m_L}{\Gamma},\quad y=\frac{\Gamma_H-\Gamma_L}{2\Gamma}. \tag{2.2}$$

The expressions for $N_{(1)\perp,2},\kappa_{(1)\perp,2},\sigma_{(1)\perp,2},\mathcal{C}_{(1)\perp,2}$ and $\mathcal{S}_{(1)\perp,2}$ are given in ref. [6]. For the sake of completeness, we record their expressions in eqs. (A.1)–(A.5). Hereafter, we evaluate an asymmetry including overall factor $N_{(1)\perp,2}\kappa_{(1)\perp,2}$ in eq. (2.1). One obtains a generic formula for the event number asymmetry of the two distinctive sets for final states; (f_1,f_2) versus (f_3,f_4) as,

$$\begin{aligned}A &\equiv \frac{\Gamma_{(f_1)\perp,f_2}-\Gamma_{(f_3)\perp,f_4}}{\Gamma_{(f_1)\perp,f_2}+\Gamma_{(f_3)\perp,f_4}}\\ &= \frac{\left(\frac{1}{\sqrt{N_R}}-\sqrt{N_R}\right)\cosh(y\Gamma t)+\Delta\sigma\sinh(y\Gamma t)+\Delta\mathcal{S}\sin(x\Gamma t)+\Delta\mathcal{C}\cos(x\Gamma t)}{\left(\frac{1}{\sqrt{N_R}}+\sqrt{N_R}\right)\cosh(y\Gamma t)+\hat{\sigma}\sinh(y\Gamma t)+\hat{\mathcal{S}}\sin(x\Gamma t)+\hat{\mathcal{C}}\cos(x\Gamma t)},\end{aligned} \tag{2.3}$$

where

$$N_R\equiv\frac{N_{(3)\perp,4}\kappa_{(3)\perp,4}}{N_{(1)\perp,2}\kappa_{(1)\perp,2}}, \tag{2.4}$$

$$\Delta X\equiv\frac{1}{\sqrt{N_R}}\frac{X_{(1)\perp,2}}{\kappa_{(1)\perp,2}}-\sqrt{N_R}\frac{X_{(3)\perp,4}}{\kappa_{(3)\perp,4}}\qquad(\text{for } X=\sigma,\mathcal{C},\mathcal{S}), \tag{2.5}$$

$$\hat{X}\equiv\frac{1}{\sqrt{N_R}}\frac{X_{(1)\perp,2}}{\kappa_{(1)\perp,2}}+\sqrt{N_R}\frac{X_{(3)\perp,4}}{\kappa_{(3)\perp,4}}\qquad(\text{for } X=\sigma,\mathcal{C},\mathcal{S}). \tag{2.6}$$

In eqs. (2.3)–(2.6), contribution from different overall factors in eq. (2.1) for two processes are taken into account. Taking the limit $N_R\to 1$ and $y\to 0$ in eq. (2.3), one finds an asymmetry whose overall normalization is eliminated, used in [4]. In eq. (2.5)–(2.6), $\Delta\mathcal{S}$ ($\Delta\mathcal{C}$) is equal to ΔS_T^+ (ΔC_T^+) defined in [6] when one takes the limit $N_R\to 1$. In practice, we only need to consider the time difference t within the interval $[0,\tau_B]$ where τ_B is the life time of B meson. Therefore, the approximation $\sinh(y\Gamma t)\simeq y\Gamma t, \cosh(y\Gamma t)\simeq 1$ is valid

JHEP02(2015)174

since $y \ll 1$ for neutral B meson system. Thus, we expand A with respect to $y\Gamma t$,

$$\begin{aligned} A &\simeq \frac{\frac{1}{\sqrt{N_R}} - \sqrt{N_R} + \Delta\sigma y\Gamma t + \Delta\mathcal{S}\sin(x\Gamma t) + \Delta\mathcal{C}\cos(x\Gamma t)}{\frac{1}{\sqrt{N_R}} + \sqrt{N_R} + \hat{\sigma} y\Gamma t + \hat{\mathcal{S}}\sin(x\Gamma t) + \hat{\mathcal{C}}\cos(x\Gamma t)} \\ &= \frac{-\frac{\Delta N_R}{2} + \frac{\Delta\sigma}{2} y\Gamma t + \frac{\Delta\mathcal{S}}{2}\sin(x\Gamma t) + \frac{\Delta\mathcal{C}}{2}\cos(x\Gamma t)}{1 + \frac{\hat{\sigma}}{2} y\Gamma t + \frac{\hat{\mathcal{S}}}{2}\sin(x\Gamma t) + \frac{\hat{\mathcal{C}}}{2}\cos(x\Gamma t)}, \end{aligned} \tag{2.7}$$

where we denote

$$N_R = 1 + \Delta N_R. \tag{2.8}$$

3 Parameter definitions in terms of flavor based state

In this section, we introduce parameters that reveal in the event number asymmetry in eq. (2.7) which we consider. In the processes which form the asymmetry, final states of B-decay are given as the same ones used for the BaBar experiment [4]. Mixing-parameters, p, q, z, p_K, q_K and z_K are defined in appendix B. Eqs. (B.3)–(B.4) lead the transformation property of mixing parameter as, $p \overset{\text{CP or T}}{\leftrightarrows} q$, $p \xrightarrow{\text{CPT}} p$, $q \xrightarrow{\text{CPT}} q$. Similarly, we obtain the transformation property of z as, $z \xrightarrow{\text{CP}} -z, z \xrightarrow{\text{T}} +z, z \xrightarrow{\text{CPT}} -z$. The transformation properties of p_K, q_K and z_K are the same as p, q and z, respectively.

Following [6], we introduce B meson decay amplitudes and inverse decay amplitudes,

$$A_f \equiv \langle f|\,T\,|B^0\rangle\,, \quad \bar{A}_f \equiv \langle f|\,T\,|\bar{B}^0\rangle\,, \quad A_f^{\text{ID}} \equiv \langle B^0|\,T\,|f^T\rangle\,, \quad \bar{A}_f^{\text{ID}} \equiv \langle \bar{B}^0|\,T\,|f^T\rangle\,, \tag{3.1}$$

where f^T is the time reversed state of f, i.e., the state with flipped momenta and spins. Note that A_f ($\bar{A}_f$) and A_f^{ID} ($\bar{A}_f^{\text{ID}}$) are exchanged under T-transformation. Throughout this paper, we introduce the notation G_f, S_f and C_f which are written in terms of amplitude ratio λ_f.

$$G_f = \frac{2\text{Re}\lambda_f}{1+|\lambda_f|^2}, \quad S_f = \frac{2\text{Im}\lambda_f}{1+|\lambda_f|^2}, \quad C_f = \frac{1-|\lambda_f|^2}{1+|\lambda_f|^2}, \tag{3.2}$$

$$G_f^2 + S_f^2 + C_f^2 = 1. \tag{3.3}$$

Using notation (3.1), we can denote following parameters,

$$\lambda_{\psi K_{S,L}} \equiv \frac{q}{p}\frac{\bar{A}_{\psi K_{S,L}}}{A_{\psi K_{S,L}}}\sqrt{\frac{1+\theta_{\psi K_{S,L}}}{1-\theta_{\psi K_{S,L}}}} = \frac{q}{p}\frac{A^{\text{ID}}_{\psi K_{S,L}}}{\bar{A}^{\text{ID}}_{\psi K_{S,L}}}\sqrt{\frac{1-\theta_{\psi K_{S,L}}}{1+\theta_{\psi K_{S,L}}}}, \tag{3.4}$$

$$\theta_{\psi K_{S,L}} = \frac{A_{\psi K_{S,L}}A^{\text{ID}}_{\psi K_{S,L}} - \bar{A}_{\psi K_{S,L}}\bar{A}^{\text{ID}}_{\psi K_{S,L}}}{A_{\psi K_{S,L}}A^{\text{ID}}_{\psi K_{S,L}} + \bar{A}_{\psi K_{S,L}}\bar{A}^{\text{ID}}_{\psi K_{S,L}}}. \tag{3.5}$$

Note that ψK_L and ψK_S are not exact CP eigenstates. $G_{\psi K_{S,L}}, S_{\psi K_{S,L}}$ and $C_{\psi K_{S,L}}$ are parameters written in terms of $\lambda_{\psi K_{S,L}}$. $\theta_{\psi K_{S,L}}, G_{\psi K_{S,L}}, S_{\psi K_{S,L}}$ and $C_{\psi K_{S,L}}$ explicitly appear

JHEP02(2015)174

in coefficients of the master formula (A.1)–(A.5) for the processes. In eq. (3.4), $\lambda_{\psi K_{S,L}}$ is written in terms of the decay amplitude that the final state is the mass eigenstate $\psi K_{S,L}$. $A^{(\mathrm{ID})}_{\psi K_{S,L}}$ and $\bar{A}^{(\mathrm{ID})}_{\psi K_{S,L}}$ can be expanded with respect to amplitudes with a flavor eigenstate as $A^{(\mathrm{ID})}_{\psi K^0}, A^{(\mathrm{ID})}_{\psi \bar{K}^0}, \bar{A}^{(\mathrm{ID})}_{\psi K^0}$ and $\bar{A}^{(\mathrm{ID})}_{\psi \bar{K}^0}$. The expressions of $A^{(\mathrm{ID})}_{\psi K_{S,L}}$ and $\bar{A}^{(\mathrm{ID})}_{\psi K_{S,L}}$ are exhibited in eqs. (B.12)–(B.19). Note that the wrong strangeness decay amplitudes given as,

$$A_{\psi \bar{K}^0}, \quad A^{\mathrm{ID}}_{\psi \bar{K}^0}, \quad \bar{A}_{\psi K^0}, \quad \bar{A}^{\mathrm{ID}}_{\psi K^0}, \tag{3.6}$$

are numerically smaller than the right strangeness decay amplitudes given as,

$$A_{\psi K^0}, \quad A^{\mathrm{ID}}_{\psi K^0}, \quad \bar{A}_{\psi \bar{K}^0}, \quad \bar{A}^{\mathrm{ID}}_{\psi \bar{K}^0}, \tag{3.7}$$

for the standard model. Thus, we ignore terms with higher power of $A^{(\mathrm{ID})}_{\psi \bar{K}^0}$ and $\bar{A}^{(\mathrm{ID})}_{\psi K^0}$. Using eqs. (B.12)–(B.19), we can calculate $\theta_{\psi K_{S,L}}$ as,

$$\theta_{\psi K_S} \simeq \theta_K - z_K, \quad \theta_{\psi K_L} \simeq \theta_K + z_K, \tag{3.8}$$

$$\theta_K = \frac{A_{\psi K^0} A^{\mathrm{ID}}_{\psi K^0} - \bar{A}_{\psi \bar{K}^0} \bar{A}^{\mathrm{ID}}_{\psi \bar{K}^0}}{A_{\psi K^0} A^{\mathrm{ID}}_{\psi K^0} + \bar{A}_{\psi \bar{K}^0} \bar{A}^{\mathrm{ID}}_{\psi \bar{K}^0}}, \tag{3.9}$$

where θ_K expresses CP and CPT violation in right strangeness decays of B meson and it corresponds to $\hat{\theta}_{\psi K}$ of [6]. Note that in [6] indirect CPT violation z_K is not taken into account. When deriving eq. (3.8), we calculated at linear order approximation with respect to z_K, θ_K and wrong strangeness decay amplitudes. Then, we can write $\lambda_{\psi K_{S,L}}$ as,

$$\lambda_{\psi K_S} \simeq \lambda(1 - \Delta\lambda_{\mathrm{wst}}), \quad \lambda_{\psi K_L} \simeq -\lambda(1 + \Delta\lambda_{\mathrm{wst}}), \tag{3.10}$$

$$\lambda \equiv \frac{q}{p}\frac{p_K}{q_K}\frac{\bar{A}_{\psi \bar{K}^0}}{A_{\psi K^0}}\sqrt{\frac{1+\theta_K}{1-\theta_K}} = \frac{q}{p}\frac{p_K}{q_K}\frac{A^{\mathrm{ID}}_{\psi K^0}}{\bar{A}^{\mathrm{ID}}_{\psi \bar{K}^0}}\sqrt{\frac{1-\theta_K}{1+\theta_K}}, \tag{3.11}$$

where $\Delta\lambda_{\mathrm{wst}}$ consists of wrong strangeness decays as,

$$\Delta\lambda_{\mathrm{wst}} = \lambda^{\mathrm{wst}}_{\psi \bar{K}^0} - \bar{\lambda}^{\mathrm{wst}}_{\psi K^0}, \tag{3.12}$$

$$\lambda^{\mathrm{wst}}_{\psi \bar{K}^0} \equiv \frac{p_K}{q_K}\frac{A_{\psi \bar{K}^0}}{A_{\psi K^0}}\sqrt{\frac{1+\theta_{\psi K^0}}{1-\theta_{\psi K^0}}} = \frac{p_K}{q_K}\frac{\bar{A}^{\mathrm{ID}}_{\psi K^0}}{\bar{A}^{\mathrm{ID}}_{\psi \bar{K}^0}}\sqrt{\frac{1-\theta_{\psi K^0}}{1+\theta_{\psi K^0}}}, \tag{3.13}$$

$$\bar{\lambda}^{\mathrm{wst}}_{\psi K^0} \equiv \frac{q_K}{p_K}\frac{\bar{A}_{\psi K^0}}{\bar{A}_{\psi \bar{K}^0}}\sqrt{\frac{1+\bar{\theta}_{\psi \bar{K}^0}}{1-\bar{\theta}_{\psi \bar{K}^0}}} = \frac{q_K}{p_K}\frac{A^{\mathrm{ID}}_{\psi \bar{K}^0}}{A^{\mathrm{ID}}_{\psi K^0}}\sqrt{\frac{1-\bar{\theta}_{\psi \bar{K}^0}}{1+\bar{\theta}_{\psi \bar{K}^0}}}, \tag{3.14}$$

$$\theta_{\psi K^0} \equiv \frac{A_{\psi K^0}\bar{A}^{\mathrm{ID}}_{\psi K^0} - A_{\psi \bar{K}^0}\bar{A}^{\mathrm{ID}}_{\psi \bar{K}^0}}{A_{\psi K^0}\bar{A}^{\mathrm{ID}}_{\psi K^0} + A_{\psi \bar{K}^0}\bar{A}^{\mathrm{ID}}_{\psi \bar{K}^0}}, \quad \bar{\theta}_{\psi \bar{K}^0} \equiv \frac{\bar{A}_{\psi \bar{K}^0}A^{\mathrm{ID}}_{\psi \bar{K}^0} - \bar{A}_{\psi K^0}A^{\mathrm{ID}}_{\psi K^0}}{\bar{A}_{\psi \bar{K}^0}A^{\mathrm{ID}}_{\psi \bar{K}^0} + \bar{A}_{\psi K^0}A^{\mathrm{ID}}_{\psi K^0}}, \tag{3.15}$$

where eq. (3.15) describes CPT violation in wrong strangeness decays. Similar to eq. (3.12), we can define a parameter including wrong sign decay amplitudes as,

$$\hat{\lambda}_{\mathrm{wst}} = \lambda^{\mathrm{wst}}_{\psi \bar{K}^0} + \bar{\lambda}^{\mathrm{wst}}_{\psi K^0}. \tag{3.16}$$

JHEP02(2015)174

Since wrong sign semi-leptonic decay amplitudes and CPT violation, $\theta_{\psi K^0}$ and $\bar{\theta}_{\psi \bar{K}^0}$, are small, we can expand eqs. (3.13), (3.14) as,

$$\lambda^{\rm wst}_{\psi \bar{K}^0} \simeq \frac{p_K}{q_K}\frac{A_{\psi \bar{K}^0}}{A_{\psi K^0}} \simeq \frac{p_K}{q_K}\frac{\bar{A}^{\rm ID}_{\psi K^0}}{\bar{A}^{\rm ID}_{\psi \bar{K}^0}}, \quad \bar{\lambda}^{\rm wst}_{\psi K^0} \simeq \frac{q_K}{p_K}\frac{\bar{A}_{\psi K^0}}{\bar{A}_{\psi \bar{K}^0}} \simeq \frac{q_K}{p_K}\frac{A^{\rm ID}_{\psi \bar{K}^0}}{A^{\rm ID}_{\psi K^0}}. \tag{3.17}$$

Eq. (3.10) indicates that $\lambda_{\psi K_{S,L}}$ is composed of the leading part λ and the sub-leading part suppressed by wrong strangeness decay amplitude. Taking the CPT conserving limit in eq. (3.10), one can obtain the relation in ref. [7]. Note that λ has the definitive transformation property of T, CP and CPT, such as $\lambda \xrightarrow{\rm T} (\lambda)^{-1}$, $\lambda \xrightarrow{\rm CP} (\lambda)^{-1}$, $\lambda \xrightarrow{\rm CPT} \lambda$. One introduces G, S and C analogous to eq. (3.2) by replacing λ_f with λ. They are transformed under T as,

$$G = \frac{2{\rm Re}\lambda}{1+|\lambda|^2} \xrightarrow{\rm T} \frac{2{\rm Re}(1/\lambda)}{1+|1/\lambda|^2} = \frac{2{\rm Re}\lambda^*}{|\lambda|^2+1} = +G, \tag{3.18}$$

$$S = \frac{2{\rm Im}\lambda}{1+|\lambda|^2} \xrightarrow{\rm T} \frac{2{\rm Im}(1/\lambda)}{1+|1/\lambda|^2} = \frac{2{\rm Im}\lambda^*}{|\lambda|^2+1} = -S, \tag{3.19}$$

$$C = \frac{1-|\lambda|^2}{1+|\lambda|^2} \xrightarrow{\rm T} \frac{1-|1/\lambda|^2}{1+|1/\lambda|^2} = \frac{|\lambda|^2-1}{|\lambda|^2+1} = -C. \tag{3.20}$$

The CP transformation property of G, S, C is the same as (3.18)–(3.20). Thus, the CPT transformation property is also determined as $G \xrightarrow{\rm CPT} +G, S \xrightarrow{\rm CPT} +S, C \xrightarrow{\rm CPT} +C$. $|\lambda|$ is close to 1 since deviation of $|q/p|, |p_K/q_K|$ and $|\bar{A}_{\psi \bar{K}^0}/A_{\psi K^0}|$ from 1 is small. Hence, we can find that C is a small parameter. One can also derive the transformation property of eqs. (3.13)–(3.14) such like $\lambda^{\rm wst}_{\psi \bar{K}^0} \xrightarrow{\rm T} \bar{\lambda}^{\rm wst}_{\psi K^0}, \lambda^{\rm wst}_{\psi \bar{K}^0} \xrightarrow{\rm CP} \bar{\lambda}^{\rm wst}_{\psi K^0}$ and $\lambda^{\rm wst}_{\psi \bar{K}^0} \xrightarrow{\rm CPT} \lambda^{\rm wst}_{\psi \bar{K}^0}$. Therefore, the parameters in eqs. (3.12), (3.16) are transformed as,

$$\Delta\lambda_{\rm wst} \xrightarrow{\rm T} -\Delta\lambda_{\rm wst}, \quad \hat{\lambda}_{\rm wst} \xrightarrow{\rm T} \hat{\lambda}_{\rm wst}. \tag{3.21}$$

The CP transformation property of the parameter (3.12), (3.16) is the same as eq. (3.21).

Note that parameters $G_{\psi K_{S,L}}, S_{\psi K_{S,L}}$ and $C_{\psi K_{S,L}}$ are related with the parameters G, S and C as,

$$G_{\psi K_S} \simeq G + S\Delta\lambda^I_{\rm wst}, \qquad G_{\psi K_L} \simeq -\left(G - S\Delta\lambda^I_{\rm wst}\right), \tag{3.22}$$

$$S_{\psi K_S} \simeq S - G\Delta\lambda^I_{\rm wst}, \qquad S_{\psi K_L} \simeq -\left(S + G\Delta\lambda^I_{\rm wst}\right), \tag{3.23}$$

$$C_{\psi K_S} \simeq C + \Delta\lambda^R_{\rm wst}, \qquad C_{\psi K_L} \simeq C - \Delta\lambda^R_{\rm wst}, \tag{3.24}$$

where we use notation for an arbitrary complex number A, $A^R \equiv {\rm Re}A$, $A^I \equiv {\rm Im}A$, throughout this paper. When deriving eqs. (3.22)–(3.24), we ignored higher order terms of C and $\Delta\lambda_{\rm wst}$. Eqs. (3.8), (3.22)–(3.24) lead relations given as,

$$\theta_{\psi K_S} + \theta_{\psi K_L} = 2\theta_K, \qquad \theta_{\psi K_S} - \theta_{\psi K_L} = -2z_K, \tag{3.25}$$

$$G_{\psi K_S} - G_{\psi K_L} = 2G, \qquad S_{\psi K_S} - S_{\psi K_L} = 2S, \qquad C_{\psi K_S} + C_{\psi K_L} = 2C, \tag{3.26}$$

$$G_{\psi K_S} + G_{\psi K_L} = 2S\Delta\lambda^I_{\rm wst}, \quad S_{\psi K_S} + S_{\psi K_L} = -2G\Delta\lambda^I_{\rm wst}, \quad C_{\psi K_S} - C_{\psi K_L} = 2\Delta\lambda^R_{\rm wst}. \tag{3.27}$$

JHEP02(2015)174

Since we have included the effect of indirect CP violation of Kaon system, we show how the correction due to ϵ_K arises. While the expression of G, C and S in eqs. (3.18)–(3.20) is invariant under the arbitrary large rephasing such as $\langle K^0| \to e^{-i\alpha_K} \langle K^0|$ and $\langle \bar{K^0}| \to e^{i\alpha_K} \langle \bar{K^0}|$, the parametrization with $\epsilon_K \ll 1$ allows only the small rephasing $\alpha_K \ll 1$.

$$\frac{p_K}{q_K} = \frac{1+\epsilon_K}{1-\epsilon_K} \simeq 1 + 2\epsilon_K. \tag{3.28}$$

Keeping only the terms which are linear to ϵ_K, G, S and C are expanded as follows,

$$\begin{aligned} G &= G' - 2S'\epsilon_K^I, \\ S &= S' + 2G'\epsilon_K^I, \\ C &= C' - 2\epsilon_K^R, \end{aligned} \tag{3.29}$$

where G', S' and C' are obtained by taking the limit $\frac{p_K}{q_K} \to 1$ in G, S and C. Namely, they are defined by replacing λ with λ' in the expression for G, S and C.

$$\lambda' = \frac{q}{p}\frac{\bar{A}_{\psi\bar{K^0}}}{A_{\psi K^0}}\sqrt{\frac{1+\theta_K}{1-\theta_K}}, \quad C' = \frac{1-|\lambda'|^2}{1+|\lambda'|^2}\,. \tag{3.30}$$

As shown in table (1), (G', S', C') equal to $(\hat{G}_{\psi K}, \hat{S}_{\psi K}, \hat{C}_{\psi K})$ defined in [6] where indirect CP violation ϵ_K is neglected. When one changes the phase convention of states as, the phase of λ' changes as follows,

$$\lambda' \to \lambda' e^{2i\alpha_K}. \tag{3.31}$$

Assuming the phase α_K is small, G', S', and ϵ_K^I change as,

$$\begin{aligned} G' &\to G' - 2\alpha_K S', \\ S' &\to S' + 2\alpha_K G', \\ \epsilon_K^I &\to \epsilon_K^I - \alpha_K, \end{aligned} \tag{3.32}$$

while C' and ϵ_K^R are invariant,

$$C' \to C', \quad \epsilon_K^R \to \epsilon_K^R. \tag{3.33}$$

Hereafter, we expand C in terms of C' and ϵ_K^R as shown in eq. (3.29) and we do not expand S and G since they are invariant under the rephasing. The numerical significance of ϵ_K^R will be discussed in the next section.

We turn to definition for parameters including semi-leptonic decay amplitudes of B meson. In the following, from eq. (3.34) to eq. (3.38), we adopt the notations of [6]. Right sign semi-leptonic decay amplitudes are denoted as,

$$\begin{aligned} A_{l^+} &= \langle l^+ X|T|B^0\rangle\,, & A_{l^+}^{\rm ID} &= \langle B^0|T|(l^+X)^T\rangle\,, \\ \bar{A}_{l^-} &= \langle l^- X|T|\bar{B}^0\rangle\,, & \bar{A}_{l^-}^{\rm ID} &= \langle \bar{B}^0|T|(l^-X)^T\rangle\,. \end{aligned} \tag{3.34}$$

Wrong sign semi-leptonic decay amplitudes are similarly given as,

$$\begin{aligned} A_{l^-} &= \langle l^- X|T|B^0\rangle\,, & A_{l^-}^{\rm ID} &= \langle B^0|T|(l^-X)^T\rangle\,, \\ \bar{A}_{l^+} &= \langle l^+ X|T|\bar{B}^0\rangle\,, & \bar{A}_{l^+}^{\rm ID} &= \langle \bar{B}^0|T|(l^+X)^T\rangle\,. \end{aligned} \tag{3.35}$$

JHEP02(2015)174

Notation of this paper	Notation of [6]	Notatin of [6]	Notation of this paper
$\lambda_{\psi K_S}$	$\frac{p_K}{q_K}\lambda_{\psi K_1}$	$\lambda_{\psi K_1}$	$\lambda'(1-\Delta\lambda_{wst})$
$\lambda_{\psi K_L}$	$\frac{p_K}{q_K}\lambda_{\psi K_2}$	$\lambda_{\psi K_2}$	$-\lambda'(1+\Delta\lambda_{wst})$
$G_{\psi K_S}$	$G_{\psi K_1}-2S_{\psi K_1}\epsilon_K^I$	$\hat{G}_{\psi K}=\frac{G_{\psi K_1}-G_{\psi K_2}}{2}$	G'
$S_{\psi K_S}$	$S_{\psi K_1}+2G_{\psi K_1}\epsilon_K^I$	$\hat{S}_{\psi K}=\frac{S_{\psi K_1}-S_{\psi K_2}}{2}$	S'
$C_{\psi K_S}$	$C_{\psi K_1}-2\epsilon_K^R$	$\hat{C}_{\psi K}=\frac{C_{\psi K_1}+C_{\psi K_2}}{2}$	C'
$G_{\psi K_L}$	$G_{\psi K_2}-2S_{\psi K_2}\epsilon_K^I$	$\Delta G_{\psi K}=\frac{G_{\psi K_1}+G_{\psi K_2}}{2}$	$S'\Delta\lambda_{wst}^I$
$S_{\psi K_L}$	$S_{\psi K_2}+2G_{\psi K_2}\epsilon_K^I$	$\Delta S_{\psi K}=\frac{S_{\psi K_1}+S_{\psi K_2}}{2}$	$-G'\Delta\lambda_{wst}^I$
$C_{\psi K_L}$	$C_{\psi K_2}-2\epsilon_K^R$	$\Delta C_{\psi K}=\frac{C_{\psi K_1}-C_{\psi K_2}}{2}$	$\Delta\lambda_{wst}^R$
θ_K	$\hat{\theta}_{\psi K}=\frac{\theta_{\psi K1}+\theta_{\psi K2}}{2}$	$\Delta\theta_{\psi K}=\frac{\theta_{\psi K1}-\theta_{\psi K2}}{2}$	0

Table 1. The correspondence of parameters in this paper and those of [6]. In this paper, ψK_1 corresponds to ψK_S and ψK_2 corresponds to ψK_L respectively in [6] where indirect CP violation parameter ϵ_K is neglected. In this paper, ψK_L and ψK_S include the effect of indirect CP and CPT violation. The first column shows the quantities defined for mass eigenstates (K_L, K_S). From the third row to the eighth row in the second column, the quantities in the first column are expanded up to the first order of ϵ_K and are written in terms of the quantities for CP eigenstates K_1, K_2. In the third column and in the fourth column, we show how $(\hat{G}_{\psi K}, \hat{S}_{\psi K}, \hat{C}_{\psi K})$ and $(\Delta G_{\psi K}, \Delta S_{\psi K}, \Delta C_{\psi K})$ in [6] are related to $(G', S', C', \Delta\lambda_{wst})$ defined in this paper. About CPT violation parameter of strangeness changing decay, one can show $\theta_{\psi K1} = \theta_{\psi K2} = \theta_K$. Therefore $\hat{\theta}_{\psi K} = \theta_K$ and $\Delta\theta_{\psi K} = 0$.

For the case of the standard model, wrong sign semi-leptonic decay amplitudes are smaller than right sign decay amplitudes. Thus, we ignore higher powers of wrong sign decay amplitudes than linear order. We define parameters including semi-leptonic decay amplitudes as,

$$\lambda_{l^+} \equiv \frac{q}{p}\frac{\bar{A}_{l^+}}{A_{l^+}}\sqrt{\frac{1+\theta_{l^+}}{1-\theta_{l^+}}} = \frac{q}{p}\frac{A^{\rm ID}_{l^-}}{\bar{A}^{\rm ID}_{l^-}}\sqrt{\frac{1-\theta_{l^+}}{1+\theta_{l^+}}}, \quad \theta_{l^+} = \frac{A_{l^+}A^{\rm ID}_{l^-} - \bar{A}_{l^+}\bar{A}^{\rm ID}_{l^-}}{A_{l^+}A^{\rm ID}_{l^-} + \bar{A}_{l^+}\bar{A}^{\rm ID}_{l^-}}, \tag{3.36}$$

$$\lambda_{l^-} \equiv \frac{q}{p}\frac{\bar{A}_{l^-}}{A_{l^-}}\sqrt{\frac{1+\theta_{l^-}}{1-\theta_{l^-}}} = \frac{q}{p}\frac{A^{\rm ID}_{l^+}}{\bar{A}^{\rm ID}_{l^+}}\sqrt{\frac{1-\theta_{l^-}}{1+\theta_{l^-}}}, \quad \theta_{l^-} = \frac{A_{l^-}A^{\rm ID}_{l^+} - \bar{A}_{l^-}\bar{A}^{\rm ID}_{l^+}}{A_{l^-}A^{\rm ID}_{l^+} - \bar{A}_{l^-}\bar{A}^{\rm ID}_{l^+}}, \tag{3.37}$$

where $\theta_{l^\pm}$ expresses CPT violation in semi-leptonic decays of B meson. One can find the transformation law such like $\lambda_{l^+} \xrightarrow{T} (\lambda_{l^-})^{-1}$, $\lambda_{l^+} \xrightarrow{CP} (\lambda_{l^-})^{-1}$, $\lambda_{l^+} \xrightarrow{CPT} \lambda_{l^+}$ by its definition (3.36)–(3.37). We assume that CPT violating parameter $\theta_{l^\pm}$ is small. At linear order approximation of $\theta_{l^\pm}$ and wrong sign semi-leptonic decay amplitudes, we obtain,

$$\lambda_{l^+} \simeq \frac{q}{p}\frac{\bar{A}_{l^+}}{A_{l^+}} \simeq \frac{q}{p}\frac{A^{\rm ID}_{l^-}}{\bar{A}^{\rm ID}_{l^-}}, \quad \lambda^{-1}_{l^-} \simeq \frac{p}{q}\frac{A_{l^-}}{\bar{A}_{l^-}} \simeq \frac{p}{q}\frac{\bar{A}^{\rm ID}_{l^+}}{A^{\rm ID}_{l^+}}, \tag{3.38}$$

where we can see that contribution of $\theta_{l^\pm}$ approximately vanishes in eq. (3.38). Following ref. [6], we also define $G_{l^\pm}, S_{l^\pm}$ and $C_{l^\pm}$ analogous to eq. (3.2) by replacing λ_f with $\lambda_{l^\pm}$. The parameters $G_{l^\pm}, S_{l^\pm}$ and $C_{l^\pm}$ explicitly appear in coefficients of master formula (A.1)–(A.5)

JHEP02(2015)174

for the processes in which the final states are given as $l^{\pm}X$. Eq. (3.38) gives approximate expressions for $G_{l^{\pm}}, S_{l^{\pm}}$ and $C_{l^{\pm}}$ as,

$$G_{l^+} = \frac{2\mathrm{Re}\lambda_{l^+}}{1+|\lambda_{l^+}|^2} \simeq 2\mathrm{Re}\lambda_{l^+}, \quad G_{l^-} = \frac{2\mathrm{Re}\lambda_{l^-}}{1+|\lambda_{l^-}|^2} \simeq 2\mathrm{Re}(\lambda_{l^-}^{-1}), \quad C_{l^{\pm}} = \frac{1-|\lambda_{l^{\pm}}|^2}{1+|\lambda_{l^{\pm}}|^2} \simeq \pm 1,$$
$$S_{l^+} = \frac{2\mathrm{Im}\lambda_{l^+}}{1+|\lambda_{l^+}|^2} \simeq 2\mathrm{Im}\lambda_{l^+}, \quad S_{l^-} = \frac{2\mathrm{Im}\lambda_{l^-}}{1+|\lambda_{l^-}|^2} \simeq -2\mathrm{Im}(\lambda_{l^-}^{-1}). \tag{3.39}$$

Note that eq. (3.39) implies that $G_{l^{\pm}}$ and $S_{l^{\pm}}$ are small numbers since λ_{l^+} and $\lambda_{l^-}^{-1}$ are suppressed. We can find the relations,

$$G_{l^+} + G_{l^-} = 2\hat{\lambda}_l^R, \qquad S_{l^+} - S_{l^-} = 2\hat{\lambda}_l^I, \tag{3.40}$$
$$G_{l^+} - G_{l^-} = 2\Delta\lambda_l^R, \qquad S_{l^+} + S_{l^-} = 2\Delta\lambda_l^I, \tag{3.41}$$

where $\hat{\lambda}_l$ and $\Delta\lambda_l$ are defined as,

$$\hat{\lambda}_l \equiv \lambda_{l^+} + \lambda_{l^-}^{-1}, \quad \Delta\lambda_l \equiv \lambda_{l^+} - \lambda_{l^-}^{-1}. \tag{3.42}$$

They transform definitively under CP, T and CPT. One obtains the transformation property of T as,

$$\hat{\lambda}_l \xrightarrow{\mathrm{T}} (\lambda_{l^-})^{-1} + \lambda_{l^+} = +\hat{\lambda}_l, \quad \Delta\lambda_l \xrightarrow{\mathrm{T}} (\lambda_{l^-})^{-1} - \lambda_{l^+} = -\Delta\lambda_l. \tag{3.43}$$

The CP transformation property of $\hat{\lambda}_l$ and $\Delta\lambda_l$ is the same as (3.43). Hence, the CPT transformation property of $\hat{\lambda}_l$ and $\Delta\lambda_l$ is also determined as $\hat{\lambda}_l \xrightarrow{\mathrm{CPT}} \hat{\lambda}_l, \Delta\lambda_l \xrightarrow{\mathrm{CPT}} \Delta\lambda_l$. Eqs. (3.22)–(3.24), (3.40)–(3.41) enable one to write down the asymmetry in eq. (2.3) for the BaBar experiment in terms of parameters which are exactly T-odd or T-even. Similarly, one defines,

$$R_M \equiv \frac{|p|^2-|q|^2}{|p|^2+|q|^2}, \quad \xi_l \equiv \frac{\bar{A}_{l^-}A_{l^+}^{\mathrm{ID}} - A_{l^+}\bar{A}_{l^-}^{\mathrm{ID}}}{\bar{A}_{l^-}A_{l^+}^{\mathrm{ID}} + A_{l^+}\bar{A}_{l^-}^{\mathrm{ID}}}, \quad C_{\xi}^l, \equiv \frac{1-|\lambda_{\xi}^l|^2}{1+|\lambda_{\xi}^l|^2}, \tag{3.44}$$

$$\lambda_{\xi}^l \equiv \frac{A_{l^+}}{\bar{A}_{l^-}}\sqrt{\frac{1+\xi_l}{1-\xi_l}} = \frac{A_{l^+}^{\mathrm{ID}}}{\bar{A}_{l^-}^{\mathrm{ID}}}\sqrt{\frac{1-\xi_l}{1+\xi_l}}. \tag{3.45}$$

In eq. (3.44), R_M expresses mixing-induced CP and T violation for B meson system [6] and is a small number. As for newly introduced parameters, ξ_l implies CP and T violation in right sign semi-leptonic decays and we also assume ξ_l is a small number. The expression of λ_{ξ}^l (3.45) includes right sign semi-leptonic decay amplitude ratio and we assume $|A_{l^+}/\bar{A}_{l^-}| \simeq 1$. Therefore, C_{ξ}^l is a small number compared with $\mathcal{O}(1)$. The parameters defined in eq. (3.44) also appear in the asymmetry in eq. (2.3).

Hereafter, we describe some significant points of the parameters defined in this section. Note that the parameters given as,

$$S, C, G, \theta_K, R_M, z, z_K, \hat{\lambda}_l, \Delta\lambda_l, \xi_l, C_{\xi}^l, \hat{\lambda}_{\mathrm{wst}} \text{ and } \Delta\lambda_{\mathrm{wst}}, \tag{3.46}$$

have definitive transformation properties exhibited in table 2. In the processes which we consider, $K_{S,L}$ is included as a final state, and the effect of mixing induced T and CP

JHEP02(2015)174

	S	C	G	θ_K	R_M	z	z_K	$\hat{\lambda}_l$	$\Delta\lambda_l$	ξ_l	C^l_ξ	$\hat{\lambda}_{\rm wst}$	$\Delta\lambda_{\rm wst}$
T	$-$	$-$	$+$	$+$	$-$	$+$	$+$	$+$	$-$	$-$	$+$	$+$	$-$
CP	$-$	$-$	$+$	$-$	$-$	$-$	$-$	$+$	$-$	$-$	$-$	$+$	$-$
CPT	$+$	$+$	$+$	$-$	$+$	$-$	$-$	$+$	$+$	$+$	$-$	$+$	$+$

Table 2. Transformation property of the parameters definitively transformed under T, CP and CPT.

	p/q	p_K/q_K	$\theta_{\psi K^0}$	θ_{l+}	λ	$\lambda^{\rm wst}_{\psi\bar{K}^0}$	λ_{l+}	λ^l_ξ
T	q/p	q_K/p_K	$-\bar{\theta}_{\psi\bar{K}^0}$	θ_{l-}	$(\lambda)^{-1}$	$\bar{\lambda}^{\rm wst}_{\psi K^0}$	$(\lambda_{l-})^{-1}$	λ^l_ξ
CP	q/p	q_K/p_K	$\bar{\theta}_{\psi\bar{K}^0}$	$-\theta_{l-}$	$(\lambda)^{-1}$	$\bar{\lambda}^{\rm wst}_{\psi K^0}$	$(\lambda_{l-})^{-1}$	$(\lambda^l_\xi)^{-1}$
CPT	p/q	p_K/q_K	$-\theta_{\psi K^0}$	$-\theta_{l+}$	λ	$\lambda^{\rm wst}_{\psi\bar{K}^0}$	λ_{l+}	$(\lambda^l_\xi)^{-1}$

Table 3. Transformation property of the parameters devoted to keep the definitive transformation property of the parameters in table 2.

violation, p_K/q_K, appears in the expressions of $G, S, C, \hat{\lambda}_{\rm wst}$ and $\Delta\lambda_{\rm wst}$. Mixing-induced CP and CPT violation in K meson system, z_K, reveals in the asymmetry as well. In the next section, the asymmetry is written in terms of parameters (3.46) and it can be explicitly separated as T-odd parts and T-even parts.

The parameters defined as,

$$p/q, p_K/q_K, \theta_{\psi K^0}, \bar{\theta}_{\psi\bar{K}^0}, \theta_{l^\pm}, \lambda, \lambda^{\rm wst}_{\psi\bar{K}^0}, \bar{\lambda}^{\rm wst}_{\psi K^0}, \lambda_{l^\pm}, \text{ and } \lambda^l_\xi, \tag{3.47}$$

are dedicated to keep the definitive transformation property of parameters that reveal in table 2. The transformation property of the parameters (3.47) is exhibited in table 3.

The parameters given as,

$$\theta_{\psi K^0}, \bar{\theta}_{\psi\bar{K}^0}, \theta_{l^\pm}, C, \theta_K, R_M, z, z_K, \hat{\lambda}_l, \Delta\lambda_l, \xi_l, C^l_\xi, \hat{\lambda}_{\rm wst} \text{ and } \Delta\lambda_{\rm wst}, \tag{3.48}$$

are small numbers, and our calculation is based on linear order approximation with respect to the parameters (3.48) throughout this paper.

4 Time dependent asymmetry including the overall constants

In this section, we apply the event number asymmetry defined in eq. (2.7) to processes for B-meson decays. One should be aware of that the asymmetry considered in this paper includes the effect of different normalization for two rates; non-zero value of ΔN_R defined in eq. (2.8). As the BaBar asymmetry investigated in [4], we also assign f_1, f_2, f_3, f_4 with $\psi K_L, l^- X$, $l^+ X, \psi K_S$, respectively. We call this process as I. We also consider the other three processes which can be obtained by interchanging $l^- X$ with $l^+ X$ and ψK_S with ψK_L

JHEP02(2015)174

in the process I. Therefore we identify the four processes as,

$$\begin{aligned}
\text{(I)} \quad & (f_1, f_2, f_3, f_4) = \left(\psi K_L, l^- X, l^+ X, \psi K_S\right), \\
\text{(II)} \quad & (f_1, f_2, f_3, f_4) = \left(\psi K_S, l^- X, l^+ X, \psi K_L\right), \\
\text{(III)} \quad & (f_1, f_2, f_3, f_4) = \left(\psi K_L, l^+ X, l^- X, \psi K_S\right), \\
\text{(IV)} \quad & (f_1, f_2, f_3, f_4) = \left(\psi K_S, l^+ X, l^- X, \psi K_L\right).
\end{aligned} \tag{4.1}$$

For all the processes which we consider, we can find $\Delta N_R, \Delta\sigma, y\Gamma t, \Delta\mathcal{C}, \hat{\mathcal{S}}, \hat{\mathcal{C}}$ are small numbers compared with $\mathcal{O}(1)$. Expanding eq. (2.7) with respect to the small parameters, one obtains the asymmetry at linear order approximation,

$$\begin{aligned}
A \simeq\ & R_T + C_T \cos(x\Gamma t) + S_T \sin(x\Gamma t) \\
& + B_T \sin^2(x\Gamma t) + D_T \sin(x\Gamma t)\cos(x\Gamma t) + E_T (y\Gamma t)\sin(x\Gamma t),
\end{aligned} \tag{4.2}$$

where,

$$R_T = -\frac{\Delta N_R}{2} + \frac{\Delta\sigma}{2} y\Gamma t \simeq -\frac{\Delta N_R}{2}, \tag{4.3}$$

$$C_T = \frac{\Delta\mathcal{C}}{2}, \quad S_T = \frac{\Delta\mathcal{S}}{2}, \tag{4.4}$$

$$B_T = -\frac{\Delta\mathcal{S}}{4}\hat{S}, \quad D_T = -\frac{\Delta\mathcal{S}}{4}\hat{C}, \tag{4.5}$$

$$E_T = -\frac{\Delta\mathcal{S}}{4}\hat{\sigma}. \tag{4.6}$$

We ignore $\Delta\sigma y$ in eqs. (4.3)–(4.6). $\hat{\sigma}$ and $\Delta\mathcal{S}$ are $\mathcal{O}(1)$ parameters and $\hat{\sigma}y$ gives rise to small contribution. The model independent parametrization in eq. (4.2) without the last term can be found in [6]. In each process, we compute the asymmetry and the coefficients $(R_T, C_T, S_T, B_T, D_T, E_T)$. We label suffix I $\sim$ IV on the quantities corresponding to each process to distinguish them. Below and in table 4, we show the asymmetry and the coefficients for the process I. For the other processes, we show them in tables 5–7. We first investigate ΔN_R in eq. (2.8) for the process I. With eq. (D.4), one obtains,

$$\Delta N_R^I = 2\left[-Sz^I + R_M + \hat{\lambda}^R_{\rm wst} - G\hat{\lambda}^R_l - C^l_\xi - \xi^R_l\right]. \tag{4.7}$$

With eq. (4.7) and eqs. (D.5)–(D.9), one can also derive the coefficients in the asymmetry,

$$R_T^I = -\frac{\Delta N_R^I}{2} = Sz^I - R_M - \hat{\lambda}^R_{\rm wst} + G\hat{\lambda}^R_l + C^l_\xi + \xi^R_l, \tag{4.8}$$

$$C_T^I = \frac{\Delta\mathcal{C}^I}{2} = C - Sz^I + \theta^R_K + S\Delta\lambda^I_l = C' - 2\epsilon^R_K - Sz^I + \theta^R_K + S\Delta\lambda^I_l, \tag{4.9}$$

$$S_T^I = \frac{\Delta\mathcal{S}^I}{2} = -[S(1 - Gz^R) - G\theta^I_K + GS\Delta\lambda^R_l], \tag{4.10}$$

$$\begin{aligned}
B_T^I &= -\frac{\Delta\mathcal{S}^I}{4}\hat{S}^I \simeq \frac{S}{2}\hat{S}^I \\
&= S[G(z^I_K - \Delta\lambda^I_{\rm wst}) - z^I + SR_M + S\hat{\lambda}^R_{\rm wst} - SC^l_\xi - S\xi^R_l],
\end{aligned} \tag{4.11}$$

$$D_T^I = -\frac{\Delta\mathcal{S}^I}{4}\hat{C}^I \simeq \frac{S}{2}\hat{C}^I = S[z^R_K - \Delta\lambda^R_{\rm wst} - Gz^R - S\hat{\lambda^I_l}], \tag{4.12}$$

$$E_T^I = -\frac{\Delta\mathcal{S}^I}{4}\hat{\sigma}^I \simeq GS. \tag{4.13}$$

JHEP02(2015)174

Note that C' and ϵ_K^R are phase convention independent parameters due to definition of C'. Therefore, we state that all of eqs. (4.8)–(4.13) are expressed as phase convention independent parameters. In eq. (4.9), effect of indirect CP violation in K meson system explicitly appears and gives rise to $\mathcal{O}(10^{-3})$ contribution to C_T^I. Assuming $|q/p|-1, |\bar{A}_{\psi\bar{K}^0}/A_{\psi K^0}|-1$, $|1+\theta_K|-1$ are small numbers, we can expand C' in eq. (3.30) as,

$$C' \simeq 2 - \left|\frac{q}{p}\right| - \left|\frac{\bar{A}_{\psi\bar{K}^0}}{A_{\psi K^0}}\right| - \theta_K^R, \quad \left|\frac{q}{p}\right| \simeq 1 - \frac{1}{2}\mathrm{Im}\left(\frac{\Gamma_{12}^d}{M_{12}^d}\right). \tag{4.14}$$

A theoretical prediction for the imaginary part of Γ_{12}^d/M_{12}^d is calculated [8], and it shows $\mathrm{Im}(\Gamma_{12}^d/M_{12}^d) \sim \mathcal{O}(10^{-4})$. Direct CP violation in $B_d^0 \to \psi K^0$ is $1 - |\bar{A}_{\psi\bar{K}^0}/A_{\psi K^0}| \simeq \mathcal{O}(10^{-3})$ [9]–[10]. Hence, $\epsilon_K^R, |\bar{A}_{\psi\bar{K}^0}/A_{\psi K^0}| \sim \mathcal{O}(10^{-3})$ are dominant in C_T^I, if CPT violations and the wrong sign decay in $B \to lX$ in eq. (4.9) are also negligible.

If R_T, C_T, S_T, B_T and D_T were genuine T-odd quantities, they would vanish in the limit of T-symmetry. In other words, if there are non-vanishing contributions in the limit of T-symmetry, R_T, C_T, S_T, B_T and D_T are not T-odd quantities. From eqs. (4.8)–(4.13), we find the T-even contributions. Some of them do not vanish in the limit of T-symmetry and they include $C_\xi^l, \hat{\lambda}_{\mathrm{wst}}^R\theta_K^R$, etc. The others are quadratic with respect to T-odd quantities and they vanish in the limit of T-symmetry. They include $S\Delta\lambda_l^I, S\Delta\lambda_{\mathrm{wst}}^R, S^2\hat{\lambda}_l^I$, etc.

Now we study condition that the asymmetry becomes a T-odd quantity. The following equations are needed for T-even terms in each coefficient to vanish,

$$\hat{\lambda}_{\mathrm{wst}}^R = 0, \quad G\hat{\lambda}_l^R = 0, \quad C_\xi^l = 0 \to R_T^I : \mathrm{T-odd}, \tag{4.15}$$

$$\theta_K^R = 0, \quad S\Delta\lambda_l^I = 0 \to C_T^I : \mathrm{T-odd}, \tag{4.16}$$

$$G\theta_K^I = 0, \quad GS\Delta\lambda_l^R = 0 \to S_T^I : \mathrm{T-odd}, \tag{4.17}$$

$$SG\Delta\lambda_{\mathrm{wst}}^I = 0, \quad S^2\hat{\lambda}_{\mathrm{wst}}^R = 0, \quad S^2C_\xi^l = 0 \to B_T^I : \mathrm{T-odd}, \tag{4.18}$$

$$S\Delta\lambda_{\mathrm{wst}}^R = 0, \quad S^2\hat{\lambda}_l^I = 0 \to D_T^I : \mathrm{T-odd}. \tag{4.19}$$

When the real part and imaginary part of λ do not vanish, both G and S are non-zero and the conditions that all the eqs. (4.15)–(4.19) are satisfied become,

$$\theta_K = \Delta\lambda_{\mathrm{wst}} = \Delta\lambda_l = \hat{\lambda}_l = \hat{\lambda}_{\mathrm{wst}}^R = C_\xi^l = 0. \tag{4.20}$$

The conditions except $C_\xi^l = 0$ agree with ones obtained in [6]. The additional condition is required since we take account of the overall constants in the asymmetry.

In the first column of table 4, we show how each coefficient of the asymmetry in eq. (4.2) depends on T-odd combination of the parameters and in the other columns we show the dependence on T-even combination of the parameters. As for T-even contribution, we identify the sources of T-even contribution to the coefficients. In the second column, the contribution of θ_K which is CP and CPT violation in right strangeness decays is shown. In the third column, the contribution of C_ξ^l which is CP and CPT violation in the right sign semi-leptonic decays is shown. In the fourth and the fifth column, T-even contribution from the wrong strangeness decays and the wrong sign semi-leptonic decays are shown, respectively. In tables 5–7, we show the coefficients for the processes (II)–(IV). In appendix E, we show a rule useful for deriving them.

JHEP02(2015)174

	T-odd terms	$\theta_K \neq 0$	$C_\xi^l \neq 0$	$A_{\psi\bar{K}^0} \neq 0, \bar{A}_{\psi K^0} \neq 0$	$\bar{A}_{l^+} \neq 0, A_{l^-} \neq 0$
R_T^I	$Sz^I - R_M + \xi_l^R$	0	C_ξ^l	$-\hat{\lambda}_{\rm wst}^R$	$G\hat{\lambda}_l^R$
C_T^I	$C - Sz^I$	θ_K^R	0	0	$S\Delta\lambda_l^I$
S_T^I	$-S\left[1 - Gz^R\right]$	$G\theta_K^I$	0	0	$-GS\Delta\lambda_l^R$
B_T^I	$S\left[Gz_K^I - z^I + SR_M - S\xi_l^R\right]$	0	$-S^2C_\xi^l$	$S^2\hat{\lambda}_{\rm wst}^R - SG\Delta\lambda_{\rm wst}^I$	0
D_T^I	$S\left[z_K^R - Gz^R\right]$	0	0	$-S\Delta\lambda_{\rm wst}^R$	$-S^2\hat{\lambda}_l^I$
E_T^I	GS	0	0	0	0

Table 4. The coefficients of the asymmetry for the process I with the final state $(f_1, f_2, f_3, f_4) = (\psi K_L, l^- X, l^+ X, \psi K_S)$ and the sources which give rise to the non-vanishing contribution to the asymmetry. The sources of the first column corresponds to T-odd terms and the other correspond to T-even terms.

	T-odd terms	$\theta_K \neq 0$	$C_\xi^l \neq 0$	$A_{\psi\bar{K}^0} \neq 0, \bar{A}_{\psi K^0} \neq 0$	$\bar{A}_{l^+} \neq 0, A_{l^-} \neq 0$
R_T^{II}	$-Sz^I - R_M + \xi_l^R$	0	C_ξ^l	$\hat{\lambda}_{\rm wst}^R$	$-G\hat{\lambda}_l^R$
C_T^{II}	$C + Sz^I$	θ_K^R	0	0	$-S\Delta\lambda_l^I$
S_T^{II}	$S\left[1 + Gz^R\right]$	$-G\theta_K^I$	0	0	$-GS\Delta\lambda_l^R$
B_T^{II}	$-S\left[Gz_K^I - z^I - SR_M + S\xi_l^R\right]$	0	$-S^2C_\xi^l$	$-S^2\hat{\lambda}_{\rm wst}^R + SG\Delta\lambda_{\rm wst}^I$	0
D_T^{II}	$S\left[z_K^R - Gz^R\right]$	0	0	$-S\Delta\lambda_{\rm wst}^R$	$-S^2\hat{\lambda}_l^I$
E_T^{II}	GS	0	0	0	0

Table 5. The coefficients of the asymmetry for the process II with the final state $(f_1, f_2, f_3, f_4) = (\psi K_S, l^- X, l^+ X, \psi K_L)$ and the sources which give rise to the non-vanishing contribution to the asymmetry. The sources of the first column corresponds to T-odd terms and the other correspond to T-even terms.

	T-odd terms	$\theta_K \neq 0$	$C_\xi^l \neq 0$	$A_{\psi\bar{K}^0} \neq 0, \bar{A}_{\psi K^0} \neq 0$	$\bar{A}_{l^+} \neq 0, A_{l^-} \neq 0$
R_T^{III}	$Sz^I + R_M - \xi_l^R$	0	$-C_\xi^l$	$-\hat{\lambda}_{\rm wst}^R$	$G\hat{\lambda}_l^R$
C_T^{III}	$-C - Sz^I$	$-\theta_K^R$	0	0	$S\Delta\lambda_l^I$
S_T^{III}	$S\left[1 + Gz^R\right]$	$-G\theta_K^I$	0	0	$-GS\Delta\lambda_l^R$
B_T^{III}	$S\left[Gz_K^I - z^I - SR_M + S\xi_l^R\right]$	0	$S^2C_\xi^l$	$S^2\hat{\lambda}_{\rm wst}^R - SG\Delta\lambda_{\rm wst}^I$	0
D_T^{III}	$S\left[z_K^R - Gz^R\right]$	0	0	$-S\Delta\lambda_{\rm wst}^R$	$-S^2\hat{\lambda}_l^I$
E_T^{III}	$-GS$	0	0	0	0

Table 6. The coefficients of the asymmetry for the process III with the final states $(f_1, f_2, f_3, f_4) = (\psi K_L, l^+ X, l^- X, \psi K_S)$ and the sources which give rise to the non-vanishing contribution to the asymmetry. The sources of the first column corresponds to T-odd terms and the other correspond to T-even terms.

JHEP02(2015)174

	T-odd terms	$\theta_K \neq 0$	$C_\xi^l \neq 0$	$A_{\psi\bar{K}^0} \neq 0, \bar{A}_{\psi K^0} \neq 0$	$\bar{A}_{l^+} \neq 0, A_{l^-} \neq 0$
R_T^{IV}	$-Sz^I + R_M - \xi_l^R$	0	$-C_\xi^l$	$\hat{\lambda}_{\rm wst}^R$	$-G\hat{\lambda}_l^R$
C_T^{IV}	$-C + Sz^I$	$-\theta_K^R$	0	0	$-S\Delta\lambda_l^I$
S_T^{IV}	$-S\left[1 - Gz^R\right]$	$G\theta_K^I$	0	0	$-GS\Delta\lambda_l^R$
B_T^{IV}	$S\left[-Gz_K^I + z^I - SR_M + S\xi_l^R\right]$	0	$S^2C_\xi^l$	$-S^2\hat{\lambda}_{\rm wst}^R + SG\Delta\lambda_{\rm wst}^I$	0
D_T^{IV}	$S\left[z_K^R - Gz^R\right]$	0	0	$-S\Delta\lambda_{\rm wst}^R$	$-S^2\hat{\lambda}_l^I$
E_T^{IV}	$-GS$	0	0	0	0

Table 7. The coefficients of the asymmetry for the process IV with the final states $(f_1, f_2, f_3, f_4) = (\psi K_S, l^+X, l^-X, \psi K_L)$ and the sources which give rise to the non-vanishing contribution to the asymmetry. The sources of the first column corresponds to T-odd terms and the other correspond to T-even terms.

Although the asymmetry in eq. (4.2) is not exactly T-asymmetry, the measurement of the coefficients are useful for constraining S and G as well as various non-standard interactions. Non-standard interactions include wrong sign decay and CPT violation. In the following subsections, we show how one can determine S and G and also show how one can constrain the various non-standard interactions. We first study the case without any assumption and in later subsections, we investigate two physically interesting cases, one corresponding to the case that CPT is a good symmetry and the other is the case without wrong sign decays. Since there are relations among the coefficients for different processes, we first identify the independent coefficients. From tables 4–7, one finds the following relations among the coefficients for the different processes.

$$
\begin{aligned}
R_T^{IV} &= -R_T^I, & R_T^{III} &= -R_T^{II}, \\
C_T^{III} &= -C_T^{II}, & C_T^{IV} &= -C_T^I, \\
S_T^{III} &= S_T^{II}, & S_T^{IV} &= S_T^I, \\
B_T^{III} &= -B_T^{II}, & B_T^{IV} &= -B_T^I, \\
D_T^I &= D_T^{II} = D_T^{III} = D_T^{IV}, \\
E_T^I &= E_T^{II} = -E_T^{III} = -E_T^{IV}.
\end{aligned}
$$

They imply that there are ten independent coefficients. In table 8, we show how ten independent combination of the coefficients can be written in terms of CPT even , CPT odd, and wrong sign decay parameters. Since there are eighteen parameters, the number of the independent coefficients is not enough to extract the parameters. However, one can still constrain the combination of the parameters. Below we investigate how to extract the parameters for the three cases.

4.1 Extracting the parameters from the coefficients: general case

Let us first examine how one can determine the parameters from the measurements of the coefficients shown in table 8. Hereafter, we discuss a method to determine the values for G and S through observing E_T. Since E_T is multiplied by y in eq. (4.2), one cannot extract

JHEP02(2015)174

	CPT even parameters	CPT violating parameters	wrong sign decays
$\frac{R_T^I+R_T^{II}}{2}$	$-R_M+\xi_l^R$	$+C_\xi^l$	0
$\frac{R_T^I-R_T^{II}}{2}$	0	Sz^I	$-\hat{\lambda}_{\rm wst}^R+G\hat{\lambda}_l^R$
$\frac{C_T^I+C_T^{II}}{2}$	C	θ_K^R	0
$\frac{C_T^I-C_T^{II}}{2}$	0	$-Sz_I$	$S\Delta\lambda_l^I$
$\frac{S_T^I+S_T^{II}}{2}$	0	SGz^R	$-SG\Delta\lambda_l^R$
$\frac{S_T^I-S_T^{II}}{2}$	$-S$	$G\theta_K^I$	0
$\frac{B_T^I+B_T^{II}}{2}$	$S^2\left(R_M-\xi_l^R\right)$	$-S^2C_\xi^l$	0
$\frac{B_T^I-B_T^{II}}{2}$	0	$S\left(Gz_K^I-z^I\right)$	$S(S\hat{\lambda}_{wst}^R-G\Delta\lambda_{wst}^I)$
D_T^I	0	$S\left(z_K^R-Gz^R\right)$	$-S\left(\Delta\lambda_{wst}^R+S\hat{\lambda}_l^I\right)$
E_T^I	GS	0	0
$\frac{B_T^I+B_T^{II}}{R_T^I+R_T^{II}}$	$-S^2$	0	0

Table 8. Combinations of the independent coefficients in the asymmetry. The sources which contribute to each combination are classified in three categories.

the value of E_T solely from the measurement of the asymmetry. Therefore, we need to determine the value of y through the other experiment. y defined in eq. (2.2) is regarding to the width difference of B meson mass eigenstate, and a method to measure $y\cos\beta\simeq Gy$ is suggested in refs. [11]–[12]. Combining the measurement of $E_T^Iy\simeq GSy$, one can determine S. Since S and G in their leading order satisfy $S^2+G^2\simeq 1-\mathcal{O}(C^2)$, the measurement of E_T determines $(\pm G,S)$ within the two-fold ambiguity. The ambiguity would be removed if we assume that the standard model contribution is dominant for the width difference. (See figure 1) As an alternative way to determine S, one can use the relation $\frac{B_T^I+B_T^{II}}{R_T^I+R_T^{II}}=-S^2$, and determine $|S|$. The sign ambiguity for S can be removed because in the leading order S is equal to $\frac{S_T^{II}-S_T^I}{2}$. Excluding the case that the sub-leading contribution changes the sign of the leading term, one can determine the sign for S through observing $\frac{S_T^{II}-S_T^I}{2}$. Having determined G and S, we consider constraining the other parameters.

We note that the following relation is satisfied,

$$\frac{R_T^I-R_T^{II}}{2}+\frac{C_T^I-C_T^{II}}{2}=-\hat{\lambda}_{\rm wst}^R+G\hat{\lambda}_l^R+S\Delta\lambda_l^I. \tag{4.21}$$

Since the right-hand side is independent of CPT violating parameters, non-vanishing contribution implies the unambiguous evidence of the presence of the wrong sign decay. Furthermore, since S is determined, one can write the CPT violating parameter θ_K^I as,

$$\theta_K^I=\frac{\frac{S_T^I-S_T^{II}}{2}+S}{G}. \tag{4.22}$$

JHEP02(2015)174

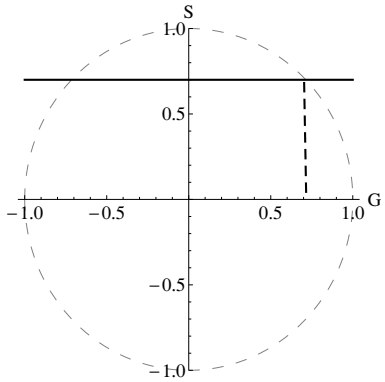

Figure 1. Determination of G and S. Due to $G^2 + S^2 \simeq 1$, G and S are on the circle of unit length. Once S is known, G is determined within two-fold ambiguity.

If the right-hand side is non-zero, it implies CPT violation in the right strangeness decay. However, the real part of θ_K cannot be singly extracted, since

$$\theta_K^R + C = \frac{C_T^I + C_T^{II}}{2}. \tag{4.23}$$

One also notes the relation,

$$-R_M + \xi_l^R + C_\xi^l = \frac{R_T^I + R_T^{II}}{2}. \tag{4.24}$$

If any one of the combinations, $\frac{R_T^I - R_T^{II}}{2}$, $\frac{C_T^I - C_T^{II}}{2}$, $\frac{S_T^I + S_T^{II}}{2}$, $\frac{B_T^I - B_T^{II}}{2}$, and D_T^I is non-zero, it implies CPT violation and/or wrong sign decay. However, if the cancellation between CPT violation and wrong sign decay occurs, they can vanish.

4.2 Extracting the parameters from the coefficients: CPT conserving limit

Next we consider the case in the limit of CPT symmetry. In the limit of CPT symmetry, all the contribution in the second column vanishes in table 8. Since all the wrong sign decay parameters are CPT even, the third column of table 8 does not vanish. In the limit C, S and $R_M - \xi_l^R$ can be determined as,

$$C = \frac{C_T^I + C_T^{II}}{2}, \tag{4.25}$$

$$S = \frac{S_T^{II} - S_T^I}{2}, \tag{4.26}$$

$$R_M - \xi_l^R = -\frac{R_T^I + R_T^{II}}{2}. \tag{4.27}$$

Moreover T-odd wrong sign semi-leptonic decay $\Delta\lambda_l$ can be determine as,

$$\Delta\lambda_l^I = \frac{C_T^I - C_T^{II}}{2S}, \tag{4.28}$$

$$\Delta\lambda_l^R = -\frac{S_T^I + S_T^{II}}{2GS}. \tag{4.29}$$

JHEP02(2015)174

For the other five wrong sign decay parameters $\hat{\lambda}^R_{\rm wst}, \hat{\lambda}^{R,I}_l \Delta\lambda^{R,I}_{\rm wst}$, one obtains the following three constraints.

$$\frac{R^I_T - R^{II}_T}{2} = -\hat{\lambda}^R_{\rm wst} + G\hat{\lambda}^R_l, \tag{4.30}$$

$$\frac{B^I_T - B^{II}_T}{2} = S\left(S\hat{\lambda}^R_{\rm wst} - G\Delta\lambda^I_{\rm wst}\right), \tag{4.31}$$

$$D^I_T = -S\left(\Delta\lambda^R_{\rm wst} + S\hat{\lambda}^I_l\right). \tag{4.32}$$

4.3 Extracting the parameters from the coefficients: case without wrong sign decay

Lastly, we consider the case without wrong sign decays. The relations in eqs. (4.22)–(4.24) are satisfied in this case. The right-hand side of eq. (4.21) vanishes. In addition to these, CP and CPT violation of the mixing parameters in B meson system is determined by

$$z^I = \frac{R^I_T - R^{II}_T}{2S}, \quad z^R = \frac{S^I_T + S^{II}_T}{2GS}. \tag{4.33}$$

CP and CPT violation in the neutral K meson system is also determined as,

$$z^I_K = \frac{D^I_T + \frac{S^I_T + S^{II}_T}{2}}{S}, \quad z^R_K = \frac{B^I_T - B^{II}_T - \left(C^I_T - C^{II}_T\right)}{2SG}. \tag{4.34}$$

The five parameters $C^l_\xi, \theta^R_K, C, R_M$ and ξ^R_l satisfy the two constraints eqs. (4.23)–(4.24).

5 Conditions for authentic time reversed process

In section 4, we showed the expression of the asymmetry that describes event number difference of figure 2 and figure 3. However, rather than figure 3, figure 4 is an authentic time reversed process of figure 2, since the two processes of figure 2 and figure 4 are related with flipping time direction. In discussion given in refs. [1]–[3], one substituted figure 3 for figure 4 because signal sides of figure 2 and figure 3 are deemed to be a time reversed process to each other. Since figure 3 is not an authentic time reversed process, the asymmetry is slightly deviated from T-odd.

In this section, we clarify why T-even parts are included in the coefficients eqs. (4.8)–(4.12), although it is naively thought to be a T-odd quantity.

One can show that, when the following conditions are simultaneously satisfied, figure 3 plays the role as a time reversed process of figure 2 and the coefficients eqs. (4.8)–(4.12) become T-odd.

1. Equivalence conditions of B meson states.

2. $\Delta N^{\rm e}_R = 0$.

Here we denote $\Delta N_R = \Delta N^{\rm o}_R + \Delta N^{\rm e}_R$ and $\Delta N^{\rm e}_R$ ($\Delta N^{\rm o}_R$) is the T-even (odd) part.

JHEP02(2015)174

The equivalence conditions indicate that the initial (final) B meson states of signal side in figures 3–4 are the same as each other. The equivalence conditions are described as,

$$\begin{cases} |B_{(\to l^+X)\perp}\rangle \propto |B_{l^-X\to}\rangle \\ |B_{\to\psi K_S}\rangle \propto |B_{(\psi K_L\to)\perp}\rangle \end{cases} . \tag{5.1}$$

Eq. (5.1) shows that B meson states in figures 3–4 are equivalent. Similarly, figure 5 is the authentic time reversed process of figure 3. When we apply the same condition to B meson states in figures 2–5, one obtains,

$$\begin{cases} |B_{(\to l^-X)\perp}\rangle \propto |B_{(l^+X\to)}\rangle \\ |B_{(\to\psi K_L)}\rangle \propto |B_{(\psi K_S\to)\perp}\rangle \end{cases} . \tag{5.2}$$

Violation of the conditions (5.1)–(5.2) is originally calculated in ref. [6]. Including overall factors and using our notation, we show the violation of the conditions (5.1)–(5.2) as follows,

$$\begin{cases} \langle B_{(\psi K_L\to)\perp}|B_{(\to\psi K_S)\perp}\rangle = N_{(\to\psi K_S)\perp}N_{(\psi K_L\to)\perp}\left(A_{\psi K^0}A^{\rm ID}_{\psi K^0} + \bar{A}_{\psi\bar{K}^0}\bar{A}^{\rm ID}_{\psi\bar{K}^0}\right)\dfrac{\theta_K+\Delta\lambda_{\rm wst}}{2} \\ \langle B_{(l^-X\to)\perp}|B_{(\to l^+X)\perp}\rangle = 2N_{(l^-\to)\perp}N_{(\to l^+)\perp}A_{l^+}\bar{A}^{\rm ID}_{l^-}\dfrac{p}{q}\lambda_{l^+}, \end{cases} \tag{5.3}$$

$$\begin{cases} \langle B_{(\psi K_S\to)\perp}|B_{(\to\psi K_L)\perp}\rangle = N_{(\to\psi K_L)\perp}N_{(\psi K_S\to)\perp}\left(A_{\psi K^0}A^{\rm ID}_{\psi K^0} + \bar{A}_{\psi\bar{K}^0}\bar{A}^{\rm ID}_{\psi\bar{K}^0}\right)\dfrac{\theta_K-\Delta\lambda_{\rm wst}}{2} \\ \langle B_{(l^+X\to)\perp}|B_{(\to l^-X)\perp}\rangle = 2N_{(l^+\to)\perp}N_{(\to l^-)\perp}\bar{A}_{l^-}A^{\rm ID}_{l^+}\dfrac{q}{p}\lambda^{-1}_{l^-}, \end{cases} \tag{5.4}$$

where we used the expression for states defined in eqs. (F.1)–(F.4), (F.6)–(F.9). In eqs. (5.3)–(5.4), effect of mixing-induced CP violation in K meson system is included in terms of our notation $\Delta\lambda_{\rm wst} \simeq \dfrac{p_K}{q_K}\dfrac{A_{\psi\bar{K}^0}}{A_{\psi K^0}} - \dfrac{q_K}{p_K}\dfrac{\bar{A}_{\psi K^0}}{\bar{A}_{\psi\bar{K}^0}}$ in comparison with ref. [6].

$\langle B_{(l^-X\to)\perp}|B_{(\to l^+X)\perp}\rangle \neq 0$ and $\langle B_{(l^+X\to)\perp}|B_{(\to l^-X)\perp}\rangle \neq 0$ indicate that one cannot exactly conduct the flavor tagging in the presence of wrong sign semi-leptonic decays. Similarly, $\langle B_{(\to\psi K_S)\perp}|B_{(\psi K_L\to)\perp}\rangle \neq 0$ and $\langle B_{(\psi K_S\to)\perp}|B_{(\to\psi K_L)\perp}\rangle \neq 0$ imply that one cannot exactly carry out the CP tagging in the presence of CPT violation in decays and wrong sign strangeness decays. Therefore, eqs. (5.3)–(5.4) describe that semi-leptonic decays and strangeness changing decays yield tagging ambiguities, and that are expressed in terms of state non-orthogonality.

Then, we turn to explanation of the second condition, $\Delta N^{\rm e}_R = 0$. We define the following quantities for the expedient sake.

$$X^{\rm o} = \frac{X_{(\psi K_L)\perp,l^+X}}{\kappa_{(\psi K_L)\perp,l^+X}} - \frac{X_{(l^-X)\perp,\psi K_S}}{\kappa_{(l^-X)\perp,\psi K_S}}, \quad X^{\rm e} = \frac{X_{(\psi K_L)\perp,l^+X}}{\kappa_{(\psi K_L)\perp,l^+X}} + \frac{X_{(l^-X)\perp,\psi K_S}}{\kappa_{(l^-X)\perp,\psi K_S}}, \tag{5.5}$$

where $X = \sigma, \mathcal{C}$ and $\mathcal{S}$ are given in eqs. (A.3)–(A.5). Consider the case that the equivalence conditions are satisfied to demonstrate that violation of $\Delta N^{\rm e}_R = 0$ gives rise to T-even

JHEP02(2015)174

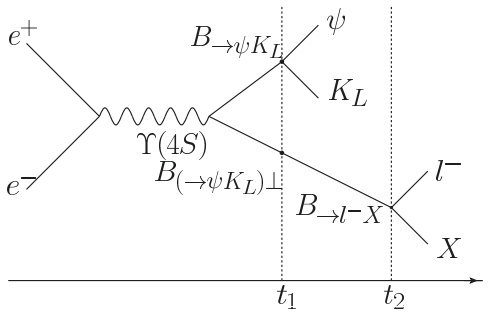

Figure 2. A process with $(f_1, f_2) = (\psi K_L, l^- X)$.

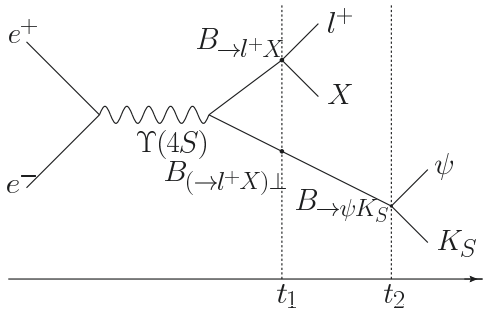

Figure 3. A process with $(f_3, f_4) = (l^+ X, \psi K_S)$. Figure 2 and figure 3 are referred as (I) in eq. (4.1). Event number asymmetry of figure 2 and figure 3. is calculated as eqs. (4.8)–(4.13).

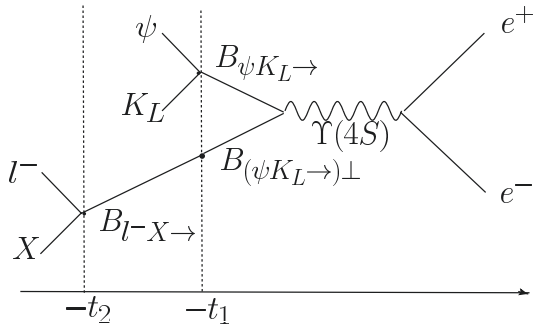

Figure 4. A process with inverse decays of B meson. Figure 2 and figure 4 are related with flipping time direction.

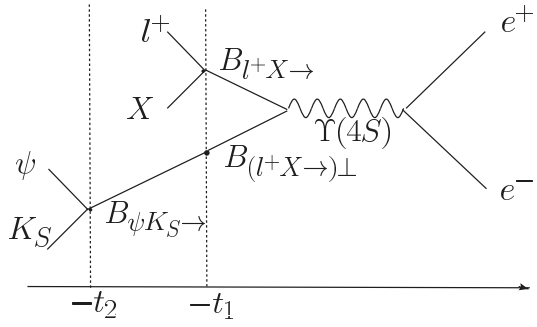

Figure 5. A process with inverse decays of B meson. Figure 3 and figure 5 are related with flipping time direction.

JHEP02(2015)174

contribution to the asymmetry. For that case, we can find that $X^{\rm o}(X^{\rm e})$ defined in eq. (5.5) is T-odd (even) due to expressions given as follows,

$$S^{\rm o} = -2S\left(1 - Gz^R\right), \qquad C^{\rm o} = 2\left[C - Sz^I\right], \qquad (\sigma^{\rm o})^l = 0, \tag{5.6}$$

$$S^{\rm e} = 2\left[Gz_K^I + \left(S^2 - 1\right)z^I\right], \qquad C^{\rm e} = 2\left[z_K^R - Gz^R\right], \qquad (\sigma^{\rm e})^l = 2G, \tag{5.7}$$

where for $\Delta\sigma$ and $\hat{\sigma}$, we write down only the leading part since small parts of $\Delta\sigma$ and $\hat{\sigma}$ are neglected when multiplied by y in the asymmetry (2.7). For the process (I), ΔX and $\hat{X}$ defined in eqs. (2.5)–(2.6) are written as,

$$\Delta X \simeq X^{\rm o} - \frac{\Delta N_R}{2}X^{\rm e} = \left(X^{\rm o} - \frac{\Delta N_R^{\rm o}}{2}X^{\rm e}\right) - \frac{\Delta N_R^{\rm e}}{2}X^{\rm e}, \tag{5.8}$$

$$\hat{X} \simeq X^{\rm e} - \frac{\Delta N_R}{2}X^{\rm o} = \left(X^{\rm e} - \frac{\Delta N_R^{\rm o}}{2}X^{\rm o}\right) - \frac{\Delta N_R^{\rm e}}{2}X^{\rm o}. \tag{5.9}$$

One finds that the T-even part of ΔN_R leads T-even contribution to ΔX in eq. (5.8). The same applies to $\hat{X}$, and it is shown that ΔX ($\hat{X}$) deviates from T-odd (even) when $\Delta N_R^{\rm e}$ has non-zero value. Therefore, we can demonstrate that $\Delta N_R^{\rm e}$ gives rise to T-even contribution to the asymmetry given in eqs. (4.3)–(4.6).

6 Conclusion

In this paper, the precise meaning of the time reversal-like asymmetry is investigated, based on the most general time dependence of the asymmetry in eq. (4.2). In analysis of BaBar [4] and [6], the difference of the overall constants for the rates is eliminated. The ratio of the overall constants for the two decay rates is deviated from unity, and the deviation $\Delta N_R = N_R - 1$ is taken into account in our analysis. If one takes the limits $\Delta N_R = 0$ and $y = 0$ in our analysis, the asymmetry of BaBar collaboration [4] is obtained. In our analysis, since the final states $\psi K_{S,L}$ are not the exact CP eigenstates, one can find the effect of mixing-induced CP violation in K meson system. The effect of ϵ_K is extracted and it gives rise to $\mathcal{O}(10^{-3})$ contribution to C_T, the coefficient of $\cos(x\Gamma t)$. ϵ_K^R and direct CP violation $|\bar{A}_{\psi\bar{K}^0}/A_{\psi K^0}|$ are dominant in C_T, if the wrong sign semi-leptonic decay and CPT violations are negligible. As well as ϵ_K, the contribution from CPT violation in Kaon system z_K is estimated.

We introduced the parameters which have the specific property under CP, T and CPT transformations, including the effect of indirect CP violation in K meson system. Taking account of the difference for overall constants, the coefficients of each time-dependent function are written in terms of such parameters, and one can find that the asymmetry consists of not only T-odd terms, but also T-even terms in the most general time dependent function for the asymmetry. Furthermore, the introduced parameters are invariant under rephasing of quarks. We also found that the asymmetry is expressed as phase convention independent quantities.

We obtained the coefficients of the asymmetry for the processes (I-IV) and studied how to extract the parameters. Assuming that the value of y, i.e., the width difference of B_d

JHEP02(2015)174

meson mass eigenstates is known, the three cases to constrain the parameters are discussed. For the most general case, combining the coefficients for different processes enables one to determine the parameters, S and G. We also find that non-zero value of some combination of the coefficient signals either CPT violation or the presence of the wrong sign decays. The other two cases correspond to CPT-conserving limit and the absence of wrong sign decays. In the CPT-conserving case, the coefficients constrain the parameters for wrong sign decays. In the absence of wrong sign decays, indirect CPT violation for B meson and K meson is constrained.

Moreover, we discussed T-even parts in the asymmetry. We found that T-even terms in the asymmetry vanish when several conditions are satisfied. These derived conditions are categorized as two parts. The first one is referred as equivalence conditions, regarding to B meson states for a time reversal-like process and an authentic time reversed process. As suggested in [6], B mesons for the two processes are not equivalent to each other, and we also showed the violation of the equivalence conditions, including the effects of mixing in K meson system. Since non-zero ΔN_R is taken into account in our study, ΔN_R can be the origin of T-even contribution to the asymmetry. We investigated that the second condition, which requires that T-even parts of ΔN_R are zero, is needed for the asymmetry to become a T-odd quantity.

A Coefficients of master formula

We record coefficients of the master formula for the time-dependent decay rate of ref. [6].

$$N_{(i)\perp,j} = \frac{1}{4}\mathcal{N}_i\mathcal{N}_j\left\{1+(C_i+C_j)\left(R_M-z^R\right)\right\}, \quad \mathcal{N}_i = |A_i|^2+|\bar{A}_i|^2, \tag{A.1}$$

$$\begin{aligned}\kappa_{(i)\perp,j} &= (1-G_iG_j)\\ &\quad +\left[(C_i+C_j)(1-G_iG_j)+C_jG_i+C_iG_j\right]z^R-(S_i+S_j)z^I\\ &\quad +G_iG_j\left(C_i\theta_i^R+C_j\theta_j^R\right)-G_iS_j\theta_j^I-G_jS_i\theta_i^I,\end{aligned} \tag{A.2}$$

$$\begin{aligned}\sigma_{(i)\perp,j} &= G_j-G_i\\ &\quad +[C_i(1+G_j-G_i)-C_j(1-G_j+G_i)]z^R+(G_iS_j-G_jS_i)z^I\\ &\quad -C_jG_j\theta_j^R+S_j\theta_j^I+C_iG_i\theta_i^R-S_i\theta_i^I,\end{aligned} \tag{A.3}$$

$$\begin{aligned}\mathcal{C}_{(i)\perp,j} &= -C_iC_j-S_iS_j\\ &\quad -[(C_i+C_j)(C_iC_j+S_iS_j)+C_iG_j+C_jG_i]z^R+(S_i+S_j)z^I\\ &\quad +G_jS_i\theta_j^I-\left[C_i\left(1-C_j^2\right)-C_jS_iS_j\right]\theta_j^R\\ &\quad +G_iS_j\theta_i^I-\left[C_j\left(1-C_i^2\right)-C_iS_iS_j\right]\theta_i^R,\end{aligned} \tag{A.4}$$

$$\begin{aligned}\mathcal{S}_{(i)\perp,j} &= C_iS_j-C_jS_i\\ &\quad +\left[C_iC_j(S_j-S_i)-\left(C_j^2+G_j\right)S_i+\left(C_i^2+G_i\right)S_j\right]z^R+(C_j-C_i)z^I\\ &\quad -C_iG_j\theta_j^I+\left[\left(C_j^2-1\right)S_i-C_iC_jS_j\right]\theta_j^R\\ &\quad +C_jG_i\theta_i^I-\left[\left(C_i^2-1\right)S_j-C_iC_jS_i\right]\theta_i^R,\end{aligned} \tag{A.5}$$

where A_i and $\bar{A}_i$ in eq. (A.1) are defined in eq. (3.1). i and j represent the final state of tagging side (f_i) and signal side(f_j) for a pair of B meson decaying respectively.

JHEP02(2015)174

B Incoming mass eigenstates and outgoing mass eigenstates in B meson and K meson system

Throughout this paper, the time reversal process of B meson decay often appears. To describe the inverse decay amplitudes, as out-states of B mesons, the reciprocal base must be used for Non-Hermitian Hamiltonian system. This is formulated in several literatures, refs. [13]–[17]. In this appendix, we show the definition of incoming states and outgoing states which are used in this paper.

The incoming mass eigenstates of effective Hamiltonian in B meson system are

$$|B_H^{\rm in}\rangle = p\sqrt{1+z}\,|B^0\rangle - q\sqrt{1-z}\,|\bar{B}^0\rangle\,, \tag{B.1}$$
$$|B_L^{\rm in}\rangle = p\sqrt{1-z}\,|B^0\rangle + q\sqrt{1+z}\,|\bar{B}^0\rangle\,, \tag{B.2}$$

where p, q are mixing parameters in indirect CP violation and z is a mixing parameter in indirect CP, CPT violation. In terms of matrix elements of effective Hamiltonian, these parameters are written as

$$\frac{p}{q} = \sqrt{\frac{M_{12} - \frac{i}{2}\Gamma_{12}}{M_{12}^* - \frac{i}{2}\Gamma_{12}^*}}, \tag{B.3}$$
$$z = \frac{M_{11} - M_{22} - \frac{i}{2}(\Gamma_{11} - \Gamma_{22})}{m_L - m_H - \frac{i}{2}(\Gamma_L - \Gamma_H)}. \tag{B.4}$$

These expressions help us understand the transformation property of λ, S, G, C, etc. Then, outgoing mass states are determined to fulfill the following conditions,

$$\langle B_H^{\rm out}|B_H^{\rm in}\rangle = 1, \langle B_H^{\rm out}|B_L^{\rm in}\rangle = 0, \langle B_L^{\rm out}|B_L^{\rm in}\rangle = 1, \langle B_L^{\rm out}|B_H^{\rm in}\rangle = 0. \tag{B.5}$$

Thus, outgoing mass eigenstates are

$$\langle B_H^{\rm out}| = \frac{1}{2pq}\left(q\sqrt{1+z}\,\langle B^0| - p\sqrt{1-z}\,\langle\bar{B}^0|\right), \tag{B.6}$$
$$\langle B_L^{\rm out}| = \frac{1}{2pq}\left(q\sqrt{1-z}\,\langle B^0| + p\sqrt{1+z}\,\langle\bar{B}^0|\right). \tag{B.7}$$

For K meson system, similarly,

$$|K_L^{\rm in}\rangle = p_K\sqrt{1+z_K}\,|K^0\rangle - q_K\sqrt{1-z_K}\,|\bar{K}^0\rangle\,, \tag{B.8}$$
$$|K_S^{\rm in}\rangle = p_K\sqrt{1-z_K}\,|K^0\rangle + q_K\sqrt{1+z_K}\,|\bar{K}^0\rangle\,, \tag{B.9}$$
$$\langle K_L^{\rm out}| = \frac{1}{2p_Kq_K}\left(q_K\sqrt{1+z_K}\,\langle K^0| - p_K\sqrt{1-z_K}\,\langle\bar{K}^0|\right), \tag{B.10}$$
$$\langle K_S^{\rm out}| = \frac{1}{2p_Kq_K}\left(q_K\sqrt{1-z_K}\,\langle K^0| + p_K\sqrt{1+z_K}\,\langle\bar{K}^0|\right). \tag{B.11}$$

Since these mass eigenstates in K meson system are shown in flavor states, we specifically can calculate the amplitudes of transition from incoming states B meson to outgoing

JHEP02(2015)174

states $\psi K_{L,S}$

$$A_{\psi K_S} = \langle \psi K_S^{\rm out} | B_0^{\rm in} \rangle = \frac{1}{2p_K q_K} \left(q_K \sqrt{1-z_K} A_{\psi K^0} + p_K \sqrt{1+z_K} A_{\psi \bar{K}^0} \right), \quad \text{(B.12)}$$

$$A_{\psi K_L} = \langle \psi K_L^{\rm out} | B_0^{\rm in} \rangle = \frac{1}{2p_K q_K} \left(q_K \sqrt{1+z_K} A_{\psi K^0} - p_K \sqrt{1-z_K} A_{\psi \bar{K}^0} \right), \quad \text{(B.13)}$$

$$\bar{A}_{\psi K_S} = \langle \psi K_S^{\rm out} | \bar{B}_0^{\rm in} \rangle = \frac{1}{2p_K q_K} \left(q_K \sqrt{1-z_K} \bar{A}_{\psi K^0} + p_K \sqrt{1+z_K} \bar{A}_{\psi \bar{K}^0} \right), \quad \text{(B.14)}$$

$$\bar{A}_{\psi K_L} = \langle \psi K_L^{\rm out} | \bar{B}_0^{\rm in} \rangle = \frac{1}{2p_K q_K} \left(q_K \sqrt{1+z_K} \bar{A}_{\psi K^0} - p_K \sqrt{1-z_K} \bar{A}_{\psi \bar{K}^0} \right). \quad \text{(B.15)}$$

Hence, we can obtain eqs. (3.11), (3.22), (3.23) and (3.24). We also can write down inverse decay amplitudes of eqs. (B.12)–(B.15)

$$A^{\rm ID}_{\psi K_S} = \langle B_0^{\rm out} | \psi K_S^{\rm in} \rangle = \left(p_K \sqrt{1-z_K} A^{\rm ID}_{\psi K^0} + q_K \sqrt{1+z_K} A^{\rm ID}_{\psi \bar{K}^0} \right), \quad \text{(B.16)}$$

$$A^{\rm ID}_{\psi K_L} = \langle B_0^{\rm out} | \psi K_L^{\rm in} \rangle = \left(p_K \sqrt{1+z_K} A^{\rm ID}_{\psi K^0} - q_K \sqrt{1-z_K} A^{\rm ID}_{\psi \bar{K}^0} \right), \quad \text{(B.17)}$$

$$\bar{A}^{\rm ID}_{\psi K_S} = \langle \bar{B}_0^{\rm out} | \psi K_S^{\rm in} \rangle = \left(p_K \sqrt{1-z_K} \bar{A}^{\rm ID}_{\psi K^0} + q_K \sqrt{1+z_K} \bar{A}^{\rm ID}_{\psi \bar{K}^0} \right), \quad \text{(B.18)}$$

$$\bar{A}^{\rm ID}_{\psi K_L} = \langle \bar{B}_0^{\rm out} | \psi K_L^{\rm in} \rangle = \left(p_K \sqrt{1+z_K} \bar{A}^{\rm ID}_{\psi K^0} - q_K \sqrt{1-z_K} \bar{A}^{\rm ID}_{\psi \bar{K}^0} \right). \quad \text{(B.19)}$$

C List of coefficients of time dependent decay rates for process (I)

In this appendix, we show the coefficients of the time dependent decay rates in eq. (2.1) which are needed for calculation of the asymmetry of process (I).

$$S_{(\psi K_L)\perp, l^- X} = S_{\psi K_L} - S_{\psi K_L} z^R - z^I - G_{\psi K_L} \theta^I_{\psi K_L}, \quad \text{(C.1)}$$

$$S_{(l^+ X)\perp, \psi K_S} = S_{\psi K_S} + S_{\psi K_S} z^R - z^I - G_{\psi K_S} \theta^I_{\psi K_S}, \quad \text{(C.2)}$$

$$C_{(\psi K_L)\perp, l^- X} = C_{\psi K_L} - S_{\psi K_L} S_{l^-} + G_{\psi K_L} z^R + S_{\psi K_L} z^I + \theta^R_{\psi K_L}, \quad \text{(C.3)}$$

$$C_{(l^+ X)\perp, \psi K_S} = -C_{\psi K_S} - S_{\psi K_S} S_{l^+} - G_{\psi K_S} z^R + S_{\psi K_S} z^I - \theta^R_{\psi K_S}, \quad \text{(C.4)}$$

$$\kappa_{(\psi K_L)\perp, l^- X} = 1 - G_{\psi K_L} G_{l^-} - (G_{\psi K_L} + 1) z^R - S_{\psi K_L} z^I, \quad \text{(C.5)}$$

$$\kappa_{(l^+ X)\perp, \psi K_S} = 1 - G_{\psi K_S} G_{l^+} + (G_{\psi K_S} + 1) z^R - S_{\psi K_S} z^I, \quad \text{(C.6)}$$

$$\sigma_{(\psi K_L)\perp, l^- X} = G_{l^-} - G_{\psi K_L} + (1 + G_{\psi K_L}) z^R - S_{\psi K_L} \theta^I_{\psi K_L}, \quad \text{(C.7)}$$

$$\sigma_{(l^+ X)\perp \psi K_S} = G_{\psi K_S} - G_{l^+} + (1 + G_{\psi K_S}) z^R + S_{\psi K_S} \theta^I_{\psi K_S}, \quad \text{(C.8)}$$

$$\frac{S_{(\psi K_L)\perp, l^- X}}{\kappa_{(\psi K_L)\perp, l^- X}} = S_{\psi K_L} + S_{\psi K_L} G_{\psi K_L} G_{l^-} + S_{\psi K_L} G_{\psi K_L} z^R + \left(S^2_{\psi K_L} - 1 \right) z^I - G_{\psi K_L} \theta^I_{\psi K_L}, \quad \text{(C.9)}$$

$$\frac{S_{(l^+ X)\perp, \psi K_S}}{\kappa_{(l^+ X)\perp, \psi K_S}} = S_{\psi K_S} + S_{\psi K_S} G_{\psi K_S} G_{l^+} - S_{\psi K_S} G_{\psi K_S} z^R + \left(S^2_{\psi K_S} - 1 \right) z^I - G_{\psi K_S} \theta^I_{\psi K_S}, \quad \text{(C.10)}$$

JHEP02(2015)174

$$\frac{C_{(\psi K_L)\perp,l^-X}}{\kappa_{(\psi K_L)\perp,l^-X}} \simeq C_{(\psi K_L)\perp,l^-X}, \tag{C.11}$$

$$\frac{C_{(l^+X)\perp,\psi K_S}}{\kappa_{(l^+X)\perp,\psi K_S}} \simeq C_{(l^+X)\perp,\psi K_S}, \tag{C.12}$$

$$\frac{\sigma_{(\psi K_L)\perp,l^-X}}{\kappa_{(\psi K_L)\perp,l^-X}} \simeq -G_{\psi K_L}, \tag{C.13}$$

$$\frac{\sigma_{(l^+X)\perp,\psi K_S}}{\kappa_{(l^+X)\perp,\psi K_S}} \simeq G_{\psi K_S}, \tag{C.14}$$

where we keep only the leading term for $\frac{\sigma}{\kappa}$, since it will be multiplied by a small number y in the formulae of the decay rate eq. (2.1).

D Expressions for $N_R, \Delta\mathcal{S}, \Delta\mathcal{C}, \Delta\sigma, \hat{\sigma}, \hat{\mathcal{S}}$ and $\hat{\mathcal{C}}$

The quantity N_R, defined in eq. (2.4), denotes the ratio of a normalization for rates. Since we compute the asymmetry including the effect of N_R, its expression should be clarified. In this appendix section, we calculate N_R, and obtain the expressions of parameters as $\Delta\mathcal{S}, \Delta\mathcal{C}, \Delta\sigma, \hat{\sigma}, \hat{\mathcal{S}}$ and $\hat{\mathcal{C}}$ for the process (I). In deriving formulae, we use eqs. (C.1)–(C.14). Expanding N_R with respect to small parameters, we obtain the general structure of N_R at first order approximation.

$$\begin{aligned}
N_R &= \frac{N_{(3)\perp,4}}{N_{(1)\perp,2}} \frac{\kappa_{(3)\perp,4}}{\kappa_{(1)\perp,2}} \\
&= \frac{\mathcal{N}_3\mathcal{N}_4 \left[1 + (C_3 + C_4)\left(R_M - z^R\right)\right]}{\mathcal{N}_1\mathcal{N}_2 \left[1 + (C_1 + C_2)\left(R_M - z^R\right)\right]} \frac{\kappa^l_{(3)\perp,4}\left(1 + \dfrac{\Delta\kappa_{(3)\perp,4}}{\kappa^l_{(3)\perp,4}}\right)}{\kappa^l_{(1)\perp,2}\left(1 + \dfrac{\Delta\kappa_{(1)\perp,2}}{\kappa^l_{(1)\perp,2}}\right)} \\
&\simeq \frac{\mathcal{N}_3\mathcal{N}_4}{\mathcal{N}_1\mathcal{N}_2} \frac{\kappa^l_{(3)\perp,4}}{\kappa^l_{(1)\perp,2}} \left[1 + (C_3 + C_4 - C_1 - C_2)\left(R_M - z^R\right) + \frac{\Delta\kappa_{(3)\perp,4}}{\kappa^l_{(3)\perp,4}} - \frac{\Delta\kappa_{(1)\perp,2}}{\kappa^l_{(1)\perp,2}}\right],
\end{aligned} \tag{D.1}$$

where superscript ^{l} expresses the leading part and Δ expresses the small part such as, $\kappa_{(1)\perp,2} = \kappa^l_{(1)\perp,2} + \Delta\kappa_{(1)\perp,2}$ and $\kappa_{(3)\perp,4} = \kappa^l_{(3)\perp,4} + \Delta\kappa_{(3)\perp,4}$. For the processes given in eq. (4.1), $\kappa^l_{(1)\perp,2} = \kappa^l_{(3)\perp,4} = 1$ ($f_1 = \psi K_L, f_2 = l^-X, f_3 = l^+X, f_4 = \psi K_S$ for process (I)) is satisfied and N^I_R is written as,

$$\begin{aligned}
N^I_R &= \frac{\mathcal{N}_{l^+X}\mathcal{N}_{\psi K_S}}{\mathcal{N}_{\psi K_L}\mathcal{N}_{l^-X}} \left[1 + (C_{\psi K_S} - C_{\psi K_L} + C_{l^+} - C_{l^-})\left(R_M - z^R\right)\right. \\
&\quad \left. + \Delta\kappa_{(l^+X)\perp,\psi K_S} - \Delta\kappa_{(\psi K_L)\perp,l^-X}\right] \\
&\simeq \frac{\mathcal{N}_{\psi K_S}\mathcal{N}_{l^+X}}{\mathcal{N}_{\psi K_L}\mathcal{N}_{l^-X}} \left[1 + 2\left(R_M - z^R\right) + 2\left(z^R - Sz^I - G\hat{\lambda}^R_l\right)\right] \\
&= \frac{\mathcal{N}_{\psi K_S}\mathcal{N}_{l^+X}}{\mathcal{N}_{\psi K_L}\mathcal{N}_{l^-X}} \left[1 + 2\left(-Sz^I + R_M - G\hat{\lambda}^R_l\right)\right].
\end{aligned} \tag{D.2}$$

JHEP02(2015)174

Deviation of $\mathcal{N}_{l^+X}/\mathcal{N}_{l^-X}$ and $\mathcal{N}_{\psi K_S}/\mathcal{N}_{\psi K_L}$ from 1 is written in terms of small parameters as,

$$\frac{\mathcal{N}_{l^+X}}{\mathcal{N}_{l^-X}} = 1 - 2\left(C_\xi^l + \xi_l^R\right), \quad \frac{\mathcal{N}_{\psi K_S}}{\mathcal{N}_{\psi K_L}} = 1 + 2\hat{\lambda}_{\rm wst}^R. \tag{D.3}$$

$$N_R^I = 1 + \Delta N_R^I = 1 + 2\left[-Sz^I + R_M + \hat{\lambda}_{\rm wst}^R - G\hat{\lambda}_l^R - C_\xi^l - \xi_l^R\right]. \tag{D.4}$$

Note that ΔN_R^I is a small number.

We can also write down the expressions of ΔS^I and ΔC^I.

$$\begin{aligned}\Delta\mathcal{S}^I &= \left(\frac{\mathcal{S}_{(\psi K_L)\perp,l^-X}}{\kappa_{(\psi K_L)\perp,l^-X}} - \frac{\mathcal{S}_{(l^+X)\perp,\psi K_S}}{\kappa_{(l^+X)\perp,\psi K_S}}\right) - \frac{\Delta N_R^I}{2}\left(\frac{\mathcal{S}_{(\psi K_L)\perp,l^-X}}{\kappa_{(\psi K_L)\perp,l^-X}} + \frac{\mathcal{S}_{(l^+X)\perp,\psi K_S}}{\kappa_{(l^+X)\perp,\psi K_S}}\right) \\ &\simeq \frac{\mathcal{S}_{(\psi K_L)\perp,l^-X}}{\kappa_{(\psi K_L)\perp,l^-X}} - \frac{\mathcal{S}_{(l^+X)\perp,\psi K_S}}{\kappa_{(l^+X)\perp,\psi K_S}} = -2\left[S\left(1 - Gz^R\right) - G\theta_K^I + GS\Delta\lambda_l^R\right], \end{aligned} \tag{D.5}$$

$$\Delta\mathcal{C}^I \simeq \frac{\mathcal{C}_{(\psi K_L)\perp,l^-X}}{\kappa_{(\psi K_L)\perp,l^-X}} - \frac{\mathcal{C}_{(l^+X)\perp,\psi K_S}}{\kappa_{(l^+X)\perp,\psi K_S}} = 2\left[C - Sz^I + \theta_K^R + S\Delta\lambda_l^I\right]. \tag{D.6}$$

We calculate only the leading part of $\Delta\sigma^I$ and $\hat{\sigma}^I$, since the sub-leading part of $\Delta\sigma^I$ and $\hat{\sigma}^I$ is suppressed when multiplied with $y\Gamma t$.

$$\Delta\sigma^{Il} = 0, \quad \hat{\sigma}^{Il} = 2G. \tag{D.7}$$

We write down the expressions for $\hat{\mathcal{S}}^I$ and $\hat{\mathcal{C}}^I$ as follows,

$$\begin{aligned}\hat{\mathcal{S}}^I &= \left(\frac{\mathcal{S}_{(\psi K_L)\perp,l^-X}}{\kappa_{(\psi K_L)\perp,l^-X}} + \frac{\mathcal{S}_{(l^+X)\perp,\psi K_S}}{\kappa_{(l^+X)\perp,\psi K_S}}\right) - \frac{\Delta N_R^I}{2}\left(\frac{\mathcal{S}_{(\psi K_L)\perp,l^-X}}{\kappa_{(\psi K_L)\perp,l^-X}} - \frac{\mathcal{S}_{(l^+X)\perp,\psi K_S}}{\kappa_{(l^+X)\perp,\psi K_S}}\right) \\ &\simeq 2G\left(z_K^I - \Delta\lambda_{\rm wst}^I\right) + 2\left(S^2 - 1\right)z^I + 2GS\hat{\lambda}_l^R + S\Delta N_R^I \\ &= 2\left[G\left(z_K^I - \Delta\lambda_{\rm wst}^I\right) - z^I + SR_M + S\hat{\lambda}_{\rm wst}^R - SC_\xi^l - S\xi_l^R\right], \end{aligned} \tag{D.8}$$

$$\hat{\mathcal{C}}^I \simeq \frac{\mathcal{C}_{(\psi K_L)\perp,l^-X}}{\kappa_{(\psi K_L)\perp,l^-X}} + \frac{\mathcal{C}_{(l^+X)\perp,\psi K_S}}{\kappa_{(l^+X)\perp,\psi K_S}} = 2\left[z_K^R - \Delta\lambda_{\rm wst}^R - Gz^R - S\hat{\lambda}_l^I\right]. \tag{D.9}$$

E The relation among coefficients of the asymmetries for processes (I)–(IV)

In this appendix, we show the relation among the coefficients for different processes (I-IV). First, we note the coefficients of the process II(IV) are obtained by changing the sign of the mixing parameter q_K and z_K of I(III). The change of the sign of q_K leads to the change of the sign for S, G and $\lambda_{\rm wst}$. Next, we show a simple rule which enables one to obtain the coefficients for table 5, with the coefficients of table 7. For this purpose we do not

JHEP02(2015)174

substitute ± 1 for $C_{l\pm}$ respectively and write the coefficients of asymmetry for process IV,

$$R_T^{IV} = -Sz^I + \frac{1}{2}(C_{l^+} - C_{l^-})R_M - \xi_l^R - C_\xi^l + \hat{\lambda}_{\rm wst}^R - G\hat{\lambda}_l^R, \tag{E.1}$$

$$C_T^{IV} = \frac{1}{2}(C_{l^-} - C_{l^+})C + Sz^I + \frac{1}{2}\left(C_{l^-}\theta_{K_L}^R - C_{l^+}\theta_{K_S}^R\right) - S\Delta\lambda_l^I, \tag{E.2}$$

$$S_T^{IV} = \frac{1}{2}(C_{l^-} - C_{l^+})S + SGz^R + \frac{G}{2}\left(C_{l^+}\theta_{K_S}^I - C_{l^-}\theta_{K_L}^I\right) \tag{E.3}$$

$$-GS\left(C_{l^+}{\rm Re}\left[\lambda_{l^+}\right] + C_{l^-}{\rm Re}\left[\lambda_{l^-}^{-1}\right]\right), \tag{E.4}$$

$$B_T^{IV} = S\left[-Gz_K^I + z^I + \frac{C_{l^-} - C_{l^+}}{2}SR_M + S\xi_l^R\right] + S^2C_\xi^l - S^2\hat{\lambda}_{\rm wst}^R + SG\Delta\lambda_{\rm wst}^I, \tag{E.5}$$

$$D_T^{IV} = S\left[z_K^R - Gz^R\right] - S\Delta\lambda_{\rm wst}^R + \frac{C_{l^-} - C_{l^+}}{2}S^2\hat{\lambda}_l^I, \tag{E.6}$$

$$E_T^{IV} = \frac{C_{l^-} - C_{l^+}}{2}GS. \tag{E.7}$$

When l^+ and l^- in eq. (D.3) are exchanged, the sign of C_ξ^l and ξ_l^R is reversed. According to eqs. (3.40)–(3.41), the sign of $\hat{\lambda}_l^I$ and $\Delta\lambda_l^R$ also changes. Additionally, one needs to interchange C_{l^+} and C_{l^-} in eqs. (E.1)–(E.7) and one can obtain the coefficients of asymmetry for process II.

F Calculation of equivalence conditions

In this appendix, we give the derivation of eqs. (5.3)–(5.4). The expression of the final state of signal side in figure (2) is,

$$|B_{(\to\psi K_S)\perp}\rangle = N_{(\to\psi K_S)\perp}\left(\bar{A}_{\psi K_S}|B^0\rangle - A_{\psi K_S}|\bar{B}^0\rangle\right), \tag{F.1}$$

since the state is orthogonal to $\langle\psi K_S|$. The state orthogonal to $|\psi K_L\rangle$ is

$$\langle B_{(\psi K_L\to)\perp}| = N_{(\psi K_L\to)\perp}\left(\bar{A}_{\psi K_L}^{\rm ID}\langle B^0| - A_{\psi K_L}^{\rm ID}\langle\bar{B}^0|\right). \tag{F.2}$$

Similarly, one can write down,

$$\langle B_{(\psi K_S\to)\perp}| = N_{(\psi K_S\to)\perp}\left(\bar{A}_{\psi K_S}^{\rm ID}\langle B^0| - A_{\psi K_S}^{\rm ID}\langle\bar{B}^0|\right), \tag{F.3}$$

$$|B_{(\to\psi K_L)\perp}\rangle = N_{(\to\psi K_L)\perp}\left(\bar{A}_{\psi K_L}|B^0\rangle - A_{\psi K_L}|\bar{B}^0\rangle\right). \tag{F.4}$$

Calculating the inner product of eqs. (F.1) and (F.2), we obtain

$$\begin{aligned}\langle B_{(\psi K_L\to)\perp}|B_{(\to\psi K_S)\perp}\rangle &= N_{(\to\psi K_S)\perp}N_{(\psi K_L\to)\perp}\left(\bar{A}_{\psi K_S}\bar{A}_{\psi K_L}^{\rm ID} + A_{\psi K_S}A_{\psi K_L}^{\rm ID}\right)\\ &= \frac{1}{2}N_{(\to\psi K_S)\perp}N_{(\psi K_L\to)\perp}\Big[A_{\psi K^0}A_{\psi K^0}^{\rm ID} - \bar{A}_{\psi\bar{K}^0}\bar{A}_{\psi\bar{K}^0}^{\rm ID}\\ &\quad - \frac{q_K}{p_K}\left(A_{\psi K^0}A_{\psi\bar{K}^0}^{\rm ID} + \bar{A}_{\psi\bar{K}^0}^{\rm ID}\bar{A}_{\psi K^0}\right) + \frac{p_K}{q_K}\left(A_{\psi\bar{K}^0}A_{\psi K^0}^{\rm ID} + \bar{A}_{\psi\bar{K}^0}\bar{A}_{\psi K^0}^{\rm ID}\right)\Big]\\ &= \frac{N_{(\to\psi K_S)\perp}N_{(\psi K_L\to)\perp}}{2}\left(A_{\psi K^0}A_{\psi K^0}^{\rm ID} + \bar{A}_{\psi\bar{K}^0}\bar{A}_{\psi\bar{K}^0}^{\rm ID}\right)[\theta_K + \Delta\lambda_{\rm wst}],\end{aligned} \tag{F.5}$$

JHEP02(2015)174

where we used eqs. (B.12)–(B.19). The inner product in eq. (F.5) was previously obtained in [6]. In eq. (F.5), we compute it with our notation including the normalization constant and have ignored the second order of small parameters $z_K, \theta_{\psi K^0}, \bar{\theta}_{\psi \bar{K}^0}, \hat{\lambda}_{\rm wst}$ and $\Delta\lambda_{\rm wst}$.

Next, we show the derivation of the first line of eq. (5.3) and the second line of eq. (5.4). The states are given as,

$$\langle B_{(l^- X\to)\perp}| = N_{(l^-\to)\perp}\left(\bar{A}^{\rm ID}_{l^-}\langle B^0| - A^{\rm ID}_{l^-}\langle \bar{B}^0|\right), \tag{F.6}$$

$$|B_{(\to l^+ X)\perp}\rangle = N_{(\to l^+)\perp}\left(\bar{A}_{l^+}|B^0\rangle - A_{l^+}|\bar{B}^0\rangle\right), \tag{F.7}$$

$$\langle B_{(l^+ X\to)\perp}| = N_{(l^+\to)\perp}\left(\bar{A}^{\rm ID}_{l^+}\langle B^0| - A^{\rm ID}_{l^+}\langle \bar{B}^0|\right), \tag{F.8}$$

$$|B_{(\to l^- X)\perp}\rangle = N_{(\to l^-)\perp}\left(\bar{A}_{l^-}|B^0\rangle - A_{l^-}|\bar{B}^0\rangle\right). \tag{F.9}$$

Their inner product is,

$$\begin{aligned}\langle B_{(l^- X\to)\perp}|B_{(\to l^+ X)\perp}\rangle &= N_{(l^-\to)\perp}N_{(\to l^+)\perp}\left(\bar{A}^{\rm ID}_{l^-}\bar{A}_{l^+} + A^{\rm ID}_{l^-}A_{l^+}\right)\\ &= 2N_{(l^-\to)\perp}N_{(\to l^+)\perp}A_{l^+}\bar{A}^{\rm ID}_{l^-}\frac{p}{q}\lambda_{l^+}.\end{aligned} \tag{F.10}$$

The proportionality to the wrong sign decay amplitude λ_{l^+} is derived in [6].

Acknowledgments

We would like to thank Dr. T. Shindou for useful comments and suggestion, and helpful correspondence by A. Efrati, Y. Nir and Y. Soreq.

References

[1] M.C. Banuls and J. Bernabeu, *CP, T and CPT versus temporal asymmetries for entangled states of the B_d-system*, *Phys. Lett.* **B 464** (1999) 117 [hep-ph/9908353] [INSPIRE].

[2] E. Alvarez and A. Szynkman, *Direct test of time reversal invariance violation in B mesons*, *Mod. Phys. Lett.* **A 23** (2008) 2085 [hep-ph/0611370] [INSPIRE].

[3] J. Bernabeu, F. Martinez-Vidal and P. Villanueva-Perez, *Time Reversal Violation from the entangled $B^0\bar{B}^0$ system*, *JHEP* **08** (2012) 064 [arXiv:1203.0171] [INSPIRE].

[4] BaBar collaboration, J.P. Lees et al., *Observation of Time Reversal Violation in the B^0 Meson System*, *Phys. Rev. Lett.* **109** (2012) 211801 [arXiv:1207.5832] [INSPIRE].

[5] K.R. Schubert, *T Violation and CPT Tests in Neutral-Meson Systems*, arXiv:1409.5998 [INSPIRE].

[6] E. Applebaum, A. Efrati, Y. Grossman, Y. Nir and Y. Soreq, *Subtleties in the BaBar measurement of time-reversal violation*, *Phys. Rev.* **D 89** (2014) 076011 [arXiv:1312.4164] [INSPIRE].

[7] Y. Grossman, A.L. Kagan and Z. Ligeti, *Can the CP asymmetries in $B \to \psi K(s)$ and $B \to \psi K(L)$ differ?*, *Phys. Lett.* **B 538** (2002) 327 [hep-ph/0204212] [INSPIRE].

JHEP02(2015)174

[8] A. Lenz and U. Nierste, *Numerical Updates of Lifetimes and Mixing Parameters of B Mesons*, arXiv:1102.4274 [INSPIRE].

[9] I.I. Bigi and A.I. Sanda, *CP violation*, *Camb. Monogr. Part. Phys. Nucl. Phys. Cosmol.* **9** (2000) 1 [INSPIRE].

[10] H.-n. Li and S. Mishima, *Penguin pollution in the $B^0 \to J/\psi K(S)$ decay*, *JHEP* **03** (2007) 009 [hep-ph/0610120] [INSPIRE].

[11] A.S. Dighe, T. Hurth, C.S. Kim and T. Yoshikawa, *Measurement of the lifetime difference of B_d mesons: possible and worthwhile?*, *Nucl. Phys.* **B 624** (2002) 377 [hep-ph/0109088] [INSPIRE].

[12] A. Dighe, T. Hurth, C.S. Kim and T. Yoshikawa, *The Width difference of B_d mesons*, PoS(HEP2001)096 [hep-ph/0112067] [INSPIRE].

[13] R.G. Sachs, *Methods for Testing the CPT Theorem*, *Phys. Rev.* **129** (1963) 2280 [INSPIRE].

[14] C.P. Enz and R.R. Lewis, *On the phenomenological description of CP-violation for K mesons and its consequences*, *Helv. Phys. Acta* **38** (1965) 860 [INSPIRE].

[15] L. Álvarez-Gaumé, C. Kounnas, S. Lola and P. Pavlopoulos, *Violation of time reversal invariance and CPLEAR measurements*, *Phys. Lett.* **B 458** (1999) 347 [hep-ph/9812326] [INSPIRE].

[16] M. Beuthe, G. Lopez Castro and J. Pestieau, *Field theory approach to K^0-$\overline{K^0}$ and B^0-$\overline{B^0}$ systems*, *Int. J. Mod. Phys.* **A 13** (1998) 3587 [hep-ph/9707369] [INSPIRE].

[17] J.P. Silva, *On the use of the reciprocal basis in neutral meson mixing*, *Phys. Rev.* **D 62** (2000) 116008 [hep-ph/0007075] [INSPIRE].

JHEP02(2015)174

Phenomenological aspects of possible vacua of a neutrino flavor model

Phenomenological aspects of possible vacua of a neutrino flavor model*

Takuya Morozumi[1,2;1)] Hideaki Okane[1;2)] Hiroki Sakamoto[1;3)] Yusuke Shimizu[1;4)]
Kenta Takagi[1;5)] Hiroyuki Umeeda[3;6)]

[1] Graduate School of Science, Hiroshima University, Higashi-Hiroshima 739-8526, Japan
[2] Core of Research for the Energetic Universe, Hiroshima University, Higashi-Hiroshima 739-8526, Japan
[3] Graduate School of Science and Engineering, Shimane University, Matsue 690-8504, Japan

Abstract: We discuss a supersymmetric model with discrete flavor symmetry $A_4 \times Z_3$. The additional scalar fields which contribute masses of leptons in the Yukawa terms are introduced in this model. We analyze their scalar potential and find that they have various vacuum structures. We show the relations among 24 different vacua and classify them into two types. We derive expressions of the lepton mixing angles, Dirac CP violating phase and Majorana phases for the two types. The model parameters which are allowed by the experimental data of the lepton mixing angles are different for each type. We also study the constraints on the model parameters which are related to Majorana phases. The different allowed regions of the model parameters for the two types are shown numerically for a given region of two combinations of the CP violating phases.

Keywords: flavor symmetry, non-Abelian discrete group, neutrino flavor model

PACS: 14.60.Pq, 14.60.St **DOI:** 10.1088/1674-1137/42/2/023102

1 Introduction

Although all the elementary particles in the standard model (SM) have now been discovered, with the discovery of the Higgs boson, there still exist phenomena which cannot be explained in the framework of the SM. One of these is the neutrino oscillation phenomenon, which implies two non-zero neutrino mass squared differences and two large lepton mixing angles. In order to explain this, many authors propose a neutrino flavor model with non-Abelian discrete flavor symmetry in the lepton sector (for reviews see [1–4]). Even before the discovery of the non-zero θ_{13} [5–7], a few authors suggested a tiny mixing angle θ_{13} based on non-Abelian discrete flavor symmetry [8]. Recent results from the T2K and NOνA experiments [9, 10] imply CP violation through the Dirac CP phase. They studied electron neutrino appearance in a muon neutrino beam. The Majorana phases are also sources of the CP violating phases if neutrinos are Majorana particles. The KamLAND-Zen experiment [11] is searching for neutrinoless double beta ($0\nu\beta\beta$) decay to check the Majorana nature of neutrinos. Therefore, it is important to predict not only mixing angles but also CP phases with the non-Abelian discrete flavor model.

The non-Abelian discrete flavor symmetry can easily explain large lepton mixing angles, e. g. tri-bimaximal mixing (TBM) [12, 13], which is a simple framework for the lepton mixing angles. Indeed, Altarelli and Feruglio (AF) proposed a simple flavor model and predicted TBM by using A_4 discrete flavor symmetry [14, 15]. They introduced $SU(2)$ gauge singlet scalar fields, so-called "flavons", and derived the TBM in the lepton sector. The non-zero θ_{13} can be realized by another A_4 non-trivial singlet flavon [8] in addition to the flavons introduced by AF. The origin of non-vanishing θ_{13} is related to a new contribution to the mass matrices. Matrices which have the same structure as that in Ref. [8] also appear in extra-dimensional models with the S_3 and S_4

Received 3 October 2017, Published online 12 January 2018

∗ Supported by JSPS KAKENHI Grant Number JP17K05418 (T.M.). This work is also supported in part by Grants-in-Aid for Scientific Research [No. 16J05332 (Y.S.), Nos. 24540272, 26247038, 15H01037, 16H00871, and 16H02189 (H.U.)] from the Ministry of Education, Culture, Sports, Science and Technology in Japan. H.O. is also supported by Hiroshima Univ. Alumni Association

1) E-mail: morozumi@hiroshima-u.ac.jp
2) E-mail: hideaki-ookane@hiroshima-u.ac.jp
3) E-mail: h-sakamoto@hiroshima-u.ac.jp
4) E-mail: yu-shimizu@hiroshima-u.ac.jp
5) E-mail: takagi-kenta@hiroshima-u.ac.jp
6) E-mail: umeeda@riko.shimane-u.ac.jp

flavor symmetries [16, 17]. The $\Delta(27)$ model also includes these matrices [18].

In this paper, we study phenomenological aspects of a supersymmetric model with $A_4\times Z_3$ symmetries. The three generations of the left-handed leptons are expressed as the A_4 triplet, $l=(l_e,l_\mu,l_\tau)$, while the right-handed charged leptons e_R, μ_R, and τ_R are A_4 singlets denoted as $\mathbf{1}$, $\mathbf{1}''$, and $\mathbf{1}'$ respectively. Three right-handed neutrinos are also described as the triplet of A_4. We introduce the $SU(2)$ gauge singlet flavons of A_4 triplets, $\phi_T=(\phi_{T1},\phi_{T2},\phi_{T3})$ and $\phi_S=(\phi_{S1},\phi_{S2},\phi_{S3})$. In addition, ξ and ξ' are also introduced as the $SU(2)$ gauge singlet flavons with the two kinds of singlet representations of A_4, $\mathbf{1}$ and $\mathbf{1}'$ respectively.

We focus on the vacuum structure of the flavor model. The scalar sectors of this model consist of many flavons in addition to the SM Higgs boson. Then, we analyze the scalar potential and show the 24 different sets of VEVs which come from 24 combinations of 4 (6) possible VEVs of the flavon ϕ_T (ϕ_S). The 24 different vacua are classified into two types which are not related to each other under the transformations A_4. Therefore, we expect that the two types of vacua have different expressions for the physical observables in terms of the model parameters such as Yukawa couplings. We ask the following question: whether these different vacua are physically distinct from each other. The purpose of this paper is to clarify the differences and relations among the VEVs and their physical consequences. In particular, we investigate the mixing angles, CP violating phase, and effective mass for neutrinoless double beta ($0\nu\beta\beta$) decay.

This paper is organized as follows. In Section 2, we introduce the supersymmetric model with $A_4\times Z_3$ symmetry. In Section 3, we study the classification of vacua and derive the formulae for the mixing angles and CP phases. In Section 4, we discuss the phenomenological aspects for mixing angles and CP violating phases. The numerical analyses for the effective mass of $0\nu\beta\beta$ decay are presented. Section 5 is devoted to a summary. In Appendix , we show the multiplication rule of the A_4 group.

2 Supersymmetric model with $A_4\times Z_3$ symmetry

In this section, we introduce a supersymmetric model with $A_4\times Z_3$ symmetry. We analyze the scalar potential and derive the mass matrices of the lepton sector.

2.1 Model

We introduce three heavy right-handed Majorana neutrinos. The leptons and scalars in our model are listed in Table 1.

Table 1. The representations of $SU(2)_L$ and A_4, and the charge assignment of Z_3 and $U(1)_R$ for leptons and scalars: $l_{e,\mu,\tau}$, $\{e,\mu,\tau\}_R$, $\{\nu_e,\nu_\mu,\mu_\tau\}_R$, and $h_{u,d}$ denote left-handed leptons, right-handed charged leptons, right-handed neutrinos, and Higgs fields, respectively. The other scalars are gauge singlet flavons and denoted as ϕ_T, ϕ_S, ξ, and ξ'. ω is the Z_3 charge and stands for $e^{2\pi i/3}$.

	$l=\begin{pmatrix}l_e\\l_\mu\\l_\tau\end{pmatrix}$	e_R	μ_R	τ_R	$\nu_R=\begin{pmatrix}\nu_{eR}\\\nu_{\mu R}\\\nu_{\tau R}\end{pmatrix}$	$h_{u,d}$	$\phi_T=\begin{pmatrix}\phi_{T1}\\\phi_{T2}\\\phi_{T3}\end{pmatrix}$	$\phi_S=\begin{pmatrix}\phi_{S1}\\\phi_{S2}\\\phi_{S3}\end{pmatrix}$	ξ	ξ'
$SU(2)_L$	2	1	1	1	1	2	1	1	1	1
A_4	3	1	$1''$	$1'$	3	1	3	3	1	$1'$
Z_3	ω	ω^2	ω^2	ω^2	ω^2	1	1	ω^2	ω^2	ω^2
$U(1)_R$	1	1	1	1	1	0	0	0	0	0

The superpotential of Yukawa interactions is

$$w_Y=w_l+w_D+w_R, \tag{1}$$

where w_l,w_D and w_R are Yukawa interactions for charged lepton, Dirac neutrino and Majorana neutrino sectors respectively:

$$\begin{aligned}w_l=&y_e(\phi_T l)_{\mathbf{1}}e_R h_d/\Lambda+y_\mu(\phi_T l)_{\mathbf{1}'}\mu_R h_d/\Lambda\\&+y_\tau(\phi_T l)_{\mathbf{1}''}\tau_R h_d/\Lambda+\text{h.c.},\end{aligned} \tag{2}$$

$$w_D=y_D(l\nu_R)_{\mathbf{1}}h_u+\text{h.c.}, \tag{3}$$

$$w_R=y_{\phi_S}\phi_S(\nu_R\nu_R)_{\mathbf{3}}+y_\xi\xi(\nu_R\nu_R)_{\mathbf{1}}+y_{\xi'}\xi'(\nu_R\nu_R)_{\mathbf{1}''}+\text{h.c.}, \tag{4}$$

where the lower indices denote A_4 representations. Moreover, the y's and Λ denote the Yukawa coupling constants and cut-off scale respectively. The multiplication rule for A_4 representations is shown in Appendix A.

In order to obtain the mass matrices of these leptons, we analyze the following superpotential of the scalar fields:

$$w_d\equiv w_d^T+w_d^S, \tag{5}$$

where

$$w_d^T=-M(\phi_0^T\phi_T)_{\mathbf{1}}+g\phi_0^T(\phi_T\phi_T)_{\mathbf{3}}, \tag{6}$$

$$\begin{aligned}w_d^S=&g_1\phi_0^S(\phi_S\phi_S)_{\mathbf{3}}+g_2(\phi_0^S\phi_S)_{\mathbf{1}}\xi+g_2'(\phi_0^S\phi_S)_{\mathbf{1}''}\xi'\\&+g_3(\phi_S\phi_S)_{\mathbf{1}}\xi_0-g_4\xi_0\xi\xi.\end{aligned} \tag{7}$$

Table 2. The driving fields and their representations and charge assignment.

	$\phi_0^T=\begin{pmatrix}\phi_{01}^T\\ \phi_{02}^T\\ \phi_{03}^T\end{pmatrix}$	$\phi_0^S=\begin{pmatrix}\phi_{01}^S\\ \phi_{02}^S\\ \phi_{03}^S\end{pmatrix}$	ξ_0
$SU(2)$	1	1	1
A_4	3	3	1
Z_3	1	ω^2	ω^2
$U(1)_R$	2	2	2

We have introduced the additional $SU(2)$ gauge singlet fields, ϕ_0^T, ϕ_0^S and ξ_0, which are called *"driving fields"*. The charge assignments of these fields are summarized in Table 2.

2.2 Potential analysis

In this subsection, we derive the VEVs for the scalar fields $\phi_T,\phi_S,\xi,\xi',\phi_0^T,\phi_0^S,\xi_0$. One can derive the scalar potential from the superpotentials in Eqs. (6) and (7) as

$$V=V_T+V_S, \tag{8}$$

where

$$\begin{aligned}V_T=\sum_X\left|\frac{\partial w_d^T}{\partial X}\right|^2=&\left|-M\phi_{T1}+\frac{2}{3}g(\phi_{T1}^2-\phi_{T2}\phi_{T3})\right|^2+\left|-M\phi_{T3}+\frac{2}{3}g(\phi_{T2}^2-\phi_{T3}\phi_{T1})\right|^2+\left|-M\phi_{T2}+\frac{2}{3}g(\phi_{T3}^2-\phi_{T1}\phi_{T2})\right|^2\\&+\left|-M\phi_{01}^T+\frac{2}{3}g(2\phi_{01}^T\phi_{T1}-\phi_{03}^T\phi_{T2}-\phi_{02}^T\phi_{T3})\right|^2+\left|-M\phi_{03}^T+\frac{2}{3}g(2\phi_{02}^T\phi_{T2}-\phi_{01}^T\phi_{T3}-\phi_{03}^T\phi_{T1})\right|^2\\&+\left|-M\phi_{02}^T+\frac{2}{3}g(2\phi_{03}^T\phi_{T3}-\phi_{02}^T\phi_{T1}-\phi_{01}^T\phi_{T2})\right|^2,\end{aligned} \tag{9}$$

and

$$\begin{aligned}V_S=\sum_Y\left|\frac{\partial w_d^S}{\partial Y}\right|^2=&\left|\frac{2}{3}g_1(\phi_{S1}^2-\phi_{S2}\phi_{S3})-g_2\phi_{S1}\xi+g_2'\phi_{S3}\xi'\right|^2+\left|\frac{2}{3}g_1(\phi_{S2}^2-\phi_{S3}\phi_{S1})-g_2\phi_{S3}\xi+g_2'\phi_{S2}\xi'\right|^2\\&+\left|\frac{2}{3}g_1(\phi_{S3}^2-\phi_{S1}\phi_{S2})-g_2\phi_{S2}\xi+g_2'\phi_{S1}\xi'\right|^2\\&+\left|\frac{2}{3}g_1(2\phi_{01}^S\phi_{S1}-\phi_{03}^S\phi_{S2}-\phi_{02}^S\phi_{S3})-g_2\phi_{01}^S\xi+g_2'\phi_{03}^S\xi'+2g_3\phi_{S1}\xi_0\right|^2\\&+\left|\frac{2}{3}g_1(2\phi_{02}^S\phi_{S2}-\phi_{01}^S\phi_{S3}-\phi_{03}^S\phi_{S1})-g_2\phi_{03}^S\xi+g_2'\phi_{02}^S\xi'+2g_3\phi_{S3}\xi_0\right|^2\\&+\left|\frac{2}{3}g_1(2\phi_{03}^S\phi_{S3}-\phi_{02}^S\phi_{S1}-\phi_{01}^S\phi_{S2})-g_2\phi_{02}^S\xi+g_2'\phi_{01}^S\xi'+2g_3\phi_{S2}\xi_0\right|^2\\&+\left|-g_2(\phi_{01}^S\phi_{S1}+\phi_{03}^S\phi_{S2}+\phi_{02}^S\phi_{S3})-2g_4\xi\xi_0\right|^2+\left|g_2'(\phi_{02}^S\phi_{S2}+\phi_{01}^S\phi_{S3}+\phi_{03}^S\phi_{S1})\right|^2\\&+\left|g_3(\phi_{s1}^2+2\phi_{S2}\phi_{S3})-g_4\xi^2\right|^2.\end{aligned} \tag{10}$$

The sum for X,Y runs over all the scalar fields:

$$X=\{\phi_{T1},\phi_{T2},\phi_{T3},\phi_{01}^T,\phi_{02}^T,\phi_{03}^T\}\ ,$$

$$Y=\{\phi_{S1},\phi_{S2},\phi_{S3},\phi_{01}^S,\phi_{02}^S,\phi_{03}^S,\xi,\xi',\xi_0\}.$$

The scalar potential V is minimized at $V=V_T=V_S=0$. There are several solutions for the minimization condition. We obtain sets of solutions denoted as η_m and $\lambda_n^{\pm}$ (m=1-4, n=1-3), where η_m and $\lambda_n^{\pm}$ are the solutions of $V_T=0$ and $V_S=0$ respectively. Hereafter, we call them the set of VEV alignments and show them explicitly as follows:

$$\eta_1\equiv\left\{\langle\phi_T\rangle=v_T\begin{pmatrix}1\\0\\0\end{pmatrix},\ \langle\phi_0^T\rangle=\begin{pmatrix}0\\0\\0\end{pmatrix}\right\}, \tag{11}$$

$$\eta_2\equiv\left\{\langle\phi_T\rangle=\frac{v_T}{3}\begin{pmatrix}-1\\2\\2\end{pmatrix},\ \langle\phi_0^T\rangle=\begin{pmatrix}0\\0\\0\end{pmatrix}\right\}, \tag{12}$$

$$\eta_3\equiv\left\{\langle\phi_T\rangle=\frac{v_T}{3}\begin{pmatrix}-1\\2\omega\\2\omega^2\end{pmatrix},\ \langle\phi_0^T\rangle=\begin{pmatrix}0\\0\\0\end{pmatrix}\right\}, \tag{13}$$

$$\eta_4\equiv\left\{\langle\phi_T\rangle=\frac{v_T}{3}\begin{pmatrix}-1\\2\omega^2\\2\omega\end{pmatrix},\ \langle\phi_0^T\rangle=\begin{pmatrix}0\\0\\0\end{pmatrix}\right\}, \tag{14}$$

$$\lambda_1^{\pm}\equiv\left\{\langle\phi_S\rangle=\pm v_S\begin{pmatrix}1\\1\\1\end{pmatrix},\ \langle\xi'\rangle=u',\ \langle\phi_0^S\rangle=\begin{pmatrix}0\\0\\0\end{pmatrix}\right\},\quad(15)$$

$$\lambda_2^{\pm}\equiv\left\{\langle\phi_S\rangle=\pm v_S\begin{pmatrix}1\\\omega\\\omega^2\end{pmatrix},\ \langle\xi'\rangle=\omega u',\ \langle\phi_0^S\rangle=\begin{pmatrix}0\\0\\0\end{pmatrix}\right\},\quad(16)$$

$$\lambda_3^{\pm}\equiv\left\{\langle\phi_S\rangle=\pm v_S\begin{pmatrix}1\\\omega^2\\\omega\end{pmatrix},\ \langle\xi'\rangle=\omega^2 u',\ \langle\phi_0^S\rangle=\begin{pmatrix}0\\0\\0\end{pmatrix}\right\},\quad(17)$$

where $v_T=\frac{3M}{2g}$, $v_S=\sqrt{\frac{g_4}{3g_3}}u$, $u'=\frac{g_2}{g_2'}u$ and u is the VEV of ξ, $\langle\xi\rangle=u$[1]. The superscript of $\lambda^{\pm}$ denotes the overall sign of the VEV $\langle\phi_S\rangle$. In total, we obtain 24 sets of vacua, since there are four sets of alignment for η_m and six sets for $\lambda_n^{\pm}$.

2.3 Mass matrix for charged leptons and neutrinos

We derive charged lepton mass matrices and neutrino mass matrices from the Yukawa interactions in Eqs. (2), (3), and (4). These matrices are expressed in various forms corresponding to the VEV alignments. The charged lepton mass matrices ${M_l}^{(m)}$ for Eqs. (11)–(14) are

$${M_l}^{(1)}=\frac{v_d v_T}{\Lambda}\begin{pmatrix}y_e&0&0\\0&y_\mu&0\\0&0&y_\tau\end{pmatrix},\quad(18)$$

$${M_l}^{(2)}=\frac{v_d v_T}{3\Lambda}\begin{pmatrix}-y_e&2y_\mu&2y_\tau\\2y_e&-y_\mu&2y_\tau\\2y_e&2y_\mu&-y_\tau\end{pmatrix}=S{M_l}^{(1)},\quad(19)$$

$${M_l}^{(3)}=\frac{v_d v_T}{3\Lambda}\begin{pmatrix}-y_e&2\omega y_\mu&2\omega^2 y_\tau\\2\omega^2 y_e&-y_\mu&2\omega y_\tau\\2\omega y_e&2\omega^2 y_\mu&-y_\tau\end{pmatrix}=T^\dagger ST{M_l}^{(1)},\quad(20)$$

$${M_l}^{(4)}=\frac{v_d v_T}{3\Lambda}\begin{pmatrix}-y_e&2\omega^2 y_\mu&2\omega y_\tau\\2\omega y_e&-y_\mu&2\omega^2 y_\tau\\2\omega^2 y_e&2\omega y_\mu&-y_\tau\end{pmatrix}=TST^\dagger{M_l}^{(1)},\quad(21)$$

respectively, where the matrices S and T are

$$S=\frac{1}{3}\begin{pmatrix}-1&2&2\\2&-1&2\\2&2&-1\end{pmatrix},\quad T=\begin{pmatrix}1&0&0\\0&\omega&0\\0&0&\omega^2\end{pmatrix}.\quad(22)$$

The Dirac mass matrix for neutrinos obtained from Eq. (3) is

$$M_D=y_D v_u\begin{pmatrix}1&0&0\\0&0&1\\0&1&0\end{pmatrix}.\quad(23)$$

It is noted that the Dirac mass matrix is determined independently of the VEV alignments. The Majorana mass matrices ${M_R^{(n)}}^{\pm}$ for the corresponding set of solutions Eqs. (15)–(17) are given as follows:

$$\begin{aligned}{M_R^{(1)}}^{\pm}=&\pm\frac{1}{3}y_{\phi_S}v_S\begin{pmatrix}2&-1&-1\\-1&2&-1\\-1&-1&2\end{pmatrix}+y_\xi u\begin{pmatrix}1&0&0\\0&0&1\\0&1&0\end{pmatrix}\\&+y_{\xi'}u'\begin{pmatrix}0&0&1\\0&1&0\\1&0&0\end{pmatrix},\end{aligned}\quad(24)$$

$$\begin{aligned}{M_R^{(2)}}^{\pm}=&\pm\frac{1}{3}y_{\phi_S}v_S\begin{pmatrix}2&-\omega^2&-\omega\\-\omega^2&2\omega&-1\\-\omega&-1&2\omega^2\end{pmatrix}+y_\xi u\begin{pmatrix}1&0&0\\0&0&1\\0&1&0\end{pmatrix}\\&+\omega y_{\xi'}u'\begin{pmatrix}0&0&1\\0&1&0\\1&0&0\end{pmatrix}=T^\dagger{M_R^{(1)}}^{\pm}T^\dagger,\end{aligned}\quad(25)$$

$$\begin{aligned}{M_R^{(3)}}^{\pm}=&\pm\frac{1}{3}y_{\phi_S}v_S\begin{pmatrix}2&-\omega&-\omega^2\\-\omega&2\omega^2&-1\\-\omega^2&-1&2\omega\end{pmatrix}+y_\xi u\begin{pmatrix}1&0&0\\0&0&1\\0&1&0\end{pmatrix}\\&+\omega^2 y_{\xi'}u'\begin{pmatrix}0&0&1\\0&1&0\\1&0&0\end{pmatrix}=T{M_R^{(1)}}^{\pm}T.\end{aligned}\quad(26)$$

In order to generate the light neutrino mass matrices, we adopt the seesaw mechanism [19–21]. The effective neutrino mass matrices are given by the well-known formula, $M_\nu=-M_D M_R^{-1}M_D^{\rm T}$, through the seesaw mechanism. We obtain the 6 different effective neutrino mass

1) There are still other solutions for $V=0$, including the trivial solution which makes all the VEVs vanish. It leads to the vanishing of all the lepton masses and mixing angles. In addition to the trivial solution, there are solutions with non-zero VEVs of the driving fields. This case leads to the breakdown of $U(1)_R$ symmetry. In this paper, we only discuss the vacua where $U(1)_R$ symmetry is conserved.

matrices from Eqs. (23)-(26) as follows:

$$M_\nu^{(1)\pm}=\pm a\begin{pmatrix}1&0&0\\0&1&0\\0&0&1\end{pmatrix}+b^\pm\begin{pmatrix}1&1&1\\1&1&1\\1&1&1\end{pmatrix}+c\begin{pmatrix}1&0&0\\0&0&1\\0&1&0\end{pmatrix}+d\begin{pmatrix}0&0&1\\0&1&0\\1&0&0\end{pmatrix}, \quad (27)$$

$$M_\nu^{(2)\pm}=T^\dagger M_\nu^{(1)\pm}T^\dagger, \quad (28)$$

$$M_\nu^{(3)\pm}=TM_\nu^{(1)\pm}T, \quad (29)$$

where

$$\begin{aligned}&a=ky_{\phi_S}v_S,\\&c=k(y_{\xi'}u'-y_\xi u),\\&d=ky_{\xi'}u',\\&b^\pm=\mp\frac{a}{3}+\frac{a^2}{2d-c}\left(\frac{1}{3}-\frac{d^2}{a^2}\right),\\&k=\frac{{y_D}^2{v_u}^2}{y_\xi^2u^2+y_{\xi'}^2u'^2-(y_{\phi_S}^2v_S^2+y_\xi uy'_\xi u')}.\end{aligned}$$

3 Classification of vacua and PMNS mixing matrix

In this section, we classify the 24 different vacua and derive the lepton mixing matrix $U_{\rm PMNS}$, called the *Pontecorvo-Maki-Nakagawa-Sakata* (PMNS) mixing matrix. In order to classify the vacua, we discuss the relations among the VEV alignments with the transformations of A_4. We show that the 24 vacua are classified into two types in the following subsection. Then, one finds the two different PMNS matrices with diagonalizing matrices for the charged lepton and effective neutrino mass matrices Eqs. (18)–(21), and (27)–(29).

3.1 Relations among sets of VEV alignments

The generators of A_4 are expressed as the following forms for the representations $\mathbf{1}$,$\mathbf{1}'$,$\mathbf{1}''$ and $\mathbf{3}$,

$$S(\mathbf{1})=S(\mathbf{1}')=S(\mathbf{1}'')=1\ ,\quad S(\mathbf{3})=\frac{1}{3}\begin{pmatrix}-1&2&2\\2&-1&2\\2&2&-1\end{pmatrix}, \quad (30)$$

$$T(\mathbf{1})=1,\ T(\mathbf{1}')=\omega,\ T(\mathbf{1}'')=\omega^2\ ,\quad T(\mathbf{3})=\begin{pmatrix}1&0&0\\0&\omega&0\\0&0&\omega^2\end{pmatrix}. \quad (31)$$

The sets of VEV alignment η_m,$\lambda_n^\pm$ are associated through the transformations of these generators. As an example, we show the T transformation on λ_1^+:

$$T[\lambda_1^+]\equiv\left\{\langle\phi_S\rangle=T(\mathbf{3})v_S\begin{pmatrix}1\\1\\1\end{pmatrix},\langle\xi'\rangle=T(\mathbf{1}')u',\langle\phi_0^S\rangle=T(\mathbf{3})\begin{pmatrix}0\\0\\0\end{pmatrix}\right\}=\left\{\langle\phi_S\rangle=v_S\begin{pmatrix}1\\\omega\\\omega^2\end{pmatrix},\langle\xi'\rangle=\omega u',\ \langle\phi_0^S\rangle=\begin{pmatrix}0\\0\\0\end{pmatrix}\right\}=\lambda_2^+. \quad (32)$$

The S and T transformations on all the sets of the VEV alignment are summarized in Fig. 1. Some transformations preserve the VEVs of either η_m or $\lambda_n^\pm$. These vacua have Z_3 or Z_2 symmetries as the residual symmetries of A_4 respectively. For the VEVs described as η_m, they are invariant under the following transformation,

$$\begin{aligned}&T[\eta_1]=T^{-1}[\eta_1]=\eta_1\ ,\quad TST[\eta_2]=(TST)^{-1}[\eta_2]=\eta_2\ ,\\&ST[\eta_3]=(ST)^{-1}[\eta_3]=\eta_3\ ,\quad TS[\eta_4]=(TS)^{-1}[\eta_4]=\eta_4\ .\end{aligned} \quad (33)$$

It is easy to confirm that such transformations correspond to Z_3 symmetries:

$$T^3=(TST)^3=(ST)^3=(TS)^3=1. \quad (34)$$

Each $\lambda_n^\pm$ has Z_2 symmetry as follows:

$$S[\lambda_1^\pm]=\lambda_1^\pm\ ,\quad TST^2[\lambda_2^\pm]=\lambda_2^\pm\ ,\quad T^2ST[\lambda_3^\pm]=\lambda_3^\pm, \quad (35)$$

where

$$S^2=(TST^2)^2=(T^2ST)^2=1. \quad (36)$$

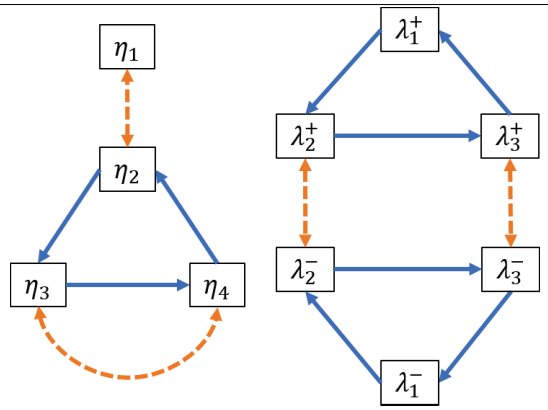

Fig. 1. (color online) Map of the transitions among the VEV alignments under the transformations S and T: The solid arrow corresponds to the transition due to T transformation and the dashed two headed arrow shows the transition due to S transformation. In the map, η_1 is invariant under T transformation while $\lambda_1^\pm$ are invariant under S transformation.

3.2 Classification of 24 vacua

In this subsection, we show the relations among the 24 different Lagrangians derived from the 24 different combinations of VEV alignments in Eqs. (11)–(17). We find the two sets of 12 equivalent Lagrangians with the appropriate field redefinitions. Then, the 24 Lagrangians are classified into two types. For simplicity, we write the Lagrangian of this model in a short form:

$$\mathcal{L}(\psi,\phi_1,\phi_2), \tag{37}$$

where ψ represents the fermion fields such as l and ν_R. ϕ_1 and ϕ_2 represent the scalar fields, which should have their VEVs written as η_m and $\lambda_n^{\pm}$ respectively. We write the Lagrangian in the broken phase for the VEV alignment $(\eta_m,\ \lambda_n^{\pm})$ with fluctuations h_1 and h_2 as

$$\mathcal{L}^{\pm}_{mn}(\psi,h_1,h_2)\equiv\mathcal{L}(\psi,\eta_m+h_1,\lambda_n^{\pm}+h_2). \tag{38}$$

Then, we prove the following equation:

$$\mathcal{L}(\psi',\eta_m+h_1',\lambda_n^{\pm}+h_2')=\mathcal{L}(\psi,G^{-1}\eta_m+h_1,G^{-1}\lambda_n^{\pm}+h_2), \tag{39}$$

where G denotes the transformation composed of S and T in Eqs. (30) and (31). There are 12 independent transformations including the identity element:

$$\begin{aligned} G;\{&e,\ T,\ T^2,\ S,\ TS,\ T^2S,\ ST,\ ST^2,\ T^2ST,\\ &TST,\ TST^2,\ T^2ST^2\}. \end{aligned} \tag{40}$$

The redefined fields are written as follows,

$$\psi'=G\psi\ ,\quad h_i'=Gh_i\quad (i=1,2). \tag{41}$$

The right-hand side of Eq. (39) corresponds to the Lagrangian for the vacuum $(G^{-1}\eta_m,G^{-1}\lambda_n^{\pm})$ while the left-hand side is the Lagrangian for the vacuum $(\eta_m,\lambda_n^{\pm})$ in terms of the redefined fields. In the symmetric phase, the Lagrangian $\mathcal{L}(\psi,\phi_1,\phi_2)$ is invariant under the G transformation,

$$\mathcal{L}(G\psi,G\phi_1,G\phi_2)=\mathcal{L}(\psi,\phi_1,\phi_2). \tag{42}$$

One obtains the following equation from Eq. (42) for the vacuum $(G^{-1}\eta_m,G^{-1}\lambda_n^{\pm})$,

$$\mathcal{L}(G\psi,\eta_m+Gh_1,\lambda_n^{\pm}+Gh_2)=\mathcal{L}(\psi,G^{-1}\eta_m+h_1,G^{-1}\lambda_n^{\pm}+h_2). \tag{43}$$

Finally, one obtains the relation Eq. (39) by applying the field definition Eq. (41) to the left-hand side of Eq. (43). The relation Eq. (39) implies the equality of the Lagrangians for the two vacua $(\eta_m,\lambda_n^{\pm})$ and $(G^{-1}\eta_m,G^{-1}\lambda_n^{\pm})$.

Here, we briefly show how to find the equivalent vacua with Fig. 1. For example, let us consider the T transformation in terms of the vacuum of (η_1,λ_1^+). One finds that η_1 is invariant and λ_1^+ transfers to λ_2^+ under the T transformation. Therefore, $\mathcal{L}_{11}^+$ and $\mathcal{L}_{12}^+$ are equivalent. One can find 12 equivalent vacua by applying 12 independent transformations in Eq. (40) to the vacuum (η_1,λ_1^+). Then, we classify the 24 Lagrangians into two types:

Type I;
$$\{\mathcal{L}_{11}^+,\mathcal{L}_{12}^+,\mathcal{L}_{13}^+,\mathcal{L}_{21}^+,\mathcal{L}_{32}^+,\mathcal{L}_{43}^+,\mathcal{L}_{22}^-,\mathcal{L}_{23}^-,\mathcal{L}_{31}^-,\mathcal{L}_{33}^-,\mathcal{L}_{41}^-,\mathcal{L}_{42}^-\}, \tag{44}$$

Type II;
$$\{\mathcal{L}_{11}^-,\mathcal{L}_{12}^-,\mathcal{L}_{13}^-,\mathcal{L}_{21}^-,\mathcal{L}_{32}^-,\mathcal{L}_{43}^-,\mathcal{L}_{22}^+,\mathcal{L}_{23}^+,\mathcal{L}_{31}^+,\mathcal{L}_{33}^+,\mathcal{L}_{41}^+,\mathcal{L}_{42}^+\}. \tag{45}$$

Type I and type II are disconnected because of the absence of a transformation which relates one type to the other. Since all the Lagrangians which belong to the same type lead to the same physical consequences, we consider only $\mathcal{L}_{11}^+$ and $\mathcal{L}_{11}^-$ as the representatives of their types:

$$\mathcal{L}^{\rm I}\equiv\mathcal{L}_{11}^+\ ,\quad \mathcal{L}^{\rm II}\equiv\mathcal{L}_{11}^-. \tag{46}$$

We also define the representative mass matrices for charged leptons and neutrinos as

$$M_l\equiv M_l^{(1)}\ ,\quad M_\nu^{\rm I}\equiv M_\nu^{(1)+}\ ,\quad M_\nu^{\rm II}\equiv M_\nu^{(1)-}. \tag{47}$$

It is noted that the charged lepton mass matrix $M_l^{(1)}$ is diagonal.

3.3 PMNS matrices for two types

In this subsection, we construct the PMNS matrices for the two types, $\mathcal{L}^{\rm I}$ and $\mathcal{L}^{\rm II}$. Since the charged lepton mass matrix M_l is diagonal, the PMNS matrix is determined so that it diagonalizes the neutrino mass matrices in Eq. (27):

$$\begin{aligned}(U^{\rm I}_{\rm PMNS})^\dagger M_\nu^{\rm I}(U^{\rm I}_{\rm PMNS})^*&=(U^{\rm II}_{\rm PMNS})^\dagger M_\nu^{\rm II}(U^{\rm II}_{\rm PMNS})^*\\ &=\begin{pmatrix} m_1 & & \\ & m_2 & \\ & & m_3\end{pmatrix},\end{aligned} \tag{48}$$

where the left-handed neutrino masses m_1,m_2 and m_3 are positive. The PMNS matrices are expressed as the following forms for the two types:

$$U^{\rm I}_{\rm PMNS}=U_{\rm TBM}U_{13}(\theta,\sigma)\begin{pmatrix} {\rm e}^{{\rm i}\phi_1} & & \\ & {\rm e}^{{\rm i}\phi_2} & \\ & & {\rm e}^{{\rm i}\phi_3}\end{pmatrix}, \tag{49}$$

$$\begin{aligned}U^{\rm II}_{\rm PMNS}&=U_{\rm TBM}\begin{pmatrix} & & -i\\ 1 & & \\ i & & \end{pmatrix}U_{13}(\theta,\sigma)\begin{pmatrix} {\rm e}^{{\rm i}\phi_1} & & \\ & {\rm e}^{{\rm i}\phi_2} & \\ & & {\rm e}^{{\rm i}\phi_3}\end{pmatrix},\\ &=U_{\rm TBM}U_{13}^*\left(\theta+\frac{\pi}{2},\sigma\right)\begin{pmatrix} -i{\rm e}^{{\rm i}(\phi_1+\sigma)} & & \\ & {\rm e}^{{\rm i}\phi_2} & \\ & & -i{\rm e}^{{\rm i}(\phi_3-\sigma)}\end{pmatrix}.\end{aligned} \tag{50}$$

The unitary matrix $U_{\rm TBM}$ is the tri-bimaximal mixing matrix and $U_{13}(\theta,\sigma)$ denotes the unitary rotation matrix:

$$U_{\rm TBM}=\begin{pmatrix}2/\sqrt{6} & 1/\sqrt{3} & 0\\ -1/\sqrt{6} & 1/\sqrt{3} & -1/\sqrt{2}\\ -1/\sqrt{6} & 1/\sqrt{3} & 1/\sqrt{2}\end{pmatrix}, \tag{51}$$

$$U_{13}(\theta,\sigma)=\begin{pmatrix}\cos\theta & 0 & {\rm e}^{-{\rm i}\sigma}\sin\theta\\ 0 & 1 & 0\\ -{\rm e}^{{\rm i}\sigma}\sin\theta & 0 & \cos\theta\end{pmatrix}. \tag{52}$$

We have introduced the parameters θ,σ and ϕ_i $(i=1,2,3)$. They are written in terms of the complex parameters of the neutrino mass matrix, a,b,c and d, in Eq. (27)[1)]. In the rest of this subsection, we derive the explicit forms of the parameters θ,σ and ϕ_i in terms of the model parameters a,b,c and d. In the first step, one rotates $M_\nu M_\nu^\dagger$ with the tri-bimaximal mixing matrix.

$$U_{\rm TBM}^\dagger M_\nu^{\rm I}(M_\nu^{\rm I})^\dagger U_{\rm TBM}=\begin{pmatrix}A & 0 & B\\ 0 & C & 0\\ B^* & 0 & D\end{pmatrix}, \tag{53}$$

$$U_{\rm TBM}^\dagger M_\nu^{\rm II}(M_\nu^{\rm II})^\dagger U_{\rm TBM}=\begin{pmatrix}D & 0 & -B^*\\ 0 & C & 0\\ -B & 0 & A\end{pmatrix}. \tag{54}$$

where

$$A=\left|a+c-\frac{d}{2}\right|^2+\left|\frac{\sqrt{3}}{2}d\right|^2, \tag{55}$$

$$B=\left(a+c-\frac{d}{2}\right)\frac{\sqrt{3}}{2}d^*+\frac{\sqrt{3}}{2}d\left(a-c+\frac{d}{2}\right)^*\equiv|B|{\rm e}^{{\rm i}\varphi_B}, \tag{56}$$

$$C=\left|\frac{a^2-(c^2-cd+d^2)}{2d-c}\right|^2, \tag{57}$$

$$D=\left|a-c+\frac{d}{2}\right|^2+\left|\frac{\sqrt{3}}{2}d\right|^2. \tag{58}$$

The mass eigenvalues are determined as

$$m_1^2=\frac{A+D}{2}\mp\frac{1}{2}\sqrt{(A-D)^2+4|B|^2}, \tag{59}$$

$$m_2^2=C, \tag{60}$$

$$m_3^2=\frac{A+D}{2}\pm\frac{1}{2}\sqrt{(A-D)^2+4|B|^2}, \tag{61}$$

where the upper and lower signs in these mass eigenvalues correspond to the normal hierarchy (NH) and the inverted hierarchy (IH). Next, we diagonalize the rotated mass matrices, Eqs. (53) and (54), with $U_{13}(\theta,\sigma)$ and $U_{13}^*(\theta+\frac{\pi}{2},\sigma)$ respectively:

$$U_{13}(\theta,\sigma)^\dagger\begin{pmatrix}A & 0 & B\\ 0 & C & 0\\ B^* & 0 & D\end{pmatrix}U_{13}(\theta,\sigma)=\begin{pmatrix}m_1^2 & & \\ & m_2^2 & \\ & & m_3^2\end{pmatrix}, \tag{62}$$

$$U_{13}\left(\theta+\frac{\pi}{2},\sigma\right)^{\rm T}\begin{pmatrix}D & 0 & -B^*\\ 0 & C & 0\\ -B & 0 & A\end{pmatrix}U_{13}\left(\theta+\frac{\pi}{2},\sigma\right)^*$$

$$=\begin{pmatrix}m_1^2 & & \\ & m_2^2 & \\ & & m_3^2\end{pmatrix}, \tag{63}$$

where θ and σ are determined as,

$$\tan2\theta=\frac{2|B|}{D-A}\ ,\ \sigma=-\varphi_B. \tag{64}$$

Finally, the other parameters ϕ_i are determined as follows,

$$\phi_1=\frac{1}{2}\left[\tan^{-1}\left[\frac{\left({\rm Im}[a]+{\rm Im}\left[c-\frac{d}{2}\right]\cos2\theta\right)\cos\sigma+\left({\rm Re}[a]\cos2\theta+{\rm Re}\left[c-\frac{d}{2}\right]\right)\sin\sigma-\frac{\sqrt{3}}{2}{\rm Im}[d]\sin2\theta}{\left({\rm Re}[a]+{\rm Re}\left[c-\frac{d}{2}\right]\cos2\theta\right)\cos\sigma-\left({\rm Im}[a]\cos2\theta+{\rm Im}\left[c-\frac{d}{2}\right]\right)\sin\sigma-\frac{\sqrt{3}}{2}{\rm Re}[d]\sin2\theta}\right]-\sigma\right], \tag{65}$$

$$\phi_2=\frac{1}{2}\tan^{-1}\left[\frac{{\rm Im}[a^2-(c^2-cd+d^2)]{\rm Re}[2d-c]-{\rm Re}[a^2-(c^2-cd+d^2)]{\rm Im}[2d-c]}{{\rm Re}[a^2-(c^2-cd+d^2)]{\rm Re}[2d-c]+{\rm Im}[a^2-(c^2-cd+d^2)]{\rm Im}[2d-c]}\right], \tag{66}$$

$$\phi_3=\frac{1}{2}\left[\tan^{-1}\left[\frac{\left({\rm Im}[a]-{\rm Im}\left[c-\frac{d}{2}\right]\cos2\theta\right)\cos\sigma-\left({\rm Re}[a]\cos2\theta-{\rm Re}\left[c-\frac{d}{2}\right]\right)\sin\sigma+\frac{\sqrt{3}}{2}{\rm Im}[d]\sin2\theta}{\left({\rm Re}[a]-{\rm Re}\left[c-\frac{d}{2}\right]\cos2\theta\right)\cos\sigma+\left({\rm Im}[a]\cos2\theta-{\rm Im}\left[c-\frac{d}{2}\right]\right)\sin\sigma+\frac{\sqrt{3}}{2}{\rm Re}[d]\sin2\theta}\right]+\sigma\right]. \tag{67}$$

1) There are six real parameters since b is written by using a,c,d.

We briefly explain the derivation of ϕ_i for the mass matrix $M_\nu^{\rm I}$. We first diagonalize $M_\nu^{\rm I}$ with the unitary matrices $U_{\rm TBM}$ and $U_{13}(\theta,\sigma)$ according to Eq. (48). However, the diagonalized neutrino mass matrix consists of complex elements. Then, the parameters ϕ_i are determined so that all the elements of the diagonalized matrix are real and positive.

4 Phenomenological aspects

We study the phenomenological aspects of this model and show the differences between the two types of vacua. The observables, such as mixing angles and CP violating phases, are described with the model parameters in different forms for the two types. In the following subsections, we discuss the relation between the observables and model parameters. The numerical analyses are also shown in this section.

4.1 Mixing angles and CP violating phases

In this subsection, we discuss the lepton mixing angles, CP violating phases and the effective mass for $0\nu\beta\beta$ decay. At first, we introduce the PDG parametrization of the PMNS matrix:

$$U_{\rm PMNS}^{\rm PDG}=\begin{pmatrix} c_{12}c_{13} & s_{12}c_{13} & s_{13}e^{-i\delta_{CP}} \\ -s_{12}c_{23}-c_{12}s_{23}s_{13}{\rm e}^{{\rm i}\delta_{CP}} & c_{12}c_{23}-s_{12}s_{23}s_{13}{\rm e}^{{\rm i}\delta_{CP}} & s_{23}c_{13} \\ s_{12}c_{23}-c_{12}c_{23}s_{13}{\rm e}^{{\rm i}\delta_{CP}} & -c_{12}s_{23}-s_{12}c_{23}s_{13}{\rm e}^{{\rm i}\delta_{CP}} & c_{23}c_{13} \end{pmatrix}\begin{pmatrix} {\rm e}^{{\rm i}\alpha} & & \\ & {\rm e}^{{\rm i}\beta} & \\ & & 1 \end{pmatrix}, \tag{68}$$

where s_{ij} and c_{ij} denote the lepton mixing angles $\sin\theta_{ij}$ and $\cos\theta_{ij}$, respectively. They are written in terms of the PMNS matrix elements:

$$\sin^2\theta_{12}=\frac{|U_{e2}|^2}{1-|U_{e3}|^2},\ \sin^2\theta_{23}=\frac{|U_{\mu3}|^2}{1-|U_{e3}|^2},\ \sin^2\theta_{13}=|U_{e3}|^2, \tag{69}$$

where $U_{\alpha i}$ denote the PMNS matrix elements. The Dirac CP violating phase δ_{CP} can be obtained with the Jarlskog invariant

$$\sin\delta_{CP}=\frac{J_{CP}}{s_{23}c_{23}s_{12}c_{12}s_{13}c_{13}^2}, \tag{70}$$

$$J_{CP}={\rm Im}\left[U_{e1}U_{\mu2}U_{\mu1}^*U_{e2}^*\right]. \tag{71}$$

In order to obtain these parameters from our model, we substitute the PMNS matrix elements in Eqs. (49) and (50). For the type I case, the matrix elements are given as follows:

$$U_{e1}=\frac{2}{\sqrt{6}}{\rm e}^{{\rm i}\phi_1}\cos\theta, \tag{72}$$

$$U_{e2}=U_{\mu2}=\frac{1}{\sqrt{3}}{\rm e}^{{\rm i}\phi_2}, \tag{73}$$

$$U_{e3}=\frac{2}{\sqrt{6}}e^{-i(\sigma-\phi_3)}\sin\theta, \tag{74}$$

$$U_{\mu1}=\left(-\frac{1}{\sqrt{6}}\cos\theta+\frac{1}{\sqrt{2}}{\rm e}^{{\rm i}\sigma}\sin\theta\right){\rm e}^{{\rm i}\phi_1}, \tag{75}$$

$$U_{\mu3}=\left(-\frac{1}{\sqrt{6}}e^{-i\sigma}\sin\theta-\frac{1}{\sqrt{2}}\cos\theta\right){\rm e}^{{\rm i}\phi_3}. \tag{76}$$

The mixing angles, Dirac CP violating phase and Majorana phases for both types are listed in Table 3.

Table 3. Mixing angles, Dirac CP phase and Majorana phases for the two types of vacua.

	Type I	Type II
$\sin^2\theta_{12}$	$\frac{1}{2+\cos2\theta}$	$\frac{1}{2-\cos2\theta}$
$\sin^2\theta_{23}$	$\frac{1}{2}\left(1+\frac{\sqrt{3}\sin2\theta}{2+\cos2\theta}\cos\sigma\right)$	$\frac{1}{2}\left(1-\frac{\sqrt{3}\sin2\theta}{2-\cos2\theta}\cos\sigma\right)$
$\sin^2\theta_{13}$	$\frac{1}{3}(1-\cos2\theta)$	$\frac{1}{3}(1+\cos2\theta)$
$\sin\delta_{CP}$	$-\frac{\sin2\theta}{\lvert\sin2\theta\rvert}\frac{(2+\cos2\theta)\sin\sigma}{\sqrt{(2+\cos2\theta)^2-3\sin^2 2\theta\cos^2\sigma}}$	$-\frac{\sin2\theta}{\lvert\sin2\theta\rvert}\frac{(2-\cos2\theta)\sin\sigma}{\sqrt{(2-\cos2\theta)^2-3\sin^2 2\theta\cos^2\sigma}}$
$\alpha+\delta_{CP}$	$\phi_1-\phi_3+\sigma$	$\phi_1-\phi_3+\sigma$
$\beta+\delta_{CP}$	$\phi_2-\phi_3+\sigma$	$\phi_2-\phi_3+\frac{\pi}{2}$

One can adopt either of the two types to predict the mixing angles and the Dirac CP violating phases, since both types give the same predictions. However, we note the following two facts. First, if one fixes $\cos2\theta\simeq1$ to obtain small $\sin^2\theta_{13}$ in type I, $\sin^2\theta_{13}$ in type II reaches 2/3, which is disfavored in the experiments. Second, as shown in Subsection 3.3, the model parameters θ, σ and ϕ_i are expressed in the same forms for the two types with a, b,

c and d of Eq. (27). Therefore, those parameters have common values for both types. Hence, the two types can not realize the experimental results simultaneously.

Next, we discuss the effective mass for $0\nu\beta\beta$ decay, $m_{ee}=\sum_i m_i U_{ei}^2$, and the Majorana phases, α and β. The effective mass is given as follows:

$$|m_{ee}^{\rm I}|=\frac{1}{3}\big|m_1(1+\cos2\theta)e^{2i\phi_1}+m_2e^{2i\phi_2} +m_3(1-\cos2\theta)e^{2i(\phi_3-\sigma)}\big|, \tag{77}$$

$$|m_{ee}^{\rm II}|=\frac{1}{3}\big|m_1(1-\cos2\theta)e^{2i(\phi_1+\sigma)}-m_2e^{2i\phi_2} +m_3(1+\cos2\theta)e^{2i\phi_3}\big|, \tag{78}$$

where the superscripts I and II denote the types of vacuum. Equivalently, one can rewrite Eqs. (77) and (78) as

$$|m_{ee}^{\rm I}|=\frac{1}{3}\big|m_1(1+\cos2\theta)e^{2i(\phi_1-\phi_3+\sigma)}+m_2e^{2i(\phi_2-\phi_3+\sigma)} +m_3(1-\cos2\theta)\big|, \tag{79}$$

$$|m_{ee}^{\rm II}|=\frac{1}{3}\big|m_1(1-\cos2\theta)e^{2i(\phi_1-\phi_3+\sigma)}-m_2e^{2i(\phi_2-\phi_3)} +m_3(1+\cos2\theta)\big|, \tag{80}$$

On the other hand, the effective mass in the PDG parametrization is written as

$$|m_{ee}|=\big|m_1c_{13}^2c_{12}^2e^{2i(\alpha+\delta_{CP})}+m_2c_{13}^2s_{12}^2e^{2i(\beta+\delta_{CP})}+m_3s_{13}^2\big|. \tag{81}$$

One can obtain the Majorana CP violating phases α and β by comparing Eqs (79)-(81),

$$\text{(Type I)}\quad \alpha+\delta_{CP}=\phi_1-\phi_3+\sigma\ ,\quad \beta+\delta_{CP}=\phi_2-\phi_3+\sigma, \tag{82}$$

$$\text{(Type II)}\quad \alpha+\delta_{CP}=\phi_1-\phi_3+\sigma\ ,\quad \beta+\delta_{CP}=\phi_2-\phi_3+\frac{\pi}{2}. \tag{83}$$

4.2 Numerical analysis

In this subsection, we show numerical analysis to find the difference between two types. We use recent experimental results with 3σ range [22], as summarized in Table 4.

Table 4. The experimental data for the mass squared differences and mixing angles with 3σ range [22].

	normal hierarchy (NH)	inverted hierarchy (IH)
$\Delta m_{21}^2/\text{eV}^2$	$(7.03\sim8.09)\times10^{-5}$	$(7.03\sim8.09)\times10^{-5}$
$\Delta m_{31}^2/\text{eV}^2$	$(2.407\sim2.643)\times10^{-3}$	$-(2.565\sim2.318)\times10^{-3}$
$\sin^2\theta_{12}$	$0.271\sim0.345$	$0.271\sim0.345$
$\sin^2\theta_{23}$	$0.385\sim0.635$	$0.393\sim0.640$
$\sin^2\theta_{13}$	$0.01934\sim0.02392$	$0.01953\sim0.02408$

As we have shown in the previous subsection, the mixing angles and Dirac CP phase are expressed in terms of the model parameters θ and σ in different forms for the two types.

The experimental data for $\sin^2\theta_{13}$ in Table 4 is realized by the following value of θ with NH or IH:

$$\text{Type I;}\quad 9.81^\circ\leqslant|\theta|\leqslant10.9^\circ\ \text{(NH)},\ 9.86^\circ\leqslant|\theta|\leqslant11.0^\circ\ \text{(IH)}, \tag{84}$$

$$\text{Type II;}\quad 79.1^\circ\leqslant|\theta|\leqslant80.2^\circ\ \text{(NH)},\ 79.0^\circ\leqslant|\theta|\leqslant80.1^\circ\ \text{(IH)}. \tag{85}$$

The value of σ is allowed in $-180^\circ\leqslant\sigma\leqslant180^\circ$ for both of the two types, since the error of $\sin^2\theta_{23}$ from the experiments is large.

Next, we discuss the parameters ϕ_i in the expressions of the Majorana phases of Eqs. (82) and (83). The effective mass $|m_{ee}|$ in Eq. (81) depends on the two combinations of Dirac and Majorana phases, $2(\alpha+\delta_{CP})$ and $2(\beta+\delta_{CP})$. If we determine both $|m_{ee}|$ and the lightest neutrino mass, we obtain the constraints on these two combinations. In order to find how the numerical constraints on ϕ_i are different in the two types, we consider a specific situation. As an example, we assume that $|m_{ee}|$ is predicted in the region as shown in Fig. 3. We note that the lightest neutrino mass is constrained from the cosmological upper bound for the neutrino mass sum, $\sum_i m_i<0.16$ eV [23]. This plot is obtained when the Dirac and Majorana phases are randomly chosen from the region A1 in Fig. 2,

$$0<\alpha+\delta_{CP}<\pi/4\ ,\ 0<\beta+\delta_{CP}<\pi/4. \tag{86}$$

In this situation, the phase differences $\phi_1-\phi_3$ and $\phi_2-\phi_3$ for one type can be distinguished from those for the other type. The constraints on the phase differences are shown in Fig. 4. For type I, the phase difference $\phi_2-\phi_3$ is proportional to $\phi_1-\phi_3$. However, for type II, $\phi_2-\phi_3$ is independent of the value of $\phi_1-\phi_3$ because σ is absent in the expression of $\phi_2-\phi_3$ in Eq. (83).

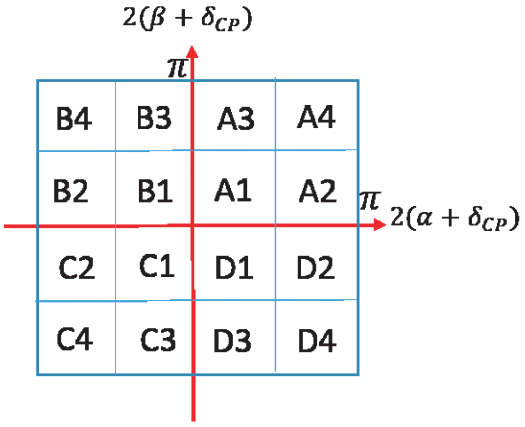

Fig. 2. (color online) 16 divided regions for $2(\alpha+\delta_{CP})$ and $2(\beta+\delta_{CP})$.

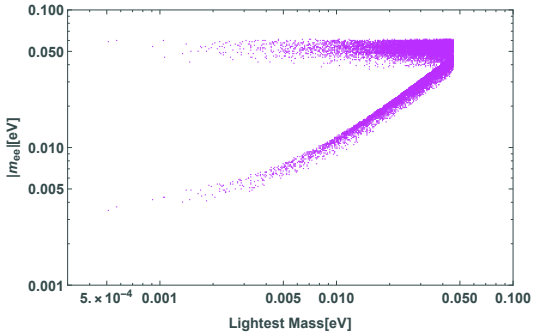

Fig. 3. (color online) The prediction of effective mass for $0\nu\beta\beta$ decay in region A1 of Fig. 2. The upper region corresponds to the IH case , while the lower one corresponds to the NH case.

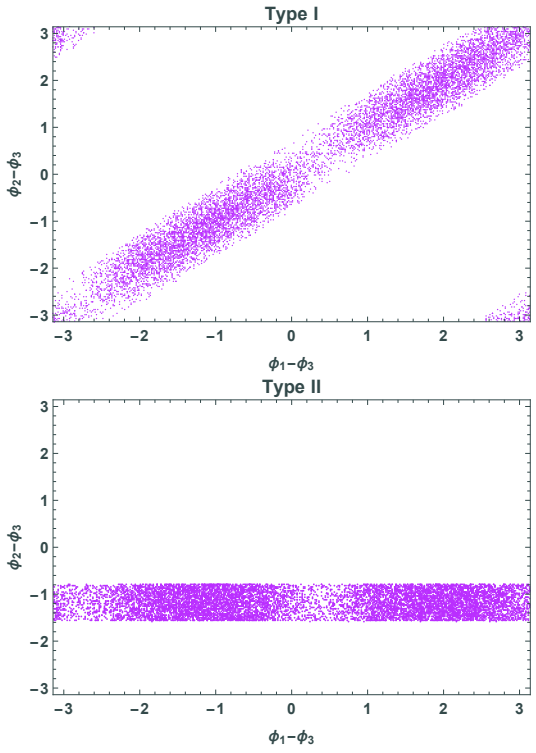

Fig. 4. (color online) The allowed regions of the model parameters, $\phi_1-\phi_3$ and $\phi_2-\phi_3$ for both types of vacua. These plots correspond to region A1 of Fig. 2.

5 Summary

We have studied phenomenological aspects of a supersymmetric model with $A_4\times Z_3$ symmetry. We found 24 degenerate vacua at the 24 minima of the scalar potential. Then, we discussed the relations among the 24 different vacua and classified them into two types. Both types consist of 12 vacua which are related to each other by transformations of A_4. We proved that the 12 vacua are equivalent and lead to the same physical consequences. However, we found that we obtain different physical consequences from the vacua of different types. Therefore, we analyzed the two types of vacua to find the different phenomenological consequences of the two types. In particular, we investigated observables such as mixing angles, Dirac CP phase, Majorana phases and effective mass for $0\nu\beta\beta$ decay.

These observables are expressed in terms of the model parameters θ, σ and ϕ_i. The angle θ and phase σ are determined by the deviation from the tri-bimaximal mixing matrix. The two types lead to different expressions for the mixing angles and Dirac CP violating phase in terms of θ and σ. Therefore, one should take different model parameters in each type in order to realize the experimental results. Although one can adopt both of the two types to predict the observable parameters, the two types cannot realize the current experimental data simultaneously. The Majorana phases α and β are parametrized in the different expressions for each type by the model parameters ϕ_i in addition to θ and σ. In order to find numerical differences between the two types of Majorana phase, we considered the specific situation where the lightest mass and effective mass for the $0\nu\beta\beta$ decay are determined in a certain region. We showed the allowed regions of the phase differences, $\phi_1-\phi_3$ and $\phi_2-\phi_3$. The regions are quite different for the two types: the phase differences for type I are proportional to each other, while those for type II are not.

The VEVs η_m and $\lambda_n^{\pm}$ transfer to the different VEVs by transformations of A_4. However, the transformations for η_m and $\lambda_n^{\pm}$ are closed differently since they have the Z_3 and Z_2 residual symmetries from A_4 respectively. We have pointed out that some combinations of the VEVs can lead to different physical consequences. When we consider models with two or more flavons, we should take account of the combination of VEVs.

Appendix A

Multiplication rule of A_4 group

In this appendix, we show the multiplication of the A_4 group. The multiplication rule of the triplets is written as follows;

$$\begin{pmatrix}a_1\\a_2\\a_3\end{pmatrix}_{\mathbf{3}}\otimes\begin{pmatrix}b_1\\b_2\\b_3\end{pmatrix}_{\mathbf{3}}=(a_1b_1+a_2b_3+a_3b_2)_{\mathbf{1}}\oplus(a_3b_3+a_1b_2+a_2b_1)_{\mathbf{1'}}\oplus(a_2b_2+a_1b_3+a_3b_1)_{\mathbf{1''}}\oplus\frac{1}{3}\begin{pmatrix}2a_1b_1-a_2b_3-a_3b_2\\2a_3b_3-a_1b_2-a_2b_1\\2a_2b_2-a_1b_3-a_3b_1\end{pmatrix}_{\mathbf{3}}\oplus\frac{1}{2}\begin{pmatrix}a_2b_3-a_3b_2\\a_1b_2-a_2b_1\\a_3b_1-a_1b_3\end{pmatrix}_{\mathbf{3}}, \tag{A1}$$

while that for singlets is,

$$\mathbf{1'}\otimes\mathbf{1''}=\mathbf{1}. \tag{A2}$$

In order to derive the A_4 invariant superpotential in Eq. (1), we have used the multiplication rules. Their derivation is shown in the reviews in Refs. [1–4].

References

1 H. Ishimori, T. Kobayashi, H. Ohki, Y. Shimizu, H. Okada, and M. Tanimoto, Prog. Theor. Phys. Suppl., **183**: 1 (2010) [arXiv:1003.3552 [hep-th]]
2 H. Ishimori, T. Kobayashi, H. Ohki, H. Okada, Y. Shimizu, and M. Tanimoto, Lect. Notes Phys., **858**: 1 (2012)
3 H. Ishimori, T. Kobayashi, Y. Shimizu, H. Ohki, H. Okada, and M. Tanimoto, Fortsch. Phys., **61**: 441 (2013)
4 S. F. King, A. Merle, S. Morisi, Y. Shimizu, and M. Tanimoto, New J. Phys., **16**: 045018 (2014) [arXiv:1402.4271 [hep-ph]]
5 F. P. An et al (Daya Bay Collaboration), Phys. Rev. Lett., **108**: 171803 (2012) [arXiv:1203.1669 [hep-ex]]
6 J. K. Ahn et al (RENO Collaboration), Phys. Rev. Lett., **108**: 191802 (2012) [arXiv:1204.0626 [hep-ex]]
7 Y. Abe et al (Double Chooz Collaboration), Phys. Lett. B, **735**: 51 (2014) [arXiv:1401.5981 [hep-ex]]
8 Y. Shimizu, M. Tanimoto, and A. Watanabe, Prog. Theor. Phys., **126**: 81 (2011) [arXiv:1105.2929 [hep-ph]]
9 K. Abe et al (T2K Collaboration), Phys. Rev. Lett., **112**: 061802 (2014) [arXiv:1311.4750 [hep-ex]]
10 P. Adamson et al (NOvA Collaboration), Phys. Rev. Lett., **116**(15): 151806 (2016) [arXiv:1601.05022 [hep-ex]]
11 A. Gando et al (KamLAND-Zen Collaboration), Phys. Rev. Lett., **117**(8): 082503 (2016); Addendum: [Phys. Rev. Lett., **117**(10): 109903 (2016)] [arXiv:1605.02889 [hep-ex]]
12 P. F. Harrison, D. H. Perkins, and W. G. Scott, Phys. Lett. B, **530**: 167 (2002) [hep-ph/0202074]
13 P. F. Harrison and W. G. Scott, Phys. Lett. B, **535**: 163 (2002) [hep-ph/0203209]
14 G. Altarelli and F. Feruglio, Nucl. Phys. B, **720**: 64 (2005) [hep-ph/0504165]
15 G. Altarelli and F. Feruglio, Nucl. Phys. B, **741**: 215 (2006) [hep-ph/0512103]
16 N. Haba, A. Watanabe, and K. Yoshioka, Phys. Rev. Lett., **97**: 041601 (2006) [hep-ph/0603116]
17 H. Ishimori, Y. Shimizu, M. Tanimoto, and A. Watanabe, Phys. Rev. D, **83**: 033004 (2011) [arXiv:1010.3805 [hep-ph]]
18 W. Grimus and L. Lavoura, JHEP, **0809**: 106 (2008) [arXiv:0809.0226 [hep-ph]]
19 P. Minkowski, Phys. Rev. B, **67**: 421 (1977)
20 T. Yanagida, *Horizontal Symmetry And Masses Of Neutrinos*, in *Workshop on the Unified Theories and the Baryon Number in the Universe*, Tsukuba, Japan, February 13-14, 1979, KEK-79-18. EDS. O. Sawada, A. Sugamoto, Conf. Proc. C, **7902131**: 95 (1979)
21 M. Gell-Mann, P. Ramond, and R. Slansky, Conf. Proc. C, **790927**: 315 (1979) [arXiv:1306.4669 [hep-th]] "Supergravity", EDS. P. van Nieuwenhuizen, D. Z. Freedman, Proceedings, Workshop At Stony Brook, 27-29 September 1979, Amsterdam, (Netherlands: North-holland, 1979) 341p
22 I. Esteban, M. C. Gonzalez-Garcia, M. Maltoni, I. Martinez-Soler, and T. Schwetz, JHEP, **1701**: 087 (2017) [arXiv:1611.01514 [hep-ph]]
23 S. Alam et al (BOSS Collaboration), arXiv:1607.03155 [astro-ph.CO]